UNIVERSITAT POLITÈCNICA
DE CATALUNYA
BARCELONATECH

Machine learning algorithms for 5G optical networks

Doctoral Thesis By:

Asmaa Ibrahim

Thesis supervisor:

Josep Prat

A thesis submitted in fulfillment of the requirements for the degree of Doctor of Philosophy in the

Department of Signal theory and communications

Barcelona, Spain, March, 2023

Acknowledgment

During the journey of this thesis many events and hard times passed, and finally all it ends up.

First, I Would like to thank Allah for his guidance and all the blessing in every single moment and step in my life.

I would like to thank Prof Josep Prat for his continuous support from the first day he accepted this supervision. Since then, he guides me patiently with his immense knowledge, and motivates me a lot as he gave me the opportunity to work on recent research topics in an amazing research environment.

I would like to thank my husband, Amir, for his great support during this journey, his amazing support always pushes and motivates me. Although the struggled times we passed through, being with me is always a blessing. I am grateful to have him.

I would like to acknowledge the help of Dr Tawfik Ismail, Ahmed El Sheikh and Ahmed Abdel Salam in this work as co-authors for the published papers. And to extend a special thanks for Dr Ahmed El Sheikh for his continuous help over fifteen years.

As in every step forward in my life, I cannot forget that this achievement could not have been possible without the support of my family: my parents, Eman and Ibrahim, and my sisters, Engy and Arwa. They supported me spiritually throughout writing this thesis and my life in general. And extend these thanks to my husband Amir.

Abstract

5G networks have envisioned to support diverse services with different quality of service (QOS), this arises 5G network slicing as a key enabler for 5G network revolution, so network slicing has been proposed as a promising technique that enables multiple virtual networks to be established on top of a common shared infrastructure. Hence, the Cloud Radio Access Network (C-RAN) has been proposed in 5G network to simply use SDN concept, as it is mainly based on fundamentals of decentralization the data plane. C-RAN consists of two main parts: Base Band Unit (BBU) and Remote Radio Heads (RRH). Moreover, 5G network mainly proposed two optical communication schemes for indoor and outdoor communication. The first scheme is the optical distribution network in C-RAN, as the transport network affects the capacity, latency, and level of intelligence of the network. Therefore, development of architectures, technologies, interfaces, and networks for 5G fronthaul has gained significant attention in the last few years. Optical Networks (ON) is considered as the best candidate for the 5G fronthaul network as it offers a reliable fronthaul network for many RRH in a cost and energy efficient manner and satisfies the capacity and delay requirements. The second scheme is Visible light communication (VLC) and it is proposed as a promising technology for wireless communication systems that promises to overcome the crowded radio spectrum and accommodates the increasing demand for data services in indoor areas.

Based on comprehensive study of the research opportunities in 5G networks, this thesis provides contributions in overcoming challenges of 5G networks in three phases. Firstly, addressing the noncoherent optical modulation in 5G optical networks and deploying the artificial intelligence capabilities to enhance it. Secondly, proposing an interference management scheme for indoor optical networks. Finally, introducing BBU-RRH assignment and interference management scheme that targeting power enhancement and handover reduction.

The first phase of this thesis introduces optical modulation schemes based on neural network architecture, regression decision tree and filter bank multicarrier technique. First, optical wireless and radio front-haul communication systems are deemed as potential technologies to the radio frequency wireless communications in several applications. Consequently, the clipped non-coherent optical modulation

Abstract

techniques have gained significant attention. The trade-off between the spectral efficiency and the power efficiency of the benchmark techniques such as asymmetrical clipping optical OFDM (ACO-OFDM) and direct clipping optical OFDM (DCO-OFDM), pose a challenge of maintaining enhanced spectral and power efficiency for the design of the optical modulation techniques. In this section, we propose a deep neural network (DNN) based optical transceiver. It uses simple but efficient DNN to predict the clipped negative parts of the transmitted signal at the receiver side. We evaluate and analyze several DNN-based optical transceiver architectures for different performance aspects. Then, we propose regression decision tree (RDT) based optical transceiver, that predicts the transmitted signal at the receiver side. The proposed transceiver compensates for the clipping noise produced by clipping the negative parts of the transmitted signal. We evaluated and analyzed the RDT based optical transceiver architectures for different performance aspects and compared the results with benchmarks techniques and alternative deep neural network (DNN) transceiver. The proposed optical OFDM transceiver enhances spectral and power efficiency compared to the latest works. Finally, Filter bank multi-carrier (FBMC) is considered a promising alternative to the Orthogonal Frequency Division Multiplexing (OFDM) scheme. It improves spectral efficiency by eliminating the need for cyclic prefix while attenuating interference due to the robustness of the out-of-band emission. In this work, we present a framework, and the performance evaluation of FBMC is a multi-carrier modulation scheme for the direct detection of optical communications. As the proposed model has higher spectral efficiency than the classical ACO-OFDM, removing the guard interval enhances the spectral efficiency. Furthermore, the perfect rectangular pulse shaping and eliminating the out of band emission of the filter bank enhances the ACO-FBMC the BER performance of the ACO-OFDM. We propose a transceiver model for Asymmetrical Clipped Optical FBMC (ACO-FBMC) based on Fast Fourier Transform (FFT) operations, analyze inter-frame interference, and offer an iterative receptive method to eliminate it. Finally, we compared the bit error rate (BER) performance of the ACO-FBMC using different overlapping factors with the ACO-OFDM.

The second phase of this thesis addresses the problem of interference management in indoor optical modulation. In VLC systems, the coverage area is divided into multiple atto-cells. In each atto-cell, multiple LED arrays are used as access points (APs) serving the assigned users. The coverage area of APs might be overlapped to avoid service discontinuity for mobile users. The overlapped coverage zones result in co-channel interference (CCI). We develop a shared frequency reuse (SFR) technique to minimize interference and maximize the system throughput. This technique divides the overall bandwidth into two parts: the shared and the reused bands. The shared band serves the users in the interference area while the reused band serves users in the non-interfering area. Then we study and evaluate the system performance

in terms of the signal-to-interference and noise ratio (SINR), total throughput, and the outage probability. The proposed system achieved total throughput of up to 800 Mbps with 40 dB SINR at the cell edge. Furthermore, the outage probability can be optimized to its minimum value when the receiver field-of-view (FOV) is taken by $40o$ when the minimum SINR is 10 dB.

In the final phase of this thesis, we address the RRH-BBU assignment and interference management in optical fronthaul network. In this section, we proposed RRH-BBU assignment based on clustering algorithm that targets minimizing the power consumption and the inter BBU handover. The proposed algorithm computes the required number of installed BBUs to accommodate the maximum traffic load, deploys time series clustering as temporal clustering method, and applies DBSCAN algorithm to divide each temporal cluster into several spatial cluster based on the cell location. Then the problem of assigning RRH of each cluster is described as a bin packing optimization problem to find the optimum number of BBUs for each cluster. The proposed algorithm has been validated using real world CDR of Milan city and it is verified by the published Milan land use map. The inter BBU handover signals have been enhanced by assigning near RRHs to the same spatial cluster and same BBU, to avoid inter BBU handover. The accurate handover rate can be computed using the user mobility between different RRHs, as stated we provide the algorithm without computing the handover rate due to lake of user mobility data. It is showed that the algorithm reduces the total power consumption of the current deployed network by 28.8 %, by assigning all the active RRHs to certain BBUs based on the traffic load and switching off the unassigned BBUs.

Table of contents

Table of contents

Table of contents

List of Figures

List of Figures

List of Tables

Abbreviation

FBMC	Filter bank multicarrier
CRAN	Centralized radio access network
VLC	Visible light communication
SDFN	Software defined network
HCRAN	Heterogeneous centralized radio access network
NFV	Network function virtualization
OFDM	Orthogonal frequency division multiplexing
ACO-OFDM	Asymmetrical clipping optical – OFDM
DCO-OFDM	Direct clipping optical – OFDM
BBU	Base Band Unit
RRH	Remote Radio Heads
ML	Machine learning
AI	Artificial intelligence
DNN	Deep neural network
RDT	Regression decision tree
ANN	Artificial neural network
HETNET	Heterogeneous network
SVM	Support vector machine
MRT	Multi regression tree
CDR	Call detailed records
QOS	Quality of service
UE	User equipment
MOPTS	Million operations per time slot

For my husband, sons, parents, and sisters

Chapter 1 : Introduction

1.1 5G networks

In this section, we present fundamental concepts and techniques of 5G networks as 5G approaches, features, software defined network (SDN), network function virtualization (NFV), cloud radio access network (CRAN). 5G network architecture has two main approaches.

I. evolutionary approach

As the 5G must scale up and improve the mobile network performance in terms of the number of served devices, traffic volume, the system throughput, heterogeneous networks (HetNet) have been proposed as a solution to achieve these enhancements. HetNets are basically composed of different cells in terms of the coverage area as (Macro cell, Pico cell, Femto cell,..) and radio access techniques as (mm wave, micro wave, ..) as shown in Fig. 1-1. Deploying these small cells improves the capacity and the coverage of the cellular network by utilizing the spatial reuse of the spectrum [2].

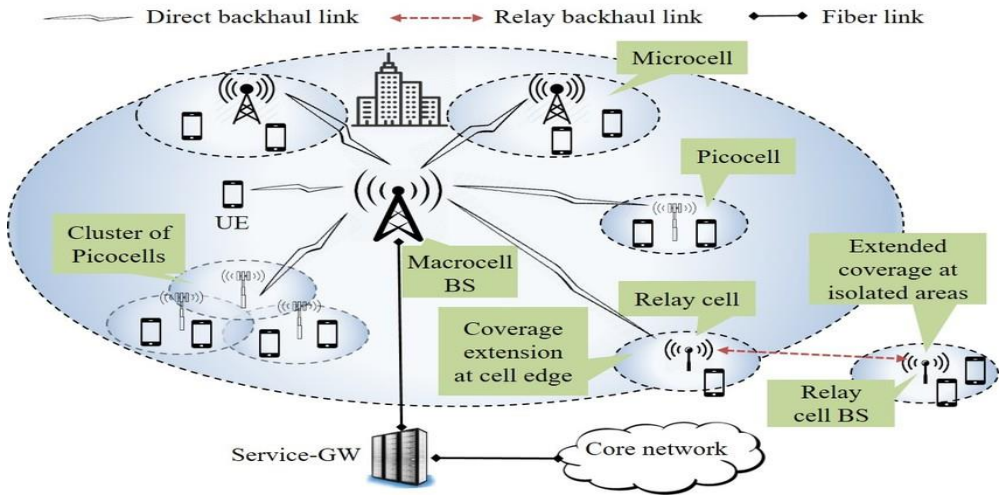

FIGURE 1-1. Network architecture of HetNets [13]

II. Service oriented approach

5G is planned as a multi service supporting different services with different quality of service (QOS), as shown in Fig. 1-2.

a. Enhanced Mobile Broad Band (eMBB) which requires huge enhancements in the throughput and user data rate supported by the current cellular network.

b. Ultra Reliable Low Latency communications (URLLC) as 5G is envisioned to support new services require low latency and high reliability as the critical communications in health care sector, for example.

c. Massive Machine Type Communications (MMTC) as 5G has to serve massive number of Internet Of Things (IOT) devices with small payloads [2]. Different techniques and network architectures have been proposed to achieve 5G network requirements.

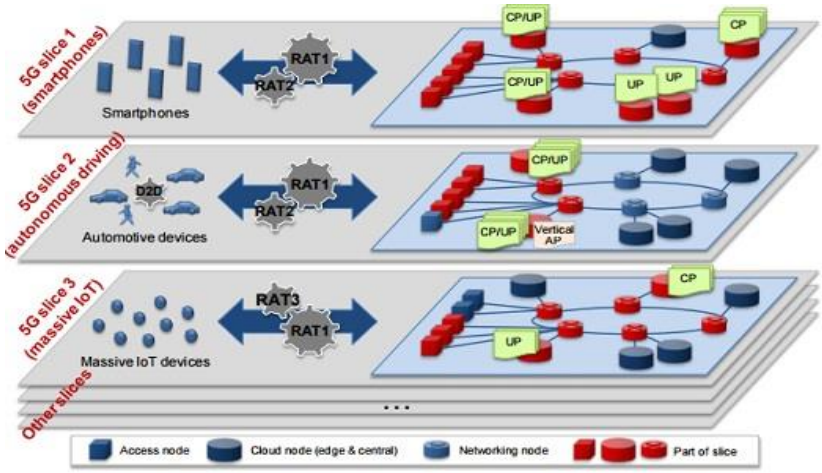

FIGURE 1-2: 5G Network Slicing [11]

In this section we will introduce several techniques and show its facilities to enable 5G networks, these techniques have been introduced as the basic partners for 5G networks [12].

1.1.1 Network slicing network

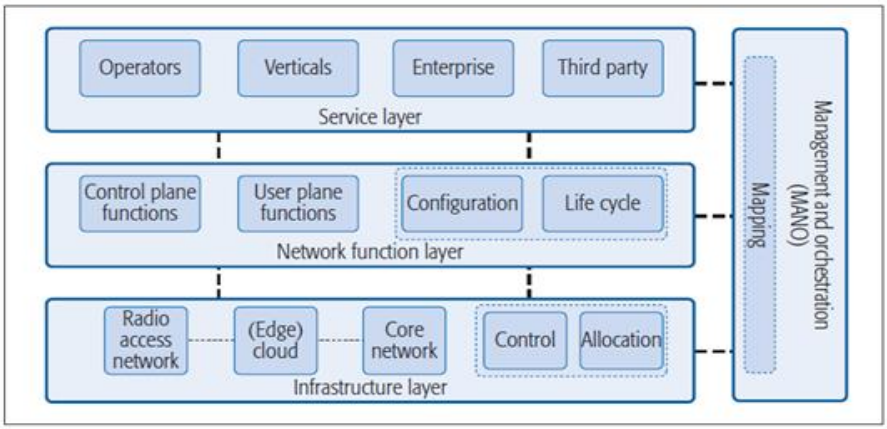

FIGURE 1-3: 5G Network layer architecture [11]

Network slicing has been proposed as a promising technique that enables multiple virtual networks to be established on top of a common shared infrastructure, so 5G network must have the ability to virtualize the underlying infrastructure and provide isolation among different services. Different organizations proposed different architectural visions that can accommodate the 5G network requirements as one fits all architecture can not support the 5G services. The Next Generation Mobile Network Alliance (NGMN) envisions the 5G architecture as flexible software network, that enables different virtual networks to be created on top of common physical infrastructure. Unlike initial proposals of network slicing which consider slicing for only core network (CN), NGMN defines the End- to- End (E2E) slicing that can be reached with slicing core network (CN) and radio access network (RAN). Its architecture is based on service management and orchestration (MANO) entity that plays the central role of orchestration [2], [3]. NGMN architecture mainly divided the 5G network into three main layers as shown in Fig. 1-3.

I. Infrastructure resources

II. Business enablement

III. Business application

The E2E MANO orchestrate the whole process in central manner, this architecture considered as a general architecture. 5G public private partnership (5G-PPP) shares the

same architecture and offers more detailed functional layers as its architecture divided as

I. Infrastructure
II. Network function
III. Orchestration
IV. Business function
V. Service function

Unlike NGMN architecture, 5G-PPP propose the orchestration as separated layer not in central manner. Mapping 5G-PPP architecture to NGMN architecture shows that the NGMN business enablement layer is divided into network and orchestration layers, while business application layer is divided into business function and service function. Network slicing of the proposed general architecture is introduced as slicing for each layer by defining the main function of each layer and the slicing of it.

1.1.2 NGMN architecture

NGMN architecture mainly divided the 5G network into three main layers

A. Infrastructure resources

This layer responsible for deployment, control, management and allocation of physical network resources including CN and RAN. For CN slicing, due to different constraints and needs of different slices the central cloud infrastructure cannot be used . Some architectures propose a mix of central and edge cloud schemes where the resource can be allocated to either of them based on the slice requirements. As URLLC slice needs low latency links that can be provided by the edge cloud part. On the other hand, the RAN composed of different LTE and Wi-Fi base stations has to be flexible to offer different services to different slices. The cloud RAN has been proposed as a promising technology that provide the RAN with high flexibility as shown in Fig. 1-4. As it composed of central base band unit with multiple remote radio heads as will be discussed.

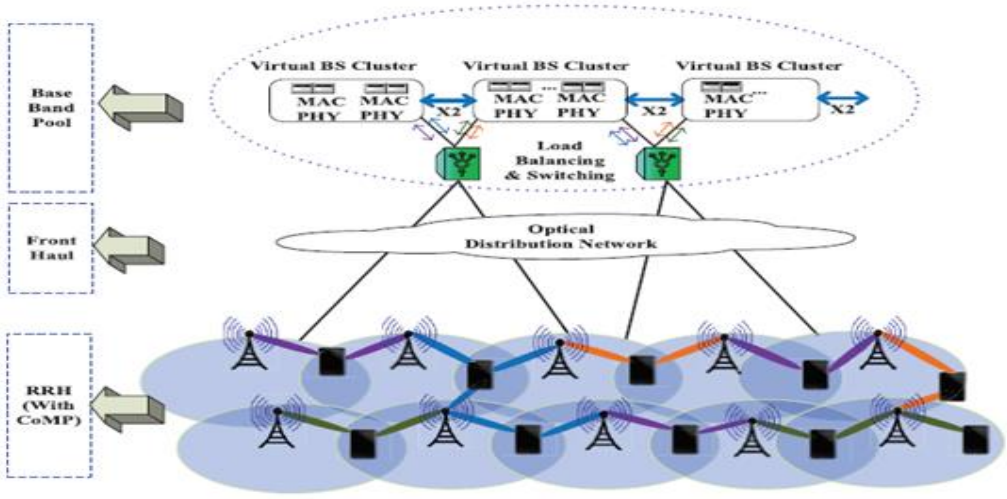

FIGURE 1-4. Cloud Radio Access Network (CRAN) architecture [6]

B. Network function

This layer offers End-to-End slicing according to the requirements of each slice by layer performing all the operations that are related to the configuration and life cycle management of the network functions after assigning virtual resources to each slice.

C. Service function

The main difference between slicing in 5G and other technologies is the End-to-End nature and need to express services through a high-level description and to map it to appropriate infrastructure elements and network function. This layer supports this service description to the network. There are two different approaches to describe the services, the first approach is simply a set of traffic characteristics and service level agreements (SLA) like network performance aspects as throughput and the latency. While the second approach is more detailed that identify specific function and the and RATs that are bundled together for the creation of slice. The first approach needs complicated orchestrator to identify the network slice from the available data, while the second description has simpler orchestrator, but it is less efficient as it allows less flexibility for the orchestrator [2].

1.1.3 5G network features

To provide different services on common shared infrastructure, 5G network must have some features that enable the network slicing as

I. Flexibility

That enables on demand configuration of networks slicing without the need of fixed contractual agreements.

II. Isolation

That assures performance guarantees and security for each tenant even when different tenants use network slices.

III. Customization

Assures that the allocated resource meets the service requirements.

IV. Elasticity

Resource elasticity can be realized by reshaping the use of resource by scaling up/ down, reallocation resources and reprogramming functionality.

V. Programmability

By providing the network with programmable resource as software defined network architecture as will be discussed.

1.1.4 Software Defined Network

In dense 5G network with multiple small cells the Configuration and maintenance of servers and network nodes become a complex challenge. Software Design Network (SDN) simplifies this complexity by separating the control functions apart from the network nodes. SDN defined as the separation between the control and the data plane as shown in Fig. 1-5. The control plane constructs the Forwarding Table to forward the data, using routing tables produced by different routing protocols, such as the Open Shortest Path First (OSPF) protocol. The data plane forwards the data packets between different network nodes. In SDN, all the forwarding decisions are taken by the controller, so it reduces the computational load on various network devices. The network administrator has a global view of the network and can handle the real time

changes in the network. Separating network intelligence from physical devices in SDN allows parallel development of software and hardware and makes it easier to experiment with new ideas and protocols [4].

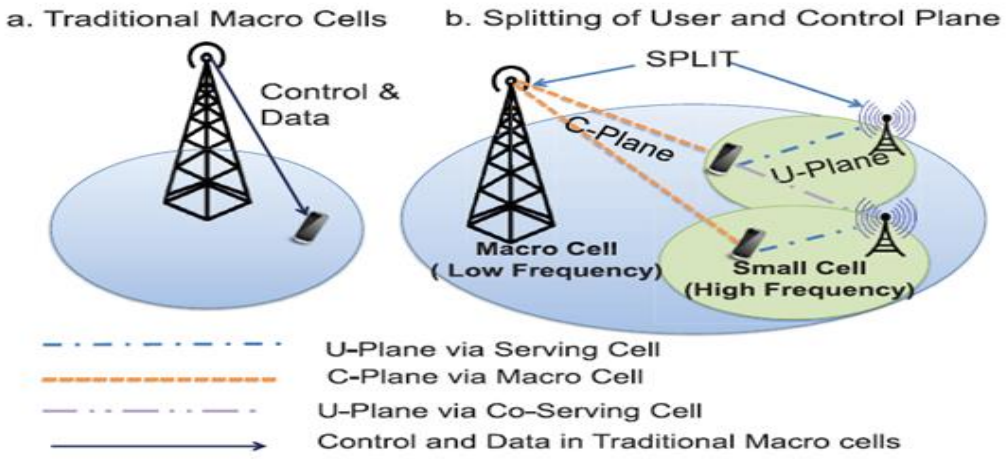

FIGURE 1-5. Control Plane and User Plane Separation [6]

The Open Systems Interconnection model (OSI model) modeled the data plane with a sensible layering, standardized by the International Organization for Standardization(ISO). The OSI model enables network applications and services to isolate the data operations to a single layer and provide interfaces between layers. Thus it seems, similar layering model is essentially needed for networks control and management plane, which was not available. This creates SDN architecture decouples control from data plane and provides it a new layering model. Open Networking Foundation (ONF) is a non-profit industry consortium which has taken the lead in standardizing critical elements for SDN architecture. One of these standards is Open Flow, which will be covered in the next section. SDN enables network slicing by providing the network with hyper-visor, while physically network is untouched). As, the hypervisor allows every individual controller to control only their own hosts (physical or virtual) on the network without affecting other parts of the network.

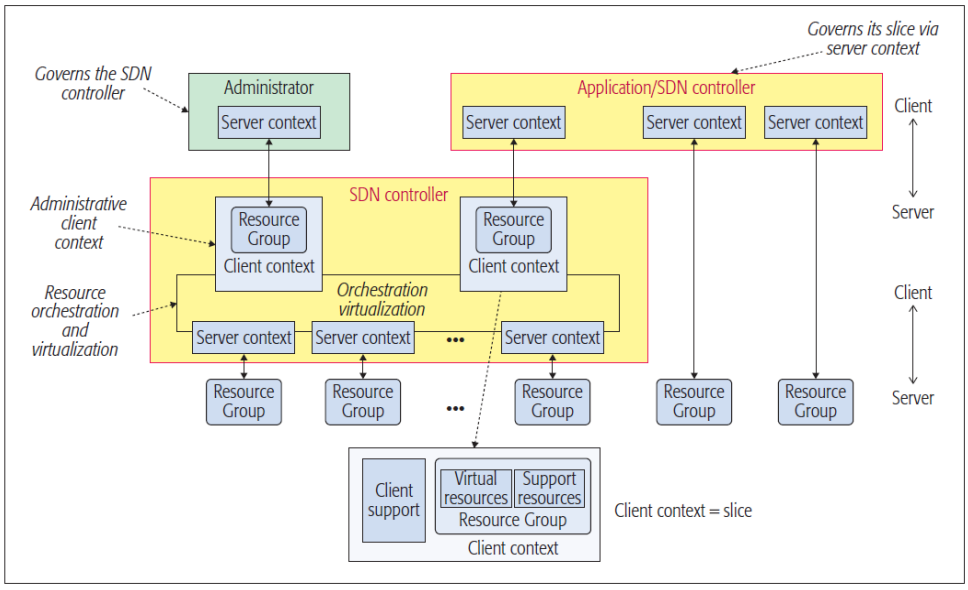

FIGURE 1-6. ONF SDN network slicing architecture [10]

As mentioned in the previous section, the communication between network devices and the controller is handled through the southbound API of the controller. As the most dominant networking technology is the Ethernet, the first standard for SDN was created to manage the controlling of Ethernet switches. Open Flow is a standardized (by ONF) protocol for SDN supported networks to handle the communication between Ethernet switches and the SDN controller as shown in Fig. 1-6. Open Flow was derived from SANE and Ethane, which were one of the first projects to decouple control and data plane. Open Flow shortly started to become more popular and as an open standard, it developed quickly to support more and more functionalities.

1.1.5 Network function virtualization

Network function virtualization (NFV) provides a new network architecture concept that depends on the virtualization of the network functions of a typical server by separating this locked-in functions from the hardware components and then gathering this separated functions to create communication services. The NFV architecture depends on three main components as shown in Fig. 1-7.

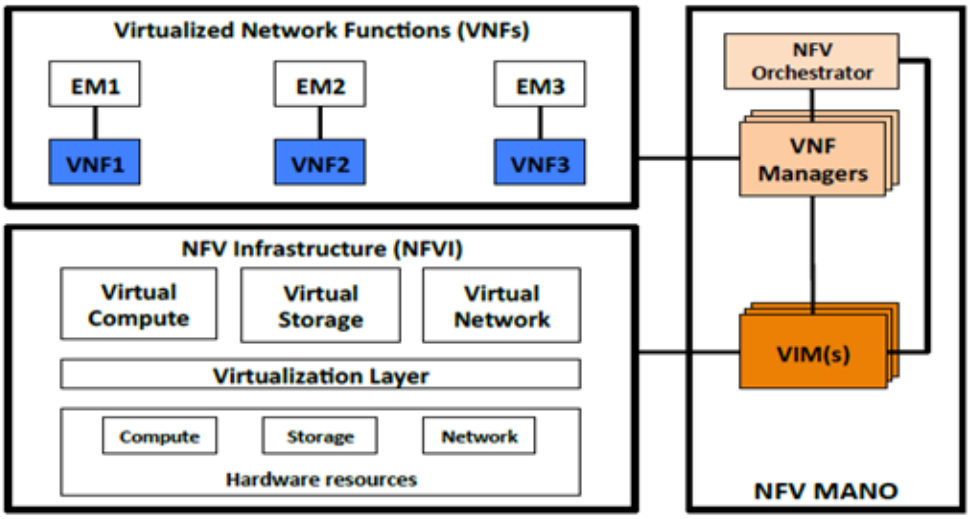

FIGURE 1-7. NFV architecture [10]

I. Virtualized Network Functions (VNFs) VNF are software network functions used to manage the network traffic based on specific network protocol and network topology on both virtual and physical resources. Moreover, the management functions for a specific VNF such as monitoring and configuring are performed by Element Management (EM)

II. NFV Infrastructure (NFVI) includes the hardware resources and the software components to manages access to physical resources. By producing a virtualization layer to create virtual resources on the available hardware.

III. Management and orchestration (MANO) The MANO is the main part of the NFV architecture as it manages the entire life-cycle of the architecture infrastructure by releasing and reallocating the resources using the virtualized infrastructure manager (VIM). and manages the legacy network management tools, interface and interact with the OSS and BSS by VNF managers. Moreover, it controls NFV Orchestrator and VNF Managers to manage physical and virtual resources in the NFVI using the Virtualized Infrastructure Managers (VIMs) [5].

1.1.6 Cloud Radio Access Network (C-RAN)

As mentioned before increasing the number of the network nodes complicates the control operations so the SDN and NFV are introduced to resolve some of the major problem associated with 5G network requirements. C-RAN architecture enables the 5G network to simply use SDN concept as it mainly based on fundamentals of decentralizing the data plane and virtualization. C-RAN consists of two main parts Base Band Unit (BBU) and Remote Radio Heads (RRH) as shown in Fig. 1-8. The base band resources are pooled at the BBU and allocated at a remote office which results in statistical multiplexing gains, energy efficient operations and cost reduction, while the RRH representing the transceiver components are distributed along the cell and connected to the BBU pool by different access technologies. C-RAN offers to improve system architecture by adding more flexibility to the system while reducing the cost of network deployment and operation [15].Moreover, the concept C-RAN is applied to the heterogeneous networks architecture producing heterogeneous Cloud Radio Access Network networks (HCRAN) architecture. In HCRAN we have HetNets composed of small cells and macro cells representing the RRH distributed among the cell area and connected to the BBU pool which performs the base band operations as shown in Fig. 1-8.

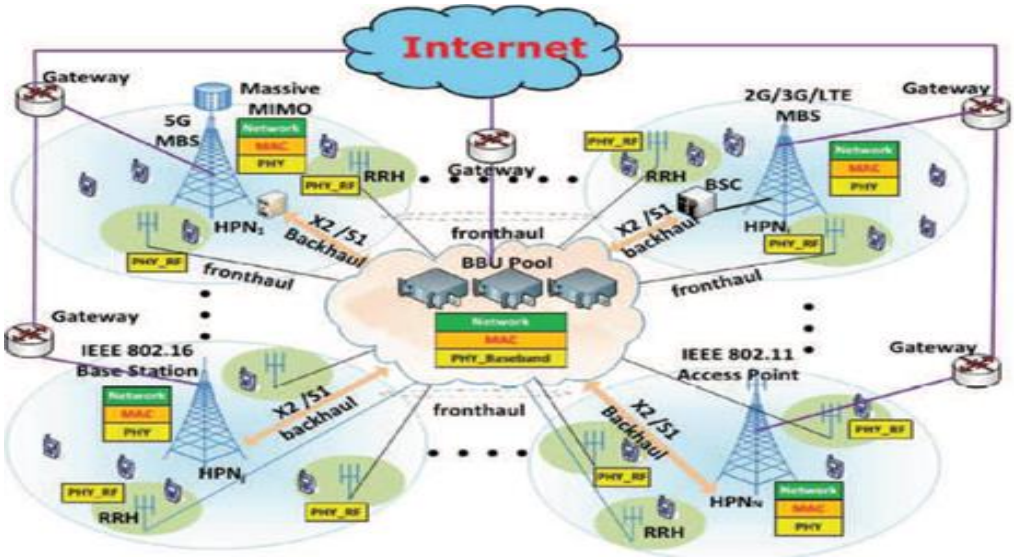

FIGURE 1-8. Heterogeneous Cloud Radio Access Network networks (HCRAN) architecture [13]

1.2 Scope and Structure of the Thesis

Throughout this thesis, we address optical modulation schemes, resource allocation and interference management for indoor (VLC) and outdoor (fronthaul) optical networks proposed by the 5G networks.

1.2.1 Optical Multicarrier Modulation

Firstly, bandwidth requirements, system cost, propagation delay and the computational complexity of the RRH, impose trade off to the design of the fronthaul transport network. This rises the development of the fronthaul transport network as a major challenge in 5G CRAN. Much research considered the optical network, amongst many wired and wireless technologies, as the best transport network for the 5G fronthaul transport network. As it offers good compromise between low latency and the high capacity, even though the compatibility between the optical fronthaul as a transport network and the radio networks must be carefully considered. On the physical layer level, the multi carrier modulation (MCM) techniques have been proved to have best spectral efficiency than the single carrier (SC) techniques. Among MCM techniques OFDM dominates the current 4G network, which enables the convergence of the optical infrastructure with existing wireless networks. These aspects proposed OFDM as a best candidate for 5G optical transport network. Nevertheless, it suffers from inter-symbol interference (ISI) and high peak to average to power ratio (PAPR). This motivates researchers to investigate alternative MCM technique addresses the drawbacks of the classical OFDM. Mainly MCM schemes can be classified on the structure level onto orthogonal, bi-orthogonal, and non-orthogonal.

A. Orthogonal schemes

They follow the matched filter techniques with orthogonal basis function which decreases spectral efficiency as in zero padding (ZP) OFDM which eliminates multipath effect by imposing guard interval between the OFDM symbols with rectangular basis function. We proposed an OFDM modulation scheme that deploys the artificial intelligence techniques (Deep Neural Networks, and Decision trees), that predict the clipped parts of the optical OFDM and overcome the tradeoff between the spectral and the power efficiency of the optical OFDM schemes .

B. Non orthogonal schemes (FBMC)

In the fronthaul network, optical transport network as stated above, optical direct detection OFDM/OQAM with RF sub bands split per user is an interesting scheme, with the interference reduction, and efficient bandwidth allocation per user. We proposed OFDM/OQAM (Filter Bank Multicarrier FBMC) on the front haul, which is compatible with optical OFDM benchmarks. The proposed algorithm overcomes the OFDM challenges as the high peak to average power ratio (PAPR) and the CP in the optical networks with high spectral efficiency.

1.2.2 Interference management schemes

A. Machine learning algorithms and energy saving scheme for transport optical fronthaul network (outdoor optical network)

Mainly 5G network topology is divided into two sub-networks the fronthaul and backhaul network as shown in Fig. 1-9 . The fronthaul network is defined as the transport network that communicating between the BBU and the RRH, while the backhaul network refers to portion of the network comprising the communication links between the core network and BBUs. Throughout this study we consider the fronthaul network and address its challenges as 5G fronthaul have high latency requirements for the transport network. Currently, the fronthaul latency budget does not exceed 30μs. We consider the modulation technique (as mentioned) and resource management schemes of the fronthaul 5G network as will be shown later. We applied orthogonal and non-orthogonal optical modulation for optical transport network that enhances the spectrum efficiency with reduced processing delay, efficiently assigns computational resources for each RRH with machine learning algorithm and finally proposes a power saving algorithm by switching off the underutilized RRH and BBU.

We will focus on the CRAN architecture challenges as the functional split between the RRH and BBU pool and the resource allocation between them. Different typologies of the function split, as providing the RRH more capabilities and increases its functionality, adds a challenge as it dramatically increases the data traffic between the RRH and BBU. Thus, it increases the complexity of the transport fronthaul network. On the other

hand, performing more functions in BBU, increase the latency of the network as it consumes much more time to support the end user. This adds a tradeoff that needs to be studied and handled. As more intelligence need to be added to the 5G network we are concerned about applying machine learning algorithm, that can adapt the allocation between the BBU pool and the RRH according to the network state. Such algorithm needs flexible network architecture.

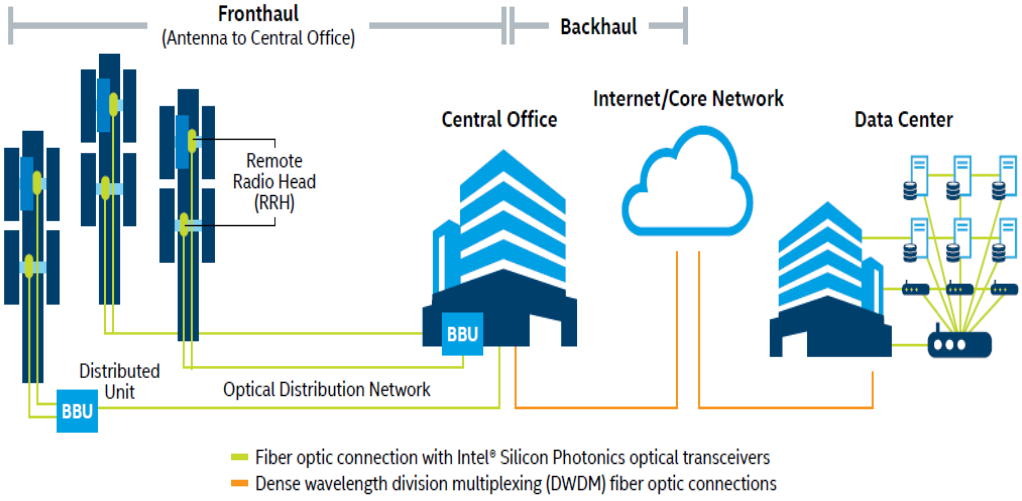

FIGURE 1-9. 5G fronthaul/backhaul network [16]

The problem of the power arises as a new challenge in the last few years, the 5G network must be a green network that saves power and consumes clean power sources. Switching off the RRH is proposed as a partner for saving network power. We are concerned about the energy efficiency challenge, as the proposed architecture supports sleep mode for some underutilized RRH and BBU that enables the green network.

B. Interference management for indoor visible light communication (Indoor optical network)

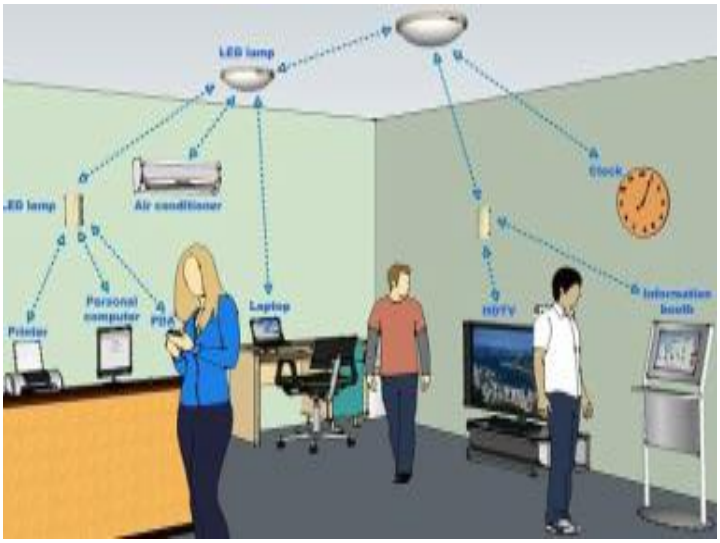

FIGURE 1-10. 5G fronthaul/backhaul network [16]

Secondly , visible light communication system (VLC) is an emerging optical wireless communication technology that is introduced to improve indoor coverage and provide high data rates. VLC is preferred over the radio frequency (RF) communications due to several benefits, including the broad unlicensed bandwidth, low-cost electronic devices, and the interference-less connections with the existing technologies.

For standalone VLC systems, the coverage areas of access points (AP) are overlapped to avoid dead zones, which causes co channel interference (CCI) at the user in the interference area (overlapping area). Hence, interference arises as a challenging problem in the VLC systems, so many interference management techniques have been investigated. We addressed the interference management in indoor optical network proposed by 5G networks (visible light communication scheme VLC). We propose an interference management technique that assigns different frequency band to the cell edge users to enhance the signal to interference plus noise ratio (SINR).

In VLC systems, the coverage area is divided into multiple atto-cells. In each atto-cell, multiple LED arrays are used as access points (APs) serving its assigned users. The coverage area of these APs might be overlapped to avoid the service discontinuity for mobile users. The overlapped zone causes co-channel interference (CCI). Hence, the

interference issue is raised in VLC systems. However, several interference management techniques are developed to overcome this issue.

A new shared frequency reuse (SFR) scheme combined with two resource allocation (RA) algorithms is proposed to minimize the interference and maximize the system throughput in the VLC system. The proposed static resource portioning technique that shows better performance than the unit frequency reuse (UFR) and the static fraction frequency reuse (FFR), although some dynamic FFR schemes shows better spectral efficiency it adds some complexities as frequent handover and computational complexity.

1.3 Dissemination of Results

The novel proposed techniques and schemes presented in this thesis have been disseminated through several research contributions.

The publication list includes: • [T]: Transaction paper • [J]: 2 journal papers. • [C]: 2 conference papers.

Also, we achieved **the best paper award** in OPJU International Technology Conference on Emerging Technologies for Sustainable Development (OTCON) , 2022.

PHASE I : Implement the OFDM/OQAM with different techniques for optical communication.	***Published paper:*** ***Journal paper*** A. *A. Ibrahim, J. Prat & T. Ismail "*Asymmetrical clipping optical filter bank multi-carrier modulation scheme*," Opt Quant Electron 53, 230 (2021).* ***Conference paper*** B. *A. Ibrahim, A. Elsheikh, A. Abdelsalam, J. Prat, "*Neural Network based Transceiver for Non-Coherent OFDM Optical Modulation *", 25th International Conference on Advanced Communication Technology Transactions (ICACT-TACT), 2022.* C. *A. Ibrahim, A. Elsheikh and J. Prat "*Non-Coherent Optical OFDM Transceiver based Machine learning : Regression Tree," *OPJU International*

	Technology Conference on Emerging Technologies for Sustainable Development (OTCON) , 2022. ***(Best Paper Award)***
PHASE II : Develop a resource allocation algorithm and interference management to be used in green CRAN based on Machine learning algorithms	***Submitted Paper (Transactions paper):*** *A. Ibrahim, A. Elsheikh and J. Prat "*Big data analysis and clustering based RRH-BBU Assignment for Green Communication Network,". *IEEE Transactions on Cognitive Communication and Networks.*
PHASE III : Indoor communication techniques	***Published paper (Journal paper):*** *A. Ibrahim, T. Ismail, K. F. Elsayed, S. M. Darweesh, and J. Prat,* "Resource Allocation and Interference Management Techniques for OFDM-Based VLC Atto-Cells*", IEEE access, vol. 8: IEEE, pp. 127431–127439, 2020.*

The thesis is organized as follows. In Chapter 2, the proposed orthogonal optical modulation using artificial intelligence techniques are introduced. The proposed non orthogonal optical modulation using FBMC are presented in chapter 3. Chapter 4 presents the interference management of indoor VLC network. The proposed resource allocation based big data analytics for green fronthaul network is introduced in Chapter 5. Finally, conclusions and future work are included in chapter 6.

Chapter 2 : Indoor Communication schemes in 5G networks : Artificial intelligent based Transceiver for Non-Coherent OFDM Optical Modulation

2.1 State of the art

2.1.1 Deep neural network-based scheme

Among many different access technologies, coherent and non-coherent optical communications are considered a perfect partner that bids unlicensed frequency, secured communications, and interfered less with the existing technologies [17]. Although non-coherent optical communication gained much attention in the last few years due to the simplicity in sending data using intensity modulation with direct detection (IM/DD), on the other hand, IM/DD imposes more requirements on the transmitted signal to have positive and real values [18]. Much research presented asymmetrical clipping optical OFDM (ACO-OFDM) and direct clipping optical OFDM (DCO-OFDM) as benchmarks techniques that accommodate real positive signal transmission.

Machine learning (ML) can play an essential role in 5G network as it has the potential to learn experienced scenarios and predict future scenarios with adaptation to the environmental fluctuations. The ML algorithms are mainly classified into three approaches, supervised, unsupervised, and reinforcement learning. As the understudy case is demonstrated as a prediction problem, the supervised learning algorithms are proposed as it can predict and classify outputs based on labelled data while generating a rule that maps the inputs to outputs. As supervised algorithms based on regression method estimate the relation between the response and the regressor values to predict one or more outputs. Recently Artificial intelligence (AI) has been deployed to provide solutions that face 5G challenges. In [19], the author proposes analytical and active ML techniques that can manage cell fault, where the fault management aims to optimize the error in the network as the cell outage. In the optical communications domain [20]

proposes a method of training and applying neural network that adaptively decode the modulation scheme of the optical camera communication. In [21] the author proposes an artificial neural network (ANN) that compensate the effect of linear and nonlinear impairments as Gaussian white noise, laser phase noise and nonlinear phase of coherent optical communication. In [22] an end-to-end optical modulation design based on deep learning is proposed, the proposed model considers pulse amplitude modulation (PAM) as base band single carrier modulation.

In this chapter we addressed the problem of predicting the clipped signal in multi-channel optical modulation (OOFDM), we describe the problem as a supervised regression problem in which the learner predicts the regressor clipped negative signal values using the response and the regressor values map obtained in the training phase. Our contribution can be concluded as We propose a deep neural network (DNN) with multiple hidden layer, and nonlinear activation function that fits the nonlinearity of the Fourier series clipping operation, The proposed model combines the power efficiency of the ACO-OFDM technique and the spectral efficiency of the DCO-OFDM.

2.1.2 Decision tree -based scheme

Scaling up and enhancing the network performance are suggested by the 5G evolutionary approach, as the 5G network must fit the massive number of served devices, increasing traffic volume and immense system throughput. The auspicious ultra-dense heterogeneous network (HetNet) architecture considered as the best candidate for the 5G network architecture, due to its heterogeneity in coverage areas along with the access technologies. HetNet proposed different cell sizes as Macro, Femto and Pico cells, that support different radio access technologies as infrared radio frequency, and optical transmission communication. For fronthaul connections, coherent and non-coherent optical communications have been recognized as promising partner among many different access technologies, as optical communications afford costless frequency, secured communications, and less interference with the existing technologies [24]. Over the last few years, much research acknowledges the non-coherent optical communication techniques due to its simplicity in transmitting data using intensity modulation with direct detection (IM/DD), although the IM/DD obliges the transmitted signal to have positive and real values [25]. Principally direct clipping optical OFDM (DCO-OFDM) adds DC component to diminish the negative values before clipping it; the added DC component significantly influences the bit error rate (BER) performance and the power efficiency of the DCO-OFDM. While asymmetrical clipping optical OFDM (ACO-OFDM) carries out hard clipping of the odd subcarriers'

negative values to zero whereas it leaves the even subcarriers unloaded to eliminate the clipping distortion, the unused subcarriers significantly reduce the spectral efficiency of the system [26],[27]. The multi-channel optical modulation problem has been proposed in much research, as in [26] the author proposed modulation technique based on separating the value and the sign by sending the absolute values and for indicating signs it merges labels in a cost-effective manner While, [28] presented a Mach–Zehnder modulator (MZM) for non-coherent optical OFDM over BPSK modulation, the proposed modulator uses to transmit Hermitian symmetry OFDM signals. Massive non coherent optical modulation techniques based on signal processing proposed in literature over the few last years. Different non coherent multi modulation techniques have been proposed to overcome the tradeoff between spectral and power efficiency as [27] presented power OFDM modulation, while we have proposed filter bank multicarrier (FBMC) as an alternative to the OOFDM [29] .

Over the past few years, the machine learning (ML) algorithms have been proposed to learn the experienced scenarios of the 5G networks and use environmental fluctuations to predict different scenarios [30]. Based on labeled data the ML algorithms proposed different classification and regression methods, that can predict binary and continuous outputs, respectively. As the understudy case is demonstrated as a multi output regression problem, we proposed different multi output regression methods that predicts the desired output based on supervised ML concept. As multi output regression methods based on supervised algorithms to predict the outputs map the relation between the response and the regressor values [25].

Recently Artificial intelligence (AI) has been deployed to overcome 5G challenges, as managing cell fault, analyzing real time mobile traffic data, etc. [30], [31] manages, collects, and analyzes real-time data, the author proposes ML algorithm that captures the traffic using the cellular provider's detail records. In [33] the author addressed the problem of the linear and nonlinear impairments in coherent optical modulation, as artificial neural network (ANN) is proposed to compensate the effect of nonlinear phase of coherent optical communication Gaussian white noise and the laser phase noise. The authors proposed an equalizer based on NN architecture for coherent OFDM optical modulation that shows robustness to DSP non linearities for up to 80 Gb/s system. In this paper, we propose an AI based optical non-coherent transceiver, that over comes the challenges of transmitting real positive values over optical transmitters. The AI module presented in this work depends on decision tree models, that predicts the clipped received signal to compensate and eliminate the clipping noise.

2.2 System model

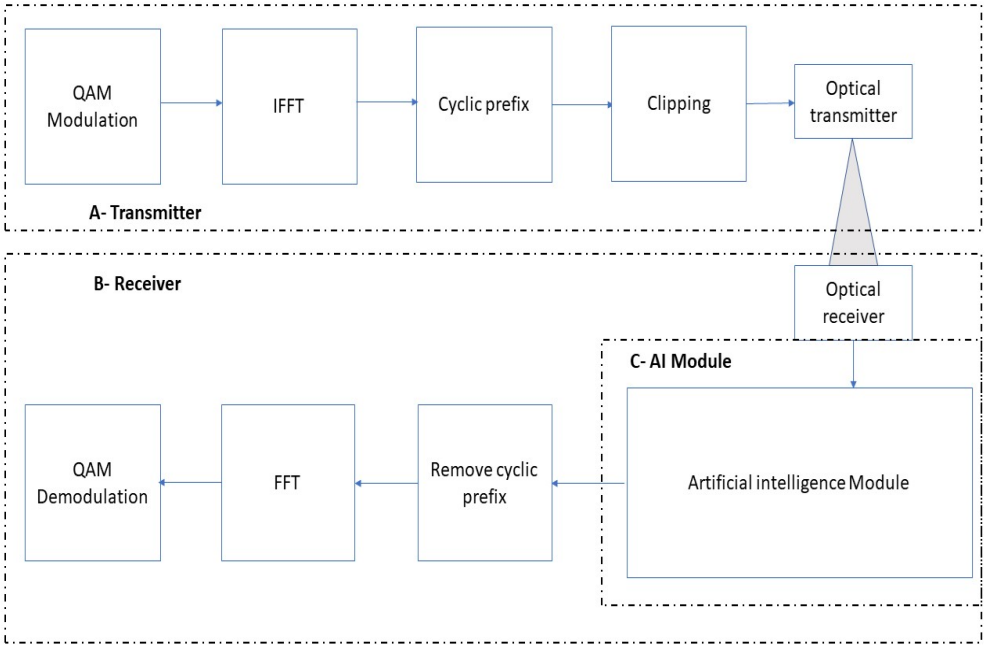

FIGURE 2-1. A- Noncoherent optical transmitter, B- Noncoherent optical receiver

In the section, we propose our system model that consists of three main modules transmitter, receiver, and the AI module. The block diagram of the proposed transceiver is shown in Fig. 2-1. The transmitter of the multi-channel optical modulation (MCM) technique is represented as the first block. The transmitter functionality is split into three parts. First, the transmitted bits are gathered as symbols using an arbitrary quadrature amplitude modulation technique (QAM). Then, these symbols are loaded to subcarriers with inverse Fourier transform operation. Finally, clipping the negative parts of the transmitted signal is performed to transmit it via an optical device. On the receiver side, the clipped received signal must be reconstructed as a bipolar signal by predicting the clipped part via AI module, that produces a bipolar signal from the transmitted unipolar signal. The predicted signal is then forwarded to the Fourier transform block to extract the data symbols from the received subcarriers and finally to the QAM demodulator to extract the received bitstream.

2.2.1 AI module: Deep neural network

The problem of predicting the clipped parts of the received signal is described as a multivariate regression model that involves multiple data variables for analysis. Multivariate regression identifies the relation between dependent and independent variables using the training data set. Linear, polynomial, and logistic regression models are commonly used models under supervised learning algorithms. According to Bussgang's theory clipping the negative parts of the Fourier series at the transmitter side is described as nonlinear operation at the receiver side. For the described problem, of predicting the clipped parts of the received subcarriers, the hard clipping of negative parts represents the nonlinear relationship between the clipped and unclipped subcarriers. According to this, we apply and compare the performance of polynomial regression model and neural network, representing logistic regression, to fit the nonlinear relation between the clipped signal representing the independent variables and the unclipped signal representing the dependent variable. Single-layer neural network (NN) with nonlinear activation function is considered a direct representation of the nonlinear regression model. As fully connected NN with single hidden layer applies a nonlinear operation to the weighted sum of the inputs according to Eq. (2.1).

$$y_j = f\left(\sum_{i=1}^{n} w_{i,j}\, x_i + b\right) \tag{2.1}$$

Where $w_{i,j}$ is the weight of each input i with neuron j, x_i is the activation inputs, y_j is the activation output, and b is the biasing of the hidden layer [20]. Deep neural network (DNN) with multiple hidden layers, are commonly used recently due to their learning capabilities and enhanced extraction, as DNN offers received signal learning hierarchy by forwarding the extracted signal from the first layers to preceding layers, and finally combines the highest-level signal to single object at the output layer.

2.2.2 AI module: Decision regression tree

We described the prediction of the received subcarriers values as multi output regression problem. Multi output regression, also known as multi variate regression, aims to identify the relation between multiple dependent and independent variables using the labeled data set for training. Multi output regression methods also utilize the prediction operation with simpler models in terms of the computational complexity. In

literature multi output regression can be classified into three main categories problem transformation methods, algorithm adaptation methods and multitask learning.

A. Problem transformation methods

Problem transformation methods depend on dividing the multi output regression problem into independent single output problems, each is solved separately using traditional regression solutions. The algorithm builds different model for each target to map the relation of each output (independent variables) and the inputs. Different methods have been proposed to solve multi output regressors as regressor chain [36] and multi output support vector machine [37]. The main drawback of these methods is ignoring the relations between multiple regressors during the prediction process.

B. Algorithm Adaptation Method

In these methods all the regressor values are determined using single model, this model maps the relation between all the inputs and every output. Moreover, it maps the relation between all the outputs themselves. The most popular algorithm adaptation methods are the SVM and multi target regression tree. Adapted versions of SVM have been proposed in literature to add the relation between all the outputs to the problem transformation model. While multi target regression tree model (MRT) is type of regression trees that can predict continuous multiple outputs.

C. Multitask Learning Method

Multitask learning methods are special type of the multioutput regression problem, as it models different tasks and identifies similarities between jointly trained tasks. Unlike the traditional multivariate regression methods, the MTL use different data sets for the training phase.

The MRT dominates other algorithm adaptation methods as it offers better identification for the dependencies between the different targets. The predictive performance of the regression trees can be improved based on the tree ensemble algorithm. The ensemble methods create different learners, the consequence ensembled multiple learner system enhances the base learner by defining the behavior of the local differences. Enormous methods have been proposed for the multiple learner construction, based on varying the training data subset, varying the training parameter,

or using totally different learning algorithms. The common approaches depend on different training sets are the boosting and bagging. Where, bagging generates multiple bootstrapped training sets with different stochastic distributions and performs equal weight voting over single learner. While, boosting changes the training sets based on the performance of the previously trained learner and uses the weighted voting algorithm [35]. The problem of predicting the unclipped subcarriers is formulated as in Equ. (2.1). We previously proposed the neural network architecture [38] to predict the clipped subcarriers as shown in Fig. 2-1. Hardware limitations on implementing the complex NN motivated this research to find simpler AI architecture in terms of hardware implementation and provide good predictivity performance. We propose the multioutput regression trees to predict the received subcarriers with accepted hardware framework.

$$Net_{trained} = F(\{Y_1 , \dots \dots Y_n | X_1 , \dots \dots X_n\}) \quad (2.2)$$

$$[\hat{Y}_1 , \dots \dots \hat{Y}_n] = Net_{trained}(Y_1 , \dots \dots Y_n) \quad (2.3)$$

were $\hat{Y}_i$represent the multi target predicted N received subcarriers, Y_i represent the N clipped subcarriers and X_1 unclipped subcarriers for training phase. During the training phase the AI module maps the relation between the clipped and the target unclipped subcarriers. The mapped function $Net_{trained}$, described in Equ. (2.2), is then called to predict the received clipped subcarriers during the transmission.

2.3 Design aspects and experimental configuration

2.3.1 Deep neural network

A. Neural network hyper parameters

The parameters of NN have a tremendous influence on the network performance as network size in terms of number of hidden layers and the size of each layer influences the network prediction efficiency. This adds tradeoff between the network design and the performance, as small networks do not bid good performance and large networks may have redundant connections on the other hand. [39], [40], [41] proposed different optimization algorithms for tuning NN hyper parameter in terms of number of hidden layers and the size of each.

I. Hidden layer size

The size of each hidden layer is defined by the number neurons in each layer, much research studied the effect of the hidden layer size on the NN performance [42],[43]. The hidden layer size has a tremendous influence on the NN performance. Using few numbers of neurons in each hidden layer causes underfitting, while increasing the number of neurons cause overfitting for the training data. As shown in Fig. 2-2, the BER and the MSE are enhanced with increasing the number of neural nodes in the hidden layer till the optimum point and it decreases again. However, the curve turning point of the proposed model is 256 neural nodes in each hidden layer, we considered 128 neural nodes as our optimum point as it bids near optimum performance with much less complexity. As 128 neural node architecture has BER of 6*10-3 and 256 architectures have BER of 4*10-3.

II. Number of hidden layers

Generally, NN architecture with input and output layers and no hidden layer solves linear regression problems, while single hidden layer NN architecture can fit any Boolean function regardless the input space [44]. Increasing the number of hidden layers to one and two layers offers good fitting to the nonlinear, additional layer can be added based on the complexity of the proposed regression model [45]. We tested the proposed model over multiple hidden layer architecture, due to the complexity of the understudy problem the architecture of three hidden layers shows the better performance over single and double hidden layers architecture in terms of BER and MSE. Increasing the number of hidden layers decrease the performance due to the overfitting problem, as shown in Fig. 2-3.

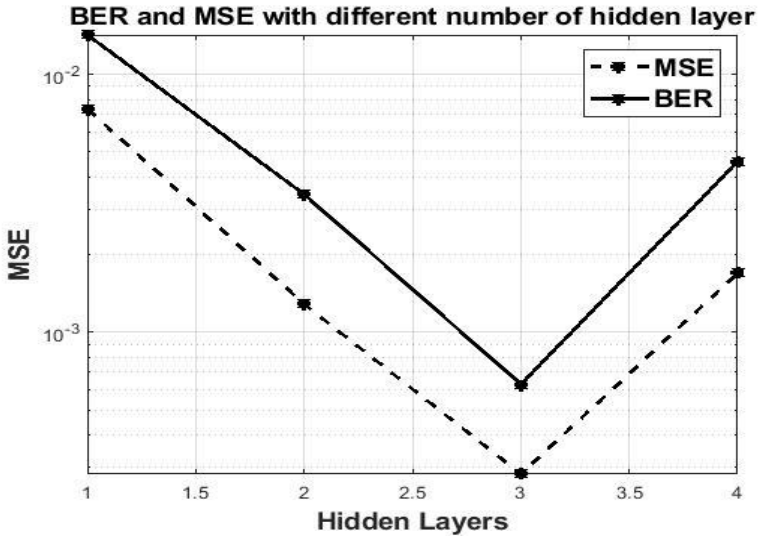

FIGURE 2-2. BER and MSE with different number of hidden layers, all the hidden layers have the same number of neural nodes. The proposed architecture has 128 Neural nodes in each layer, PRELU activation function, 4 QAM modulation and 16 subcarriers.

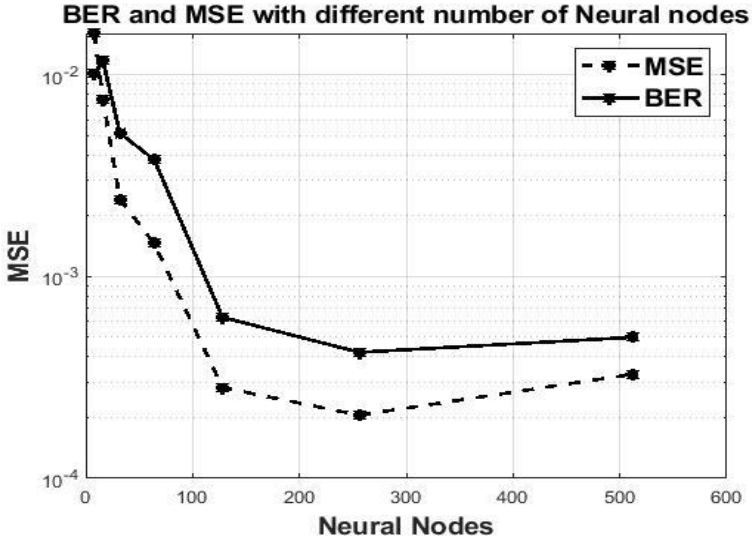

FIGURE 2-3. BER and MSE with different number of neural nodes in each hidden layer, all the hidden layers have the same number of neural nodes. The proposed architecture has 3 hidden layers, PReLU activation function, 4 QAM modulation and 16 subcarriers.

III. Activation function

Various nonlinear activation functions add nonlinearity to the DNN, as the conventional nonlinear functions sigmoid, hyperbolic tangent (tanh), rectified linear unit (ReLU). Recently variate versions of ReLU have been proposed as leaky ReLU (LReLU) [46] and parametric ReLU (PReLU) [47]. Although tanh and sigmoid activation functions are the most popular for nonlinear applications, they show poor performance in our study. On the other hand, the PReLU shows good performance as it satisfies the linearity for positive input parts and nonlinearity for negative parts, as shown in Fig. 2-4.

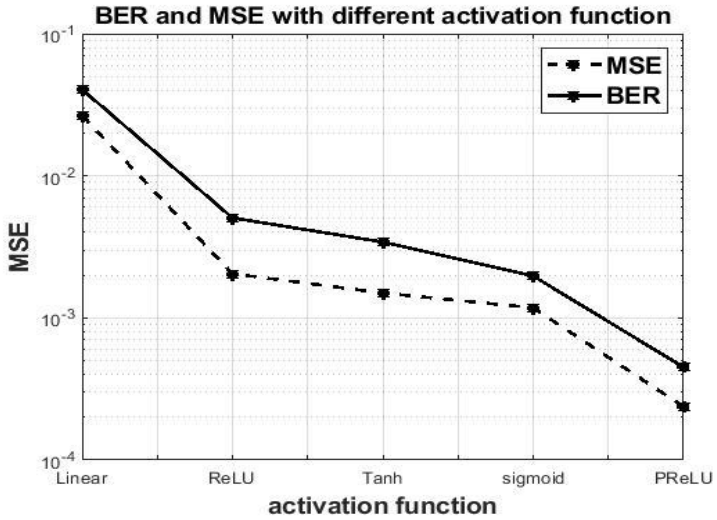

FIGURE 2-4. BER and MSE with different linear and nonlinear activation functions. The proposed architecture has 3 hidden layers, 128 neural nodes in each hidden layer, 4 QAM modulation and 16 subcarriers.

B. Communication system Parameters

In this section we proposed the effect of the communication system parameters on the system performance. We studied the effect of the modulation order, subcarrier spacing.

I. Modulation order

As increasing the modulation order decreases the decision boundaries between each pair of symbols on the constellation diagram, consequently increasing the inter symbol interference. Although the modulation order does not effect on the NN mean

square error, as it is an end-to-end transmission aspect, it effects on the received symbol BER. Fig. 2-5 shows the BER performance of the proposed architecture under 4 ,8 ,16, and 32 QAM. As shown, increasing the modulation order decrease the system BER as discussed, although it increases the system spectral efficiency on the other hand.

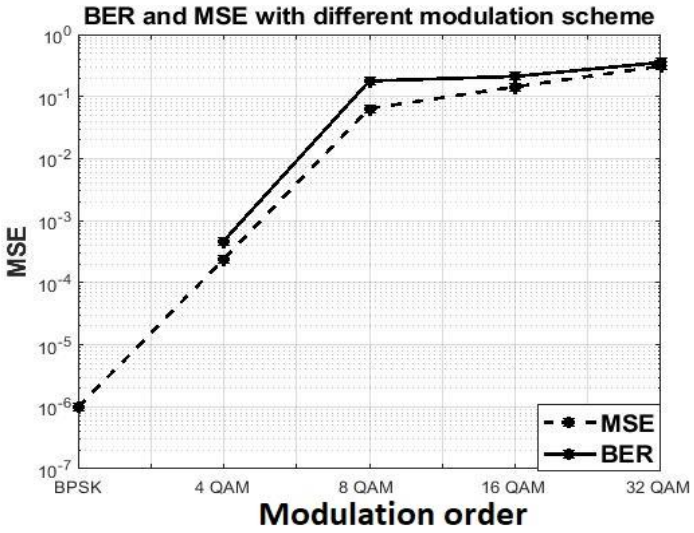

FIGURE 2-5. BER and MSE with BER performance with 3 hidden layers, 128 neural nodes in each hidden layer, 4 QAM modulation and 16 subcarriers.

II. Subcarrier spacing

In multi-channel modulation scheme, as OFDM, the channel is divided into multiple subcarriers. The subcarrier spacing represents the reciprocal of the symbol time, so narrow subcarrier spacing causes better channel equalization and robustness. Although decreasing subcarrier spacing increases the number of subchannels. This imposes more complexity to the NN architecture as it increases the number of dependent and independent regressors represent the received clipped signal and the predicted clipped signals, respectively. This tradeoff in choosing the subcarrier spacing adds challenge to designing the transceiver system. We tested our system over different subcarrier spacing. Fig. 2-6 shows the BER performance and MSE of the NN respectively, we run this simulation over the same NN architecture

in terms of activation function, number of hidden layers and neurons in each layer. Decreasing the subcarrier will increase the size of the input and output layer, this requires increasing the size of the hidden layers to efficiently extract features in each layer and forward it to higher layers. As shown Increasing the input layer size over constant hidden layer size will dramatically impact on the performance of the NN and the end-to-end performance. Consequently, the MSE and the BER performance decreases with decreasing the subcarrier spacing.

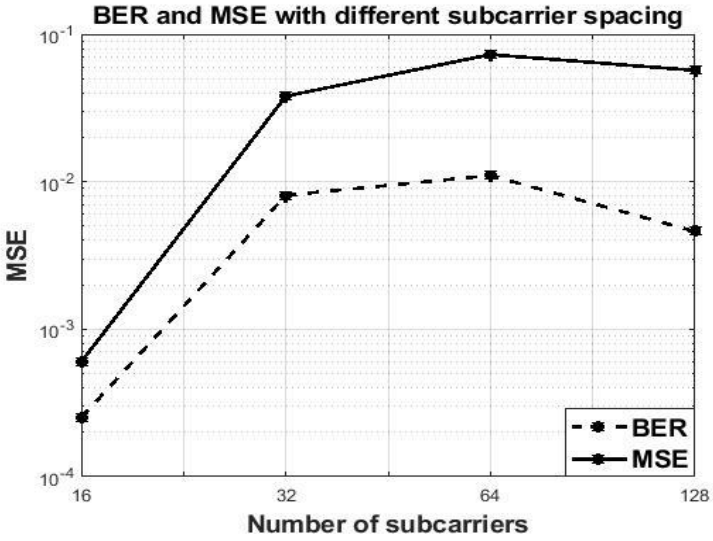

FIGURE 2-6. BER and MSE with different subcarrier spacing.

C. Training processing time

In this section we analyze the training processing time of different DNN architecture. The DNN architecture aspects as the number of hidden layers and the number of neural nodes. We compared the training processing time on AMD PRO A10-8700B R6, 10 compute cores 4C+6G 1.8 GHZ processor with 16 GB RAM and 64-bit operating system. As shown in Fig. 2-7 increasing the number of hidden layers and the neural node in each layer increases the complexity of the network and increases the training phase processing time.

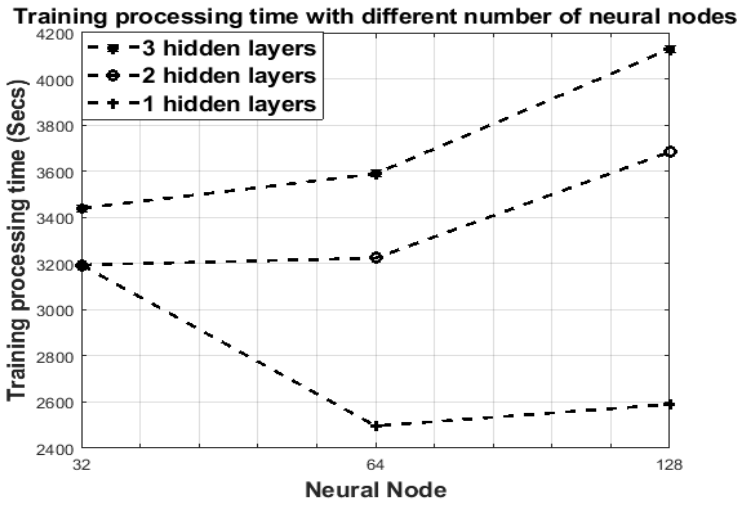

FIGURE 2-7. Training processing time with different number of hidden layers and neural nodes.

2.3.2 Decision tree

In this section, first we introduce comparison between the proposed trained algorithm and the benchmarks optical OFDM in terms of BER performance over additive white Gaussian noise (AWGN). Then, we discuss the hardware implementation possibilities of the proposed transceiver.

A. Simulation parameters

All the simulations were done with 10,000 training validation samples, with 90 percent as training samples. While 100,000 samples were used for testing the system. Over TensorFlow [48] as project interpreter with Keras library [49] for machine learning algorithms, Pandas library [50] for representing data frames analysis and Scikit - Commpy library [51] for representing digital communication techniques.

B. Communication system parameters

As mentioned in [34] the subcarrier spacing, and the modulation order highly influence the performance of the optical transceiver. Fig. 2-8 shows the BER performance of the proposed architecture under 4 ,8 ,16,

and 32 QAM. As shown, increasing the modulation order decrease the system BER as discussed, on the other hand it increases the system spectral efficiency. In the proposed transceiver the prediction operation adds another dimension of increasing the inter symbol interference, as the prediction error increases the added noise. As a result, the BER of the proposed transceiver is dramatically affected by increasing the modulation order as shown in Fig. 2-8. As shown for low modulation order as BPSK and 4 QAM the RDT shows excellent prediction, while increasing the modulation order increases the noise and decreases the BER.

Fig. 2-9 shows the BER performance of the NN and DT respectively, we run this simulation over the same NN architecture in terms of activation function, number of hidden layers and neurons in each layer. Decreasing the subcarrier increases the size of the input and output layer, this requires increasing the size of the hidden layers to efficiently extract features in each layer and forward it to higher layers. For the RDT, decreasing the subcarrier spacing increases the number of the subchannels, regressors and the responses of the regression operation, this increases the computational complexity due to increasing the number of inputs and the outputs. The number of the DT increases as the number of the predicted targets increases. Moreover, the arithmetic operation in each tree increases as the number of the regressors increases with low predictivity. As shown in Fig. 2-9 the BER of NN shows better performance than the DT for high subcarrier spacing.

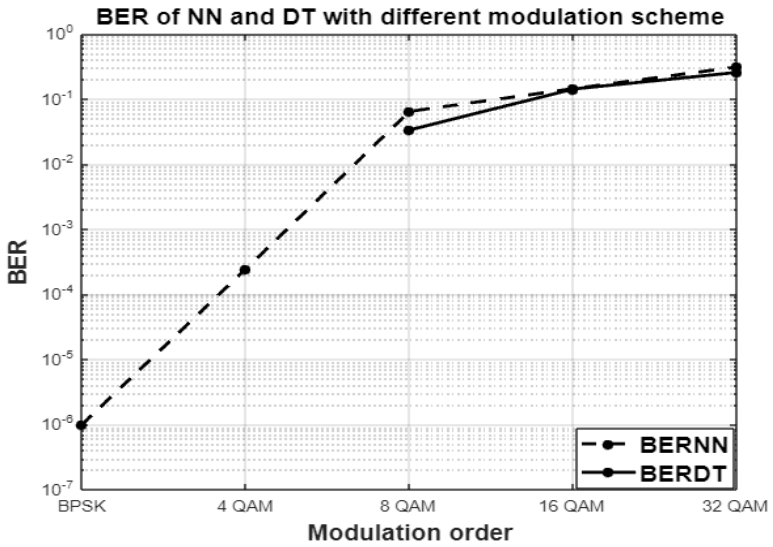

FIGURE 2-8. BER performance with different modulation order of neural network has 3 hidden layers, 128 neural nodes in each hidden layer, and decision tree.

C. ACO, DCO- OFDM versus DNN and RDT algorithm

ACO and DCO-OFDM introduce a tradeoff between the spectral efficiency and the power efficiency of the optical transmission. The ACO_OFDM interleaves the even subcarriers to compensate the clipping noise, whereas the DCO-OFDM dramatically increases the BER of the received signal due to adding DC component to the transmitted signal. On the other hand, the proposed model depends on predicting the clipped negative parts by the trained DNN. The trained network shows better performance in terms of spectral and power efficiency of the optical transmission. Although it adds computational and hardware complexity due to the training phase and the AI module in the transceiver.

As shown in Fig. 2-10 the proposed model enhances the BER of the DCO-OFDM. Moreover, it compensates the clipping noise by loading the data on all the subcarriers and predicting the clipped parts via AI module. This results on doubling the spectral efficiency of the ACO-OFDM. While the regression tree perfectly eliminates the clipping noise

the used modulation scheme as shown in Fig. 2-10, as it shows perfect symbol detection with no BER.

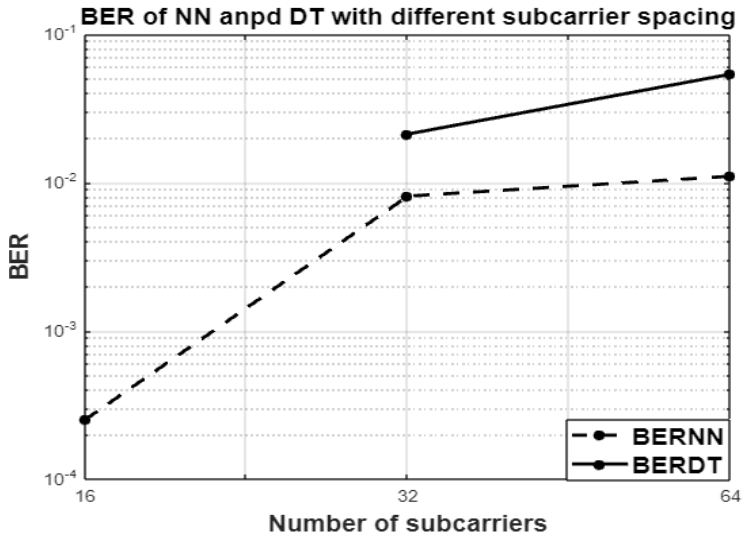

FIGURE 2-9. BER performance with different subcarrier spacing 4QAM modulation of neural network has 3 hidden layers, 128 neural nodes in each hidden layer, and decision tree.

D. Hardware implementation

As the concept of SDN raised in 5G network, the software defined network (SDR) implementation of the system transceiver is highly motivated. The SDR of the communication systems have three approaches field programmable gate array (FPGA), embedded digital signal processor (DSP), and general-purpose processor (GPP). Traditionally the OFDM transceiver is implemented on FPGA as a programmable hardware module, as it offers cost efficient , and high flexibility. On the other side, the AI module hardware implementation on FPGA has been recently proposed as it offers parallel and high-speed designs [52], [53], [54]. Despite these features more research need to be investigated to offer various implementation of different AI architecture as neural networks and regression decision tree. We propose GPP architecture as it provides easier and flexible programmable platform, that implements both the AI and the communication transceiver efficiently. Raspberry pi 4 board is deployed in the workstation as GPP

to implement the proposed transceiver. As the RPI module is based on ARM processor with relatively low capabilities CPU and very capable GPU that enhances the processing speed. The proposed transceiver is implemented considering wired communications to eliminate wireless communication noise, as the RDT is trained in noiseless environment.

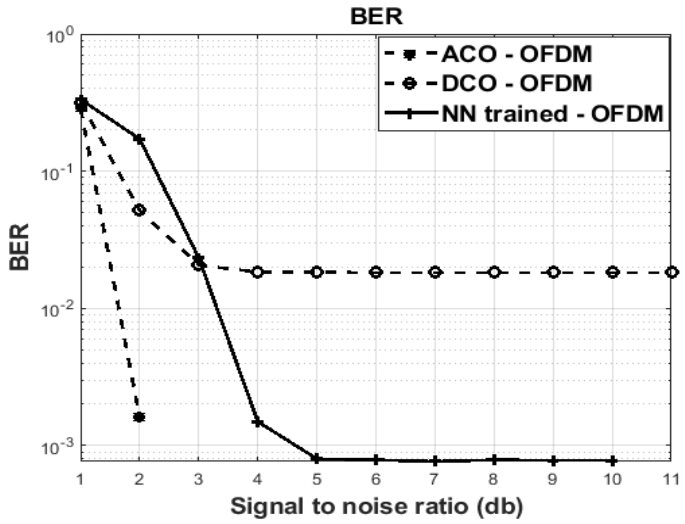

FIGURE 2-10. BER of DCO, ACO-OFDM and the proposed modulation scheme over additive white Gaussian noise channel (AWGN). The proposed architecture has 3 hidden layers, 128 neural nodes in each hidden layer, PReLU activation function and 16 subcarriers.

Chapter 3 : Indoor Communication schemes in 5G networks

(Asymmetrical Clipping Optical Filter Bank Multi-Carrier Modulation Scheme)

3.1 State of the art

In this chapter, we investigate the physical layer of 5G networks challenges, such as bandwidth requirements, system costs, spread delay, and computational complexity of the remote radio heads (RRHs) that become trade-offs on the design process of the front-line transport network. To achieve this network flexibility, the cloud radio access network (CRAN) has been introduced, as it offers a solution by decentralizing the data plane and virtualize the network function. In CRAN architecture, the baseband function is pooled at the baseband unit (BBU) and allocated at the remote central office. Simultaneously, RRH, which represents the transceiver components, is distributed along with the cell, and connected to the BBU pool. In C-RAN, the fronthaul links such as optical fibers, free-space optic or mmWave that connect the BBU and RRH suffer from the capacity, latency, and level of intelligence of the network. This increases the development of wireless transport as a significant challenge for 5G network design. Many research types have identified the optical network as the best transport network for the 5G front-haul transport network, among many wired and wireless technologies. It offers a good compromise between low latency and high capacity even though the compatibility between the optical fronthaul as a transport network and the radio networks has to be carefully considered [56][57].

The multi-carrier modulation (MCM) techniques have been proved to have better spectral efficiency than the single carrier (SC) techniques on the physical layer level. Among MCM techniques, Orthogonal frequency division multiplexing (OFDM) dominates the current 4G network, enabling the convergence of the optical infrastructure with existing wireless networks [58]. These aspects proposed OFDM as the best candidate for the 5G optical transport network. Nevertheless, it suffers from inter-symbol interference (ISI) and a high peak to the average to power ratio (PAPR). This motivates researchers to investigate alternative MCM technique addresses the drawbacks of the classical OFDM. Mainly MCM schemes can be classified at the structure level as MCM schemes can be categorized at the structural level into ”orthogonal,” ”biorthogonal,” and ”non-orthogonal structures.” Orthogonal patterns

that adopt matched filter techniques with orthogonal base functions reduce spectral efficiency in OFDM zero padding (ZP). This eliminates the multipath effect by imposing a guard interval between OFDM symbols with a rectangular base function. Bi-orthogonal patterns are represented by an orthogonal base function on both sides, which contradicts the matched filter approach as the Cyclic Prefix (CP) OFDM. It causes a more extended rectangular shape base function on the transmitter of the attached data. Finally, this analysis will incorporate non-orthogonal schemes that will be introduced throughout this chapter.

In the front-haul network, the optical transport network, as mentioned above, the optical detection of OFDM/OQAM with RF sub bands separated by the user is a promising scheme. It reduces interference and efficiently allocates bandwidth per user [59]. In the subject matter, presently, we are looking into OFDM/OQAM (Filter Bank Multi-carrier (FBMC)) for the front haul and studying its compatibility with the optical OFDM benchmarks. Our goal is to address the challenges of OFDM, including the high peak-to-average power ratio (PAPR) and the CP that occurs within optical networks with high spectral efficiency. The main contribution of this work is the first development, to the best of our knowledge, of the asymmetric clipping optical transceiver FBMC based on the Fast Fourier Transform (FFT). However, the authors use DC optical filter bank multi-carrier (DCO-FBMC in [60]. Their system is affected by the computational complexity of the corresponding filtering scheme and the high clipping noise. We also introduced an orthogonal dimension other than FBMC for RF systems. We then proposed spatial orthogonality between adjacent frames using odd indexed and even indexed asymmetrical optical clipping (ACO-FBMC). We modelled and eliminated the interframe clipping distortion using the iterative method on the receiver side.

3.2 System model

In this section, we illustrate the ACO-FBMC system model, as the transmitter and the design of the receiver are precisely proposed.

3.2.1 OQAM-FBMC

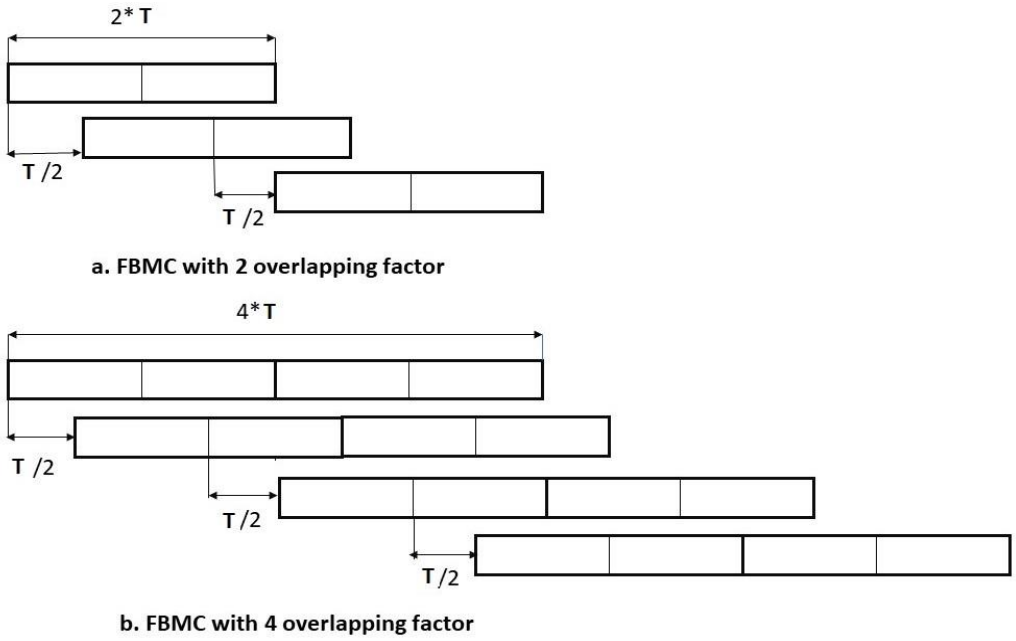

FIGURE 3-1.: OQAM-FBMC frames with 2 and 4 overlap factors.

The general form of the OQAM-FBMC frames is shown in Fig. 3-1. The discrete baseband time OQAM signal can be written as

$$x(t) = \sum_{k=-\infty}^{\infty} \sum_{l=0}^{L-1} p_{l,k}(t) * X_{l,k} \tag{3.1}$$

where Xl,k is the transmitted M-ary QAM signal at subcarrier l and time k, pl,k is the transmitted basis function where

$$p_{l,k} = p(t - KT) * e^{j2\pi lF(t-kT)} * e^{j\theta_{l,k}} \tag{3.2}$$

where F is the frequency and time k, unlike the OFDM, the OQAM system loses the complex orthogonality. Hence, the complex symbol's real and imaginary parts have to be separated into two frames [62].

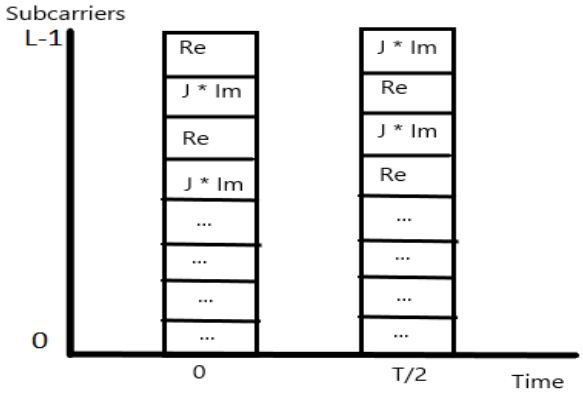

Figure 3-2: OQAM-FBMC subcarriers

IFFT Implementation of the FBMC system has been proposed in recent research as an efficient implementation. In [61], the author proposed an IFFT implementation based on the overlap and add the scheme to shape each subcarrier of the OFDM symbol. In this technique the phase $\theta l,k$ is chosen to be $(\pi/2)(l + k)$. Based on this implementation, the FBMC procedure will first perform IFFT for the QAM modulated symbols. Secondly, this frame will be repeated based on an arbitrary overlap factor O, representing the number of multicarrier symbols that overlap in the time domain, as shown in Fig. 3-2. Finally, the prototype filter is modified in combination with the repeated filter to reshape the FBMC frame subcarriers.

In OQAM-FBMC, multiple frames separated by the T/2- time shift send simultaneously. Implicitly, the first frame is carried by the real component, whereas the second frame is carried by the imaginary component of the transmitted signal, representing the phase orthogonality between the concurrently transmitted frames.

3.2.2 Transmitter design

The block diagram of the ACO-FBMC transmitter is shown in Fig. 3-3, where the quadrature and in-phase components are processed separately and combined into

an OQAM-FBMC symbol. The transmitter functionality is broken down into three main parts. First, OQAM is pre-processed, then combines the FBMC with the ACO scheme and, finally, clips the two components and transmits the shifted versions.

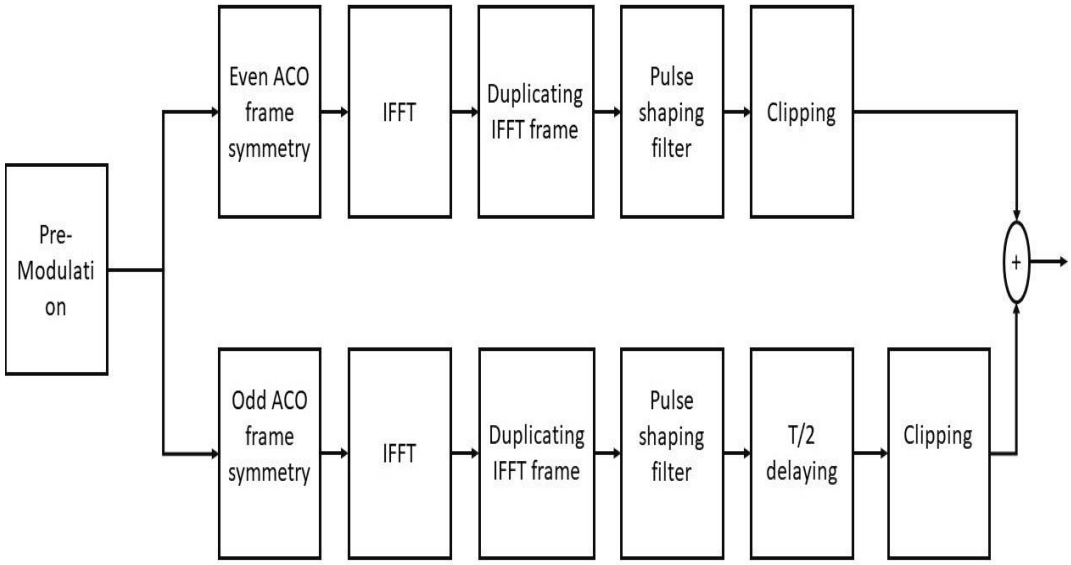

FIGURE 3-3. OQAM-FBMC Transmitter

The typical bipolar OFDM signal modifies to be sent over intensity modulation with direct detection (IM/DD) optical system in the optical domain. As in IM/DD systems, the transmitted signal is modulated and carried by the optical carrier's intensity. Accordingly, this requires the optically transmitted signal to be pure real and positive valued. Many types of research over the past decade addressed this challenge and introduced the unipolar OFDM schemes. Several optical OFDM techniques have been developed as the direct current (DC) biased optical OFDM (DCO-OFDM) [63][65], the asymmetrically clipped optical OFDM (ACO-OFDM) [64][65]. These schemes are based on generating real baseband OFDM signal by enforcing the input signal to have Hermitian symmetry. In the DCO system, a DC component is appended to the real signal to produce a real positive valued signal, and then it is clipped to eliminate the negative parts. The added DC value is a challenge in the DCO system as it highly reduces the power efficiency of the DCO-OFDM scheme. In [60], DCO-FBMC has been proposed along with FBMC transceiver based on the matched filtering

process. This system with a complex FBMC transmitter suffers from computational complexity and high clipping noise from eliminating negative parts. On the other hand, the ACO schemes are based on utilizing only the odd subcarriers and adding zeros on the even subcarriers. It has been shown that even subcarriers carry the clipping distortion [63]. The ACO-OFDM has high power efficiency and low spectral efficiency as only the odd subcarriers carry the data. Therefore, its spectral efficiency is half of the DCO-OFDM. The ACO-FBMC, dissimilar to the OQAM-FBMC, carries all the data on the only real component of the transmitted data. The clipping distortion affects the imaginary component of all transmitted subcarriers. Alternatively, another dimension of orthogonality must be added to send multiple shifted frames simultaneously. We propose a subcarrier orthogonality scheme to be implemented to ensure the orthogonality between the two components of the OQAM signal transmitted. In each frame sequence, the first frame will be sent over an odd indexed ACO according to (3), as shown in Fig. 3-4.

$$\begin{aligned} X\left(\frac{L}{2}+i+1\right) &= X\left(\frac{L}{2}-i+1\right) \quad \text{for odd } i \\ X(i) &= 0 \qquad\qquad\qquad\quad \text{for even } i \end{aligned} \tag{3.3}$$

Furthermore, the second frame will be sent over even indexed ACO according to Equ. 3.4 as shown in Fig. 3-5.

$$\begin{aligned} X\left(\frac{L}{2}+i+1\right) &= X\left(\frac{L}{2}-i+1\right) \quad \text{for odd } i \\ X(i) &= 0 \qquad\qquad\qquad\quad \text{for even } i \end{aligned} \tag{3.4}$$

Mapping the ACO scheme to the FBMC system discussed above produces the frames structures shown in Fig. 3-6. This structure verifies Hermitian symmetry, real output signal as both Frames are pure imaginary, and finally, it satisfies the OQAM-FBMC frame structure. Negative parts of the OFDM output frame will be clipped and transmitted over the optical device.

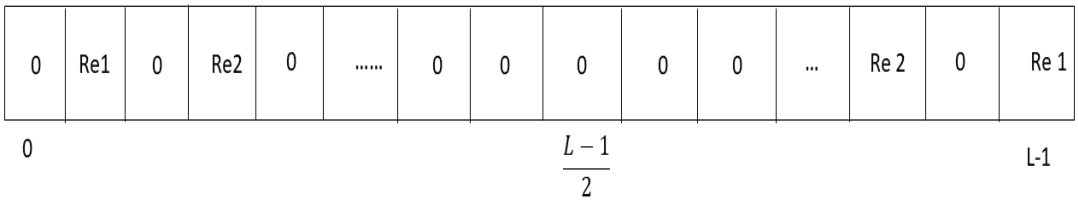

FIGURE 3-4. Odd Indexed ACO frames.

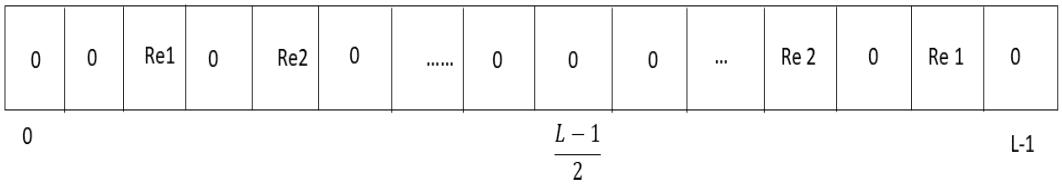

FIGURE 3-5. Even Indexed ACO frames.

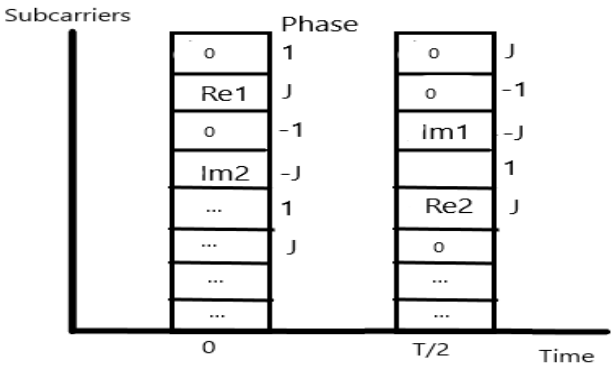

FIGURE 3-6. ACO-FBMC frames.

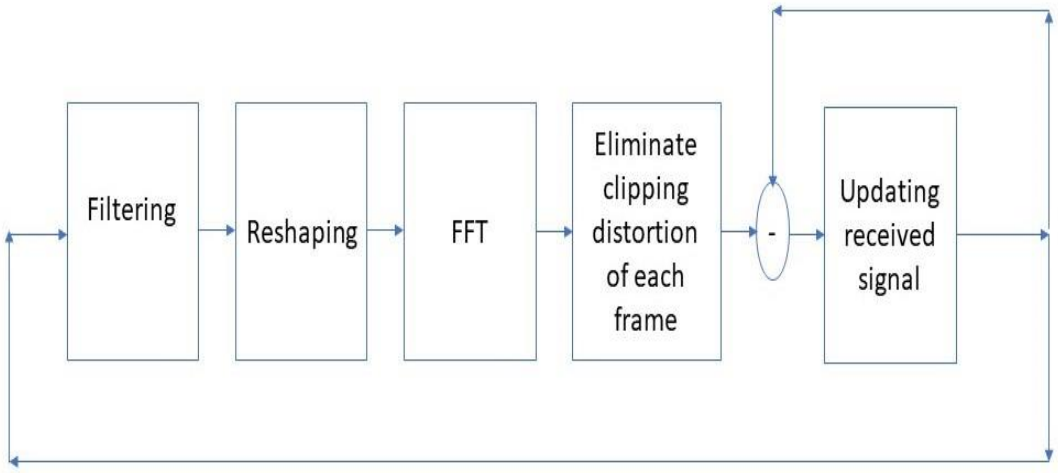

FIGURE 3-7. OQAM-FBMC Receiver

3.2.3 Receiver design

At the receiver shown in Fig. 3-7, the received signal is divided into windows, each of which is multiplied by a filter and reshaped to multiple segments with the size T × O, where T is the symbol duration, and O is the overlapping factor then FFT on the first window to produce the first received frame. Partially eliminating inter-frame interference is represented by regenerating the transmitted signal by performing IFFT on the first received frame to be subtracted from the total received frame. This process is repeated until the last frame has been detected. These received frames are used in iterative manner to eliminate all the clipping distortion. Fig. 3-8 shows the receiver procedure.

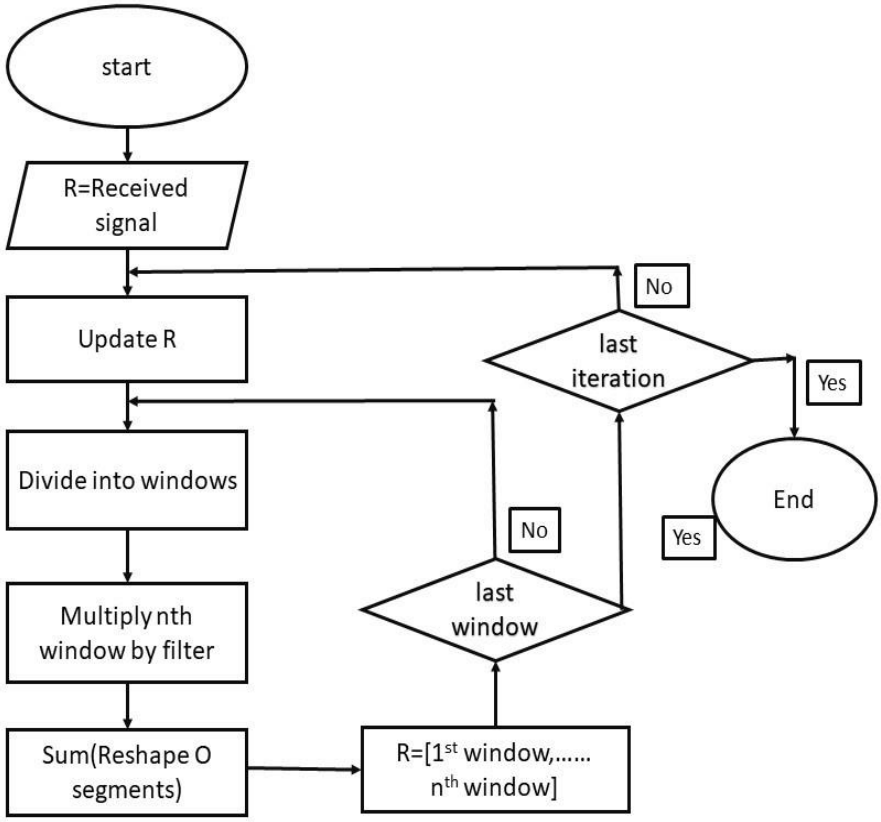

FIGURE 3-8.: The receiver procedure flow chart

3.3 Simulations and results

This section shows the simulation results of the ACO-FBMC signal transmission. The total number of subcarriers is set at L = 32. All simulations were performed on Matlab based on Monte Carlo simulations with 10, 000 in iterations. In each iteration, the system transmits 8 frames, each separated by T2 , where T is the duration of the frame. In the first place, the clipping distorted by the receiver is measured by transmitting and detecting signals over the flat channel. As shown in Fig. 3-9, the signal

received after the second iteration of the distortion cancelation has better performance than the signal obtained after the first iteration.

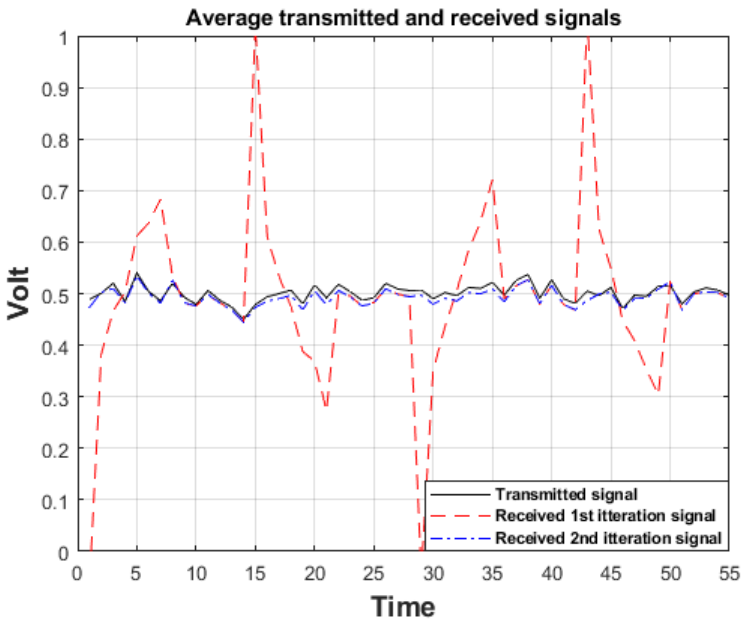

FIGURE 3-9. Average transmitted and received signals.

Secondly, the BER performance of the ACO-FBMC scheme over additive white Gaussian noise (AWGN) is studied using Hermit [66], [67] and PHYDYAS [68] filter, as shown in Fig. 3-10. The hermit filter shows better BER performance by only 0.5 db. Fig. 3-11 shows the bit error rate (BER) of ACO-FBMC frames with an overlapping factor of 8 and the ACO-OFDM. As shown, the FBMC enhances the BER performance by 4 dB over the ACO-OFDM scheme as the filter bank shapes the transmitted signal as perfectly rectangular and eliminates the out of band emission. Furthermore, it enhances spectral efficiency due to CP cancellation.

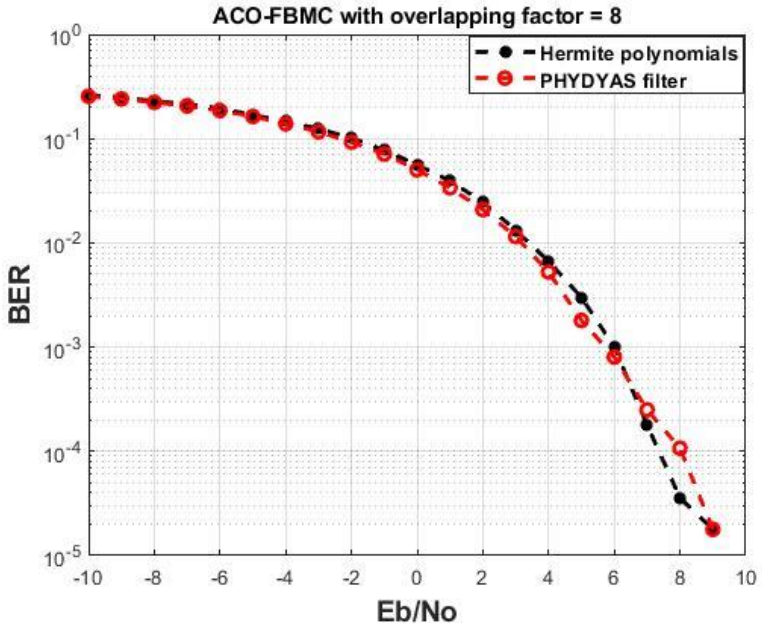

FIGURE 3-10. BER of ACO-FBMC Hermit and PHYDYAS filter

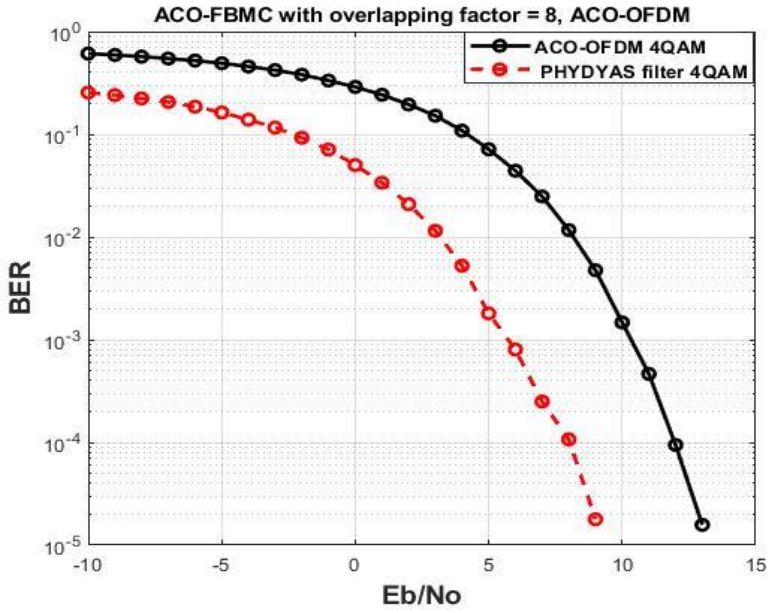

FIGURE 3-11. : BER of ACO-FBMC with 8 overlapping factor and ACO- OFDM

Fig. 3-12 shows the overlapping factor on the BER performance as the overlapping factor of 8 presents the BER performance, as the overlapping factor O characterizes the filter bank and gives different filter windows [69]. Increasing the overlapping factor narrows the filter window and increases the robustness to the inter-frame interference, enhancing the BER performance. On the other hand, it increases system complexity.

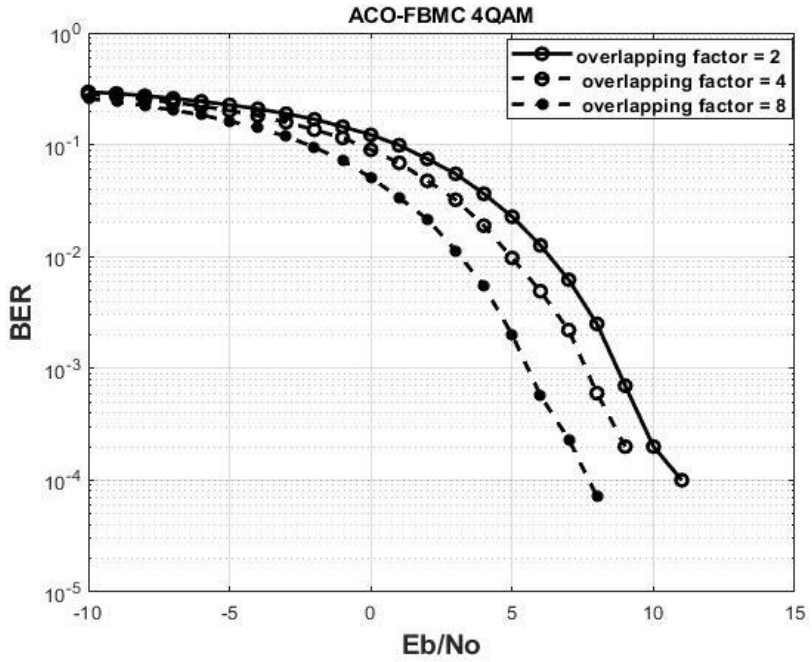

FIGURE 3-12. BER of ACO-FBMC with 2,4,8 overlapping factor

Chapter 4 : Resource Allocation and Interference Management Techniques for OFDM-Based VLC Atto-Cells

4.1 State of the art

A visible light communication system (VLC) is an emerging optical wireless communication technology that is introduced to improve indoor coverage and provide high data rates. VLC has preferred over the radio frequency (RF) communications due to several benefits, including the broad unlicensed bandwidth, low-cost electronic devices, and the interference-less connections with the existing technologies [71]. In the VLC system, the transmitted signal is modulated on the intensity or the phase of the optical transmitter. However, intensity modulation (IM) is considered as the most suitable technique for the VLC system due to its simplicity. On the receiver side, the received intensity-modulated signal is demodulated by the optical detector using direct detection (DD) technique. The optical detector generates an electrical signal proportional to the intensity of the received signal [70].

Optical wireless communication using LED as a transmitter, known as VLC, have been deployed for intelligent transport system and smart home networks [72]. VLC using LED offers low cost optical wireless communications [73]. Orthogonal frequency division multiplexing (OFDM) has been proposed as the most spectrally efficient technique that provides a high data rate and significantly improves the system capacity due to its robustness to the multipath fading [74]. A VLC system using a white LED as a communication source requires a real unipolar signal, so optical OFDM techniques have been introduced as asymmetrically clipped optical OFDM (ACO-OFDM), DC-biased optical OFDM (DCO-OFDM) [75], asymmetrically clipped DC-biased optical OFDM (ADO-OFDM) [76] and odd clipped optical OFDM (OCO-OFDM) [77]. In DCO-OFDM, Hermitian symmetry is imposed on all the subcarriers that carry the data, which produces a real bipolar signal, then DC offset is added to get the unipolar signal. While in ACO-OFDM and ADO-OFDM, only the odd subcarriers carry the data to satisfy Hermitian symmetry. However, ADO-OFDM is more optically power-efficient than conventional ACO-OFDM and DCO-OFDM [75][78]. In OCO-OFDM, Hermitian symmetry is replaced by odd symmetry of Fourier transform, which enhances its spectral efficiency for the real-modulation technique as OCO-OFDM uses

pure imaginary odd input signal to produce pure real odd output. The oddness of the output signal adds an advantage to the clipped signal, such that clipping odd real signals do not affect its amplitude, and the distortion is added on the imaginary part of the subcarrier only.

In VLC systems, the coverage area is divided into multiple atto-cells. In each atto-cell, multiple LED arrays are used as access points (APs) serving its assigned users. The coverage area of these APs might be overlapped to avoid the service discontinuity for mobile users. The overlapped zone causes co-channel interference (CCI). Hence, the interference issue is raised in VLC systems. However, several interference management techniques are developed to overcome this issue. In [79], traditional unity-frequency-reuse (UFR) is proposed, and the interference is mitigated using RF technology in the overlapped area. In [80], the authors introduce a static-resource-partitioning technique, which uses different frequencies in the adjacent cells to eliminate the interference. The static resource partitioning technique effectively eliminates the CCI at the cost of reducing the spectral efficiency. Furthermore, the interference-aware resource partitioning is investigated in [81], which depends on broadcasting a busy burst (BB) from the user intending to receive data in the next time slot. The BB adds extra complexity, but it enhances spectral efficiency. In [82], different approach of FFR is introduced as a cost-effective technique that achieves reasonable spectral efficiency with low complexity. This technique depends on assigning different frequency bands to the cell-edge users to mitigate the CCI and using the full frequency band for the cell-center user. However, frequent handovers are the main drawback of this technique.

In contrast, [83] suggested dynamic FFR splitting the cell region into two virtual classes rather than separating the users of the cells. Each cell had a supergroup covering all cell areas and a regular group covering the cell area by dividing it into three sectors. The Radio Network Controller (RNC) dynamically assigns different subcarriers to each group and its users based on the SINR of that subcarrier and based on the fairness between its users. Super and regular subcarrier groups serve both center and edge users in the entire area and the sector. In [84], the authors suggested that the dynamic strict FFR would depend on the spatial scheduling of channels that would eliminate interference. The cell is dynamically divided into sectors, unlike the strict static FFR, which divides it into three static sectors. The Joint Scheduler is used to assign channels, divide the cells into sectors, and select the best modulation and coding regime. The authors in [85] suggested FFR optical dynamics that interact with the interference graph in neighboring cells. This interference graph links all interfered access points and used dynamic FFR to increase spectral efficiency in each subgraph.

Alternative optical dynamic FFR based on bidirectional double tabu list tabu search and interference graph that analyzes the potential interference between users is proposed in [86] .The author reached the optimal dynamic scheme by combining the interference graph and the bidirectional search. A static and dynamic multicolor scheduler was proposed in [87]. The authors presented a static scheduler that assigns a different color to each cell edge to mitigate ICI and dynamic color assignment based on linear programming and greedy color assignment to improve cell-edge throughput. Also, the authors in [88] proposed interference mitigation in the colored VLC cell, which assigns users to each AP based on the minimum distance principle and assigns a channel based on the weighted user graph to mitigate the ICI and improve the network throughput.

In this chapter, a new shared frequency reuse (SFR) scheme combined with two resource allocation (RA) algorithms is proposed to minimize the interference and maximize the system throughput in the VLC system. The proposed scheme and resource allocation algorithms are applied over different OFDM techniques in a VLC system. The simulation results show that the proposed scheme and algorithms improved the signal-to-interference and noise ratio (SINR), total system throughput, and the outage probability. Furthermore, the resource allocation algorithms satisfy the demand rates with small computational complexity compared to the fixed-rate and max-min fairness algorithm, which are proposed in [89] and [90], respectively.

The contributions are listed as follows : We proposed a static resource portioning technique that shows better performance than the UFR and the static FFR, although some dynamic FFR schemes show better spectral efficiency it adds some complexities as frequent handover and computational complexity. We adapted our optimized resource allocation algorithm proposed in [89] and the max min fair algorithm [90] to suit the multi cell optical OFDM system in both interference area and the cell area. Finally, we compared the proposed interference management under different modulation and resource allocation schemes.

4.2 System model

In this section, a system model of the optical atto-cell is presented. This model represents the downlink, which consists of one AP acting as a transmitter and multiple receivers. The AP could serve several users according to its power, available capacity, and coverage area.

4.2.1 Indoor channel gain

The downlink channel between the AP and the user equipment (UE) is considered as a flat channel like a DC channel gain with considering the line-of-sight (LOS) path only and neglects the shadowing and non-line of sight (NLOS) transmission [89].

$$G = \frac{(m+1)A_{pd}}{2\pi d^2}\cos(\varphi)^m T_S(\omega) g_c(\omega)\cos(\omega) \tag{4.1}$$

where m denotes the Lambertian emission order which is given by:

$$m = \frac{-\ln(2)}{\ln\left(\cos\left(\varphi_{1/2}\right)\right)} \tag{4.2}$$

where $\varphi_{1/2}$ is the angle at which the radiated power reduces to half its value. T_S is the optical filter gain, and g_c is the concentrator gain, it is given by:

$$g_c(\omega) = \begin{cases} \dfrac{n^2}{\sin(FOV)^2} & 0 < \omega < FOV \\ 0 & \omega > FOV \end{cases} \tag{4.3}$$

The FOV of the receiver can be adjusted to control the coverage area of each AP. The proposed model uses several AP to cover an entire region. A user can communicate with at least one AP, as shown in Fig. 4-1, where ψ is the receiver angle of UE at the cell edge, r is the cell radius, R is the distance between AP and UE, and h is the distance between the plane containing the UE and the ceiling. We introduce a condition on the receiver's FOV that minimizes the interference area between the cells while keeping no dead zones. Thus, the FOV should be higher than the receiver angle of UE at the cell edge ψ, where ψ is given by:

$$\boldsymbol{\psi = \tan^{-1}\left(\frac{R}{h}\right)} \tag{4.4}$$

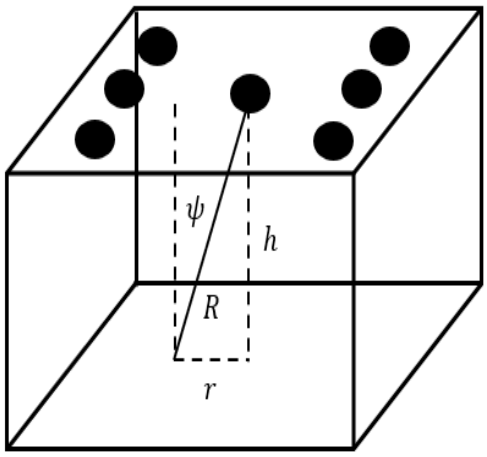

FIGURE 4-1. AP deployment in the simulated room

4.2.2 Optical OFDM Modulation and Multiple Access

Intensity modulation with direct detection (IM/DD) technique has been proved to be the most suitable technique for indoor VLC systems due to its simplicity and the low-cost end devices since the IM/DD technique is a real value unipolar signal.

In the DCO-OFDM shown in Fig. 4-2 (a), Hermitian symmetry is applied on the frequency domain OFDM frame X[k] before the inverse fast Fourier transform (IFFT) operation [75]. The Hermitian symmetry requires:

$$X[k] = X\,[N-k] \tag{4.5}$$

$$X[0] = X\left[\frac{N}{2}\right] = 0 \tag{4.6}$$

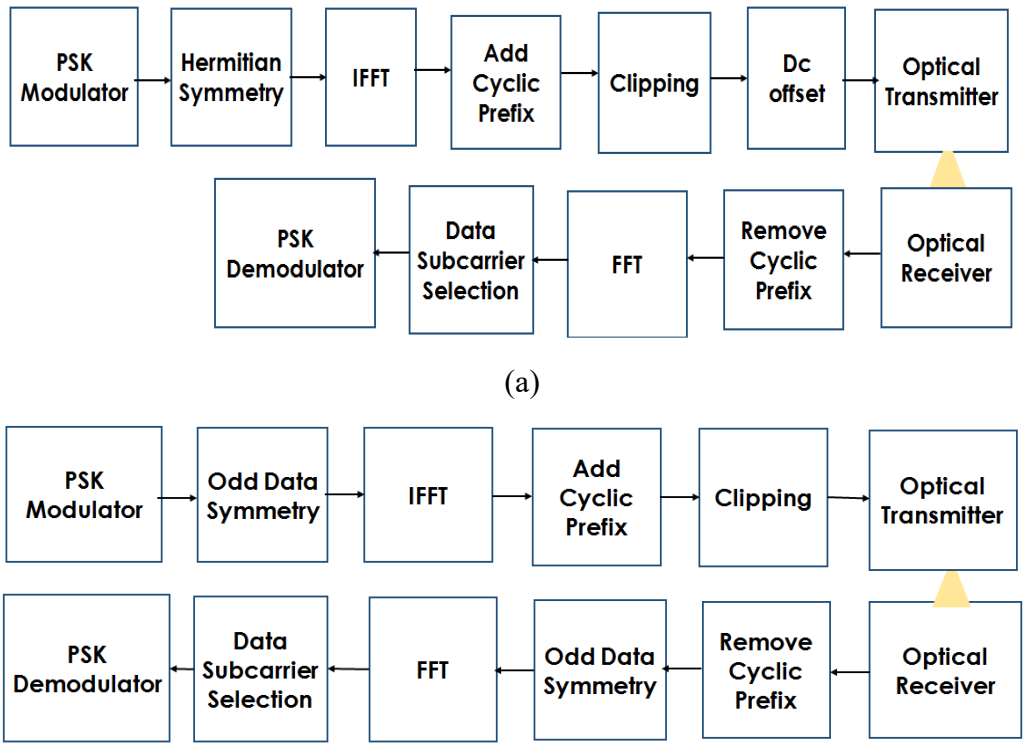

FIGURE 4-2. (a) DCO (b) OCO Modulation Techniques

In the DCO-OFDM shown in Fig. 4-2 (a), Hermitian symmetry is applied on the frequency domain OFDM frame X[k] before the inverse fast Fourier transform (IFFT) operation [75]. The Hermitian symmetry requires:

$$X[k] = X\,[N-k] \tag{4.5}$$

$$X[0] = X\left[\frac{N}{2}\right] = 0 \tag{4.6}$$

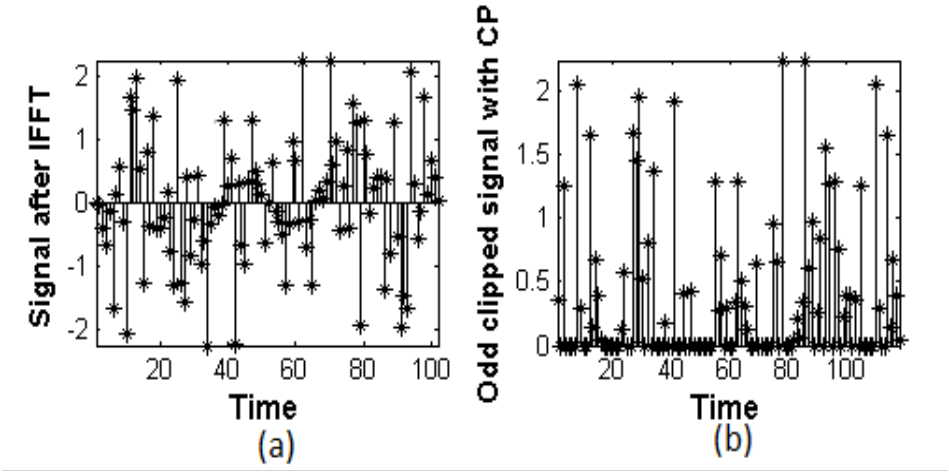

FIGURE 4-3. (a) unclipped signal (b) OCO clipped signal

The DCO-OFDM signal is made positive by adding a DC bias and after the IFFT is given by:

$$X'(t) = X(t) + DC_{\text{offset}} \tag{4.7}$$

The DCO-OFDM has relatively high spectral efficiency as all subcarriers carry information. However, it has a low power efficiency as the optical (P_{opt}) to electrical (P_{elec}) power conversion γ is affected by the DC_{offset} and given by [91][92]:

$$P_{\text{elec}} = \frac{P_{\text{opt}}^2}{\gamma^2} \tag{4.8}$$

In OCO-OFDM technique shown in Fig. 4-2 (b), a real unipolar signal is produced by applying odd symmetry on the frequency domain OFDM frame before the IFFT operation [77]. The odd symmetry requires that:

$$\boldsymbol{X[k] = -X[N-k]} \tag{4.9}$$

After the IFFT and clipping circuit, the unipolar signal can be generated which is represented as:

$$\boldsymbol{X_C(n)} = \begin{cases} \boldsymbol{X(n)} & \boldsymbol{X(n) > 0} \\ \boldsymbol{0} & \boldsymbol{X(n) < 0} \end{cases} \tag{4.10}$$

As can be seen, the clipping distortion does not affect the unipolar real information carried by the subcarrier [92].

$$\boldsymbol{P_{elec} = \pi * P_{opt}^2} \tag{4.11}$$

4.2.3 Performance Metrics

A. Signal to Interference and Noise Ratio (SINR)

SINR for user k in AP u is given by:

$$\mathrm{SINR}_{k,u} = \frac{R_{pd}^2 \; {G_{k.u}}^2 P_{\mathrm{elec}}}{\sum_{i=1.i!=u}^{i=AP} R_{pd}^2 \; {G_{k.i}}^2 P_{\mathrm{elec}} + N_o \, B_T} \tag{4.12}$$

where N_o is the noise spectral density, R_{pd} is the photodector and B_T is the system bandwidth.

B. *System Throughput*

A system throughput is defined as the sum of all rates that are required by the users. These required rates are computed bounded by the Shannon-Hartley formula. The total rate (R) is defined as the sum of the K user's rates and it is given by [81].

$$\boldsymbol{R = \rho * \sum_{k=1}^{K} N_K * B \; * \log_2(1 + P_{Kn} * g_k)} \tag{4.13}$$

where B is the bandwidth of a sub-carrier, ρ is the capacity utilization, g_k is the DC optical channel gain for user k and P_{Kn} is the power assigned for user k on subcarrier n.

C. The Outage Probability of the System

The outage probability of a system is the likelihood of the SNR being below the threshold SINR_{th} and it denoted as:

$$\boldsymbol{P_{outage} = P_r(SINR < SINR_{th})} \tag{4.14}$$

This is an example for writing thesis in word This is an example for writing thesis in word This is an example for writing thesis in word This is an example for writing thesis in word This is an example for writing thesis in word This is an example for writing thesis in word This is an example for writing thesis in word This is an example for writing thesis in word.

4.3 Resource allocation and interference management

In this section, we introduce a radio resource allocation algorithm that provides reasonable high capacity while satisfying the user rate requirements for the indoor VLC system. Then, we propose a shared-band interference management algorithm that compromises the performance of the UFR and the PFR algorithms.

4.3.1 Resource Partitioning Technique

A resource partitioning technique is proposed to resolve the inter-carrier interference (ICI) problem at the cell edge. In this technique, the covered area is partitioned into two regions, non-overlapped and overlapped. The whole band is distributed between the two regions. The reused band (N_{reused}) is assigned to the non-overlapped region and the shared band (N_{shared}) is reserved for overlapped region as shown in Fig. 4-4. The shared band is separated to small, dedicated bands N_1, N_2, N_3 and N_4 and distributed on AP_1, AP_2, AP_3 and AP_4, respectively. In this design, the maximum capacity of the system is given by:

$$\boldsymbol{C_{\max} = B_T \left[\frac{M N_{\text{reused}} + N_{\text{shared}}}{N_{\text{total}}} \right]} \tag{4.15}$$

where M is the number of APs. The shared band affects the outage probability as well as the overall system throughput. When this band is increased, the outage probability and the system throughput are decreased, and vice versa. Thus, a radio resource allocation algorithm is proposed to determine the optimal value of the shared band to provide better system efficiency.

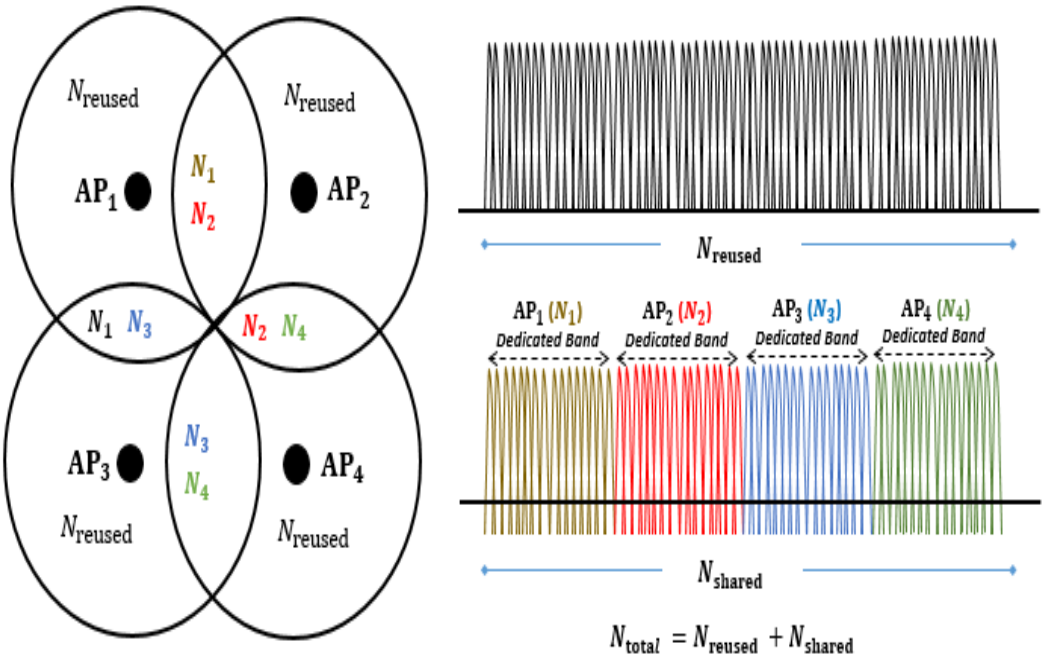

FIGURE 4-4, Resource partitioning of 4 APs

4.3.2 Resource Allocation Algorithms

Several resource allocation techniques are used to optimally assign the subcarriers of the OFDM frame to differentiate users in a multi-user environment. Fig. 4-5 shows the common resource allocation techniques that can be used with different OFDM modulation schemes.

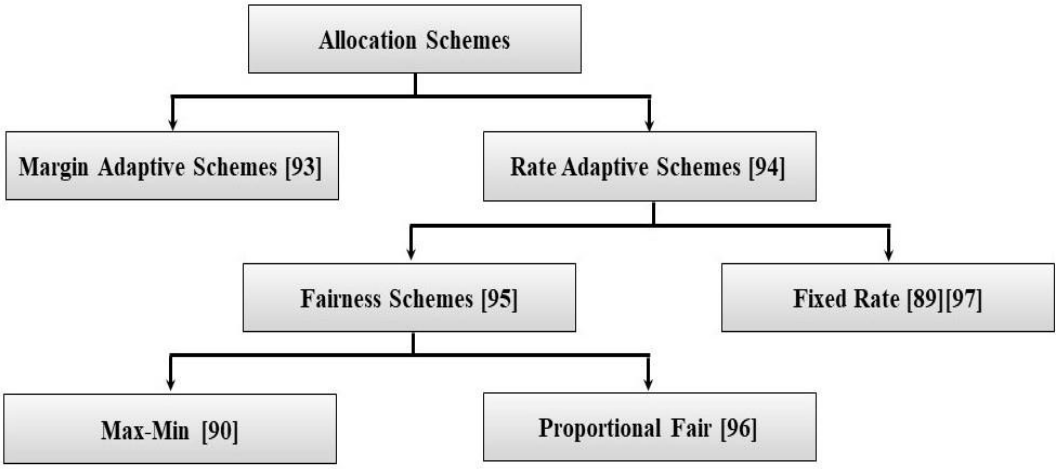

FIGURE 4-5. Resource Allocation Techniques

Margin adaptive and rate-adaptive algorithms are the two major classes of dynamic resource allocation schemes. The margin adaptive schemes focus on minimizing the total transmission power and provisioning each user with the desired data rate [93]. The rate-adaptive schemes concentrate on maximizing the overall data rate and on satisfying the power constraints [94]. The adaptive rate schemes are classified into fairness or fixed rate requirements algorithms [95]. Resource allocation with fairness algorithms attempts to maximize the total data rate while satisfying fairness among the users. For example, proportional-fair [96] and the max-min fair [90] algorithms have been introduced to allocate the radio resources. The proportional fair resource scheduling technique provides an efficient resource to most users and improves the cell-edge user throughputs. While the max-min fairness maximizes the minimum rate of the users subject to the link-capacity constraint. In [93], the proposed scheme assigns a single carrier to each user and increases the assigned resources to the user that has the least rate in each iteration. In contrast, resource allocation with fixed-rate algorithms maximizes the total data rate while providing each user with its rate requirements as in [97].

We assume that the users are uniformly distributed over the VLC area, and they are requesting different rates in the downlink transmission. Accordingly, we modified the previous resource allocation algorithms, where each cell assigns its radio resources to the attached users in the non-interference area. While in the interference area, the

radio resources are assigned by a central unit. As mentioned before each cell contributes with a portion of the total subcarriers $\boldsymbol{N_{shared}}$ and portion of the total power $\boldsymbol{P_{shared}}$ to serve the users in the interference area and $\boldsymbol{N_{reused}}$, $\boldsymbol{P_{reused}}$ to serve the users in the cell area.

4.4 Simulation and results

ITABLE I: Interference management simulation parameters

Parameter	**Value**
Room size	5 x 5 x 3
P_{opt}	8 watts
Transmitter semi angle	60^o
Receiver field of view (FOV)	40^o
PD Responsivity	0.28 A/W
Number of subcarriers	512
PD area	1 cm^2
Threshold $SINR_{th}$	10 dB
Refractive Index of a PD	1.5
Noise power spectral density	10^{-21} A^2/Hz
Bandwidth	20 MHz
Data subcarriers	255
FFT size	512
Cyclic prefix	16
Modulation technique	64 QAM

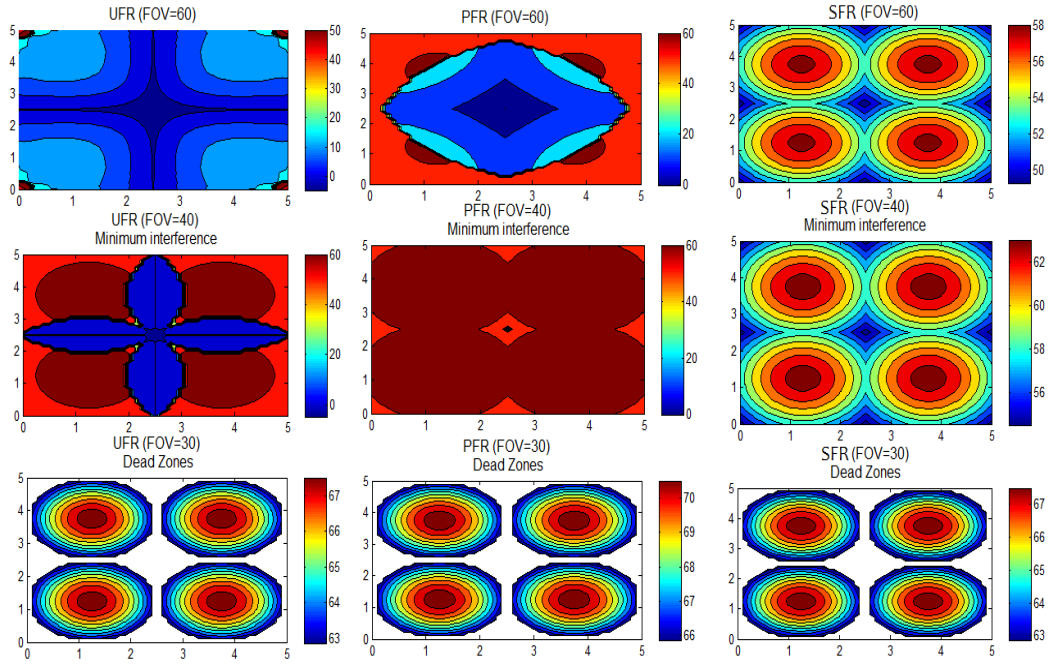

FIGURE 4-6, Spatial distributions of the received SINR with OCO, ACO, ADO-OFDM

In this section, we present the simulation results of the resource allocation algorithms 1 and 2. We consider a $\mathbf{5} \times \mathbf{5} \times \mathbf{3}$ cubic meters room with $\mathbf{4}$ APs. The users are distributed uniformly in the area. In the downlink scenario, the communication channels are assumed to be a flat time-invariant channel. We use DCO-OFDM or OCO-OFDM with $\mathbf{512}$ subcarriers. The maximum acceptable signal electrical power of $\mathbf{7}$ dB DC offset is calculated according to [10, Eq. 5]. Each cell contributes $\mathbf{10}\%$ of the total bandwidth in the interference area. Simulation results are collected from random positions of 12 users over 10,000 iterations. The parameters that are used in this simulation are presented in Table I.

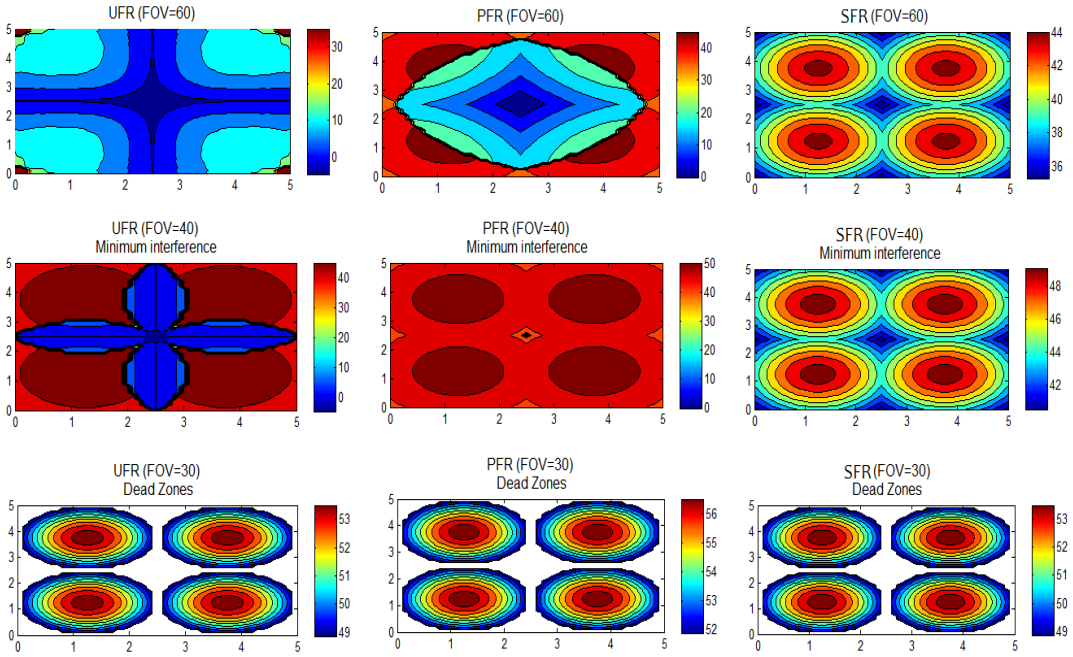

FIGURE 4-7. Spatial distributions of the received SINR with DCO-OFDM

. Fig. 4-7 shows the spatial distribution of the SINR with DCO-OFDM. As can be seen, the FOV highly affects the SINR. The proposed system is successful in achieving an optimum value of the FOV equals 40°, which depends on the room geometry and the APs location.

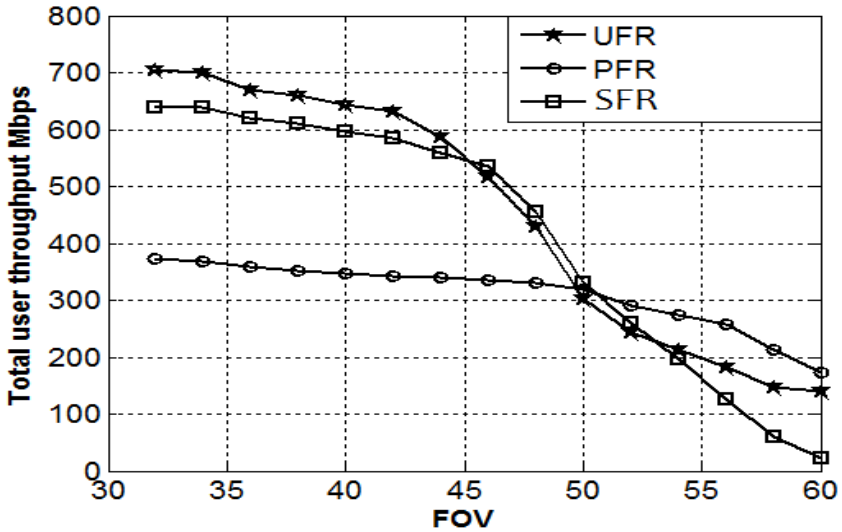

FIGURE 4-8. Total system throughput with DCO-OFDM

Fig. 4-8 and Fig. 4-9 compare the total system throughput that is achieved while applying the different resource partitioning algorithms in the DCO-OFDM and the OCO-OFDM techniques, respectively. It can be shown that the UFR and SFR enhance the overall system throughput at $\mathbf{FOV} \leq \mathbf{50}^{o}$. However, the PFR enhances system throughput when the $\mathbf{FOV} > \mathbf{50}^{o}$. From figures 4-6, 4-7, 4-8, and 4-9, we conclude that it is better to use the proposed UFR and SFR algorithms in the DCO-OFDM and OCO-OFDM systems with FOV equal to $\mathbf{40}^{o}$. This configuration provides a system throughput of 650 Mbps in the DCO-OFDM and 800 Mbps in the OCO-OFDM.

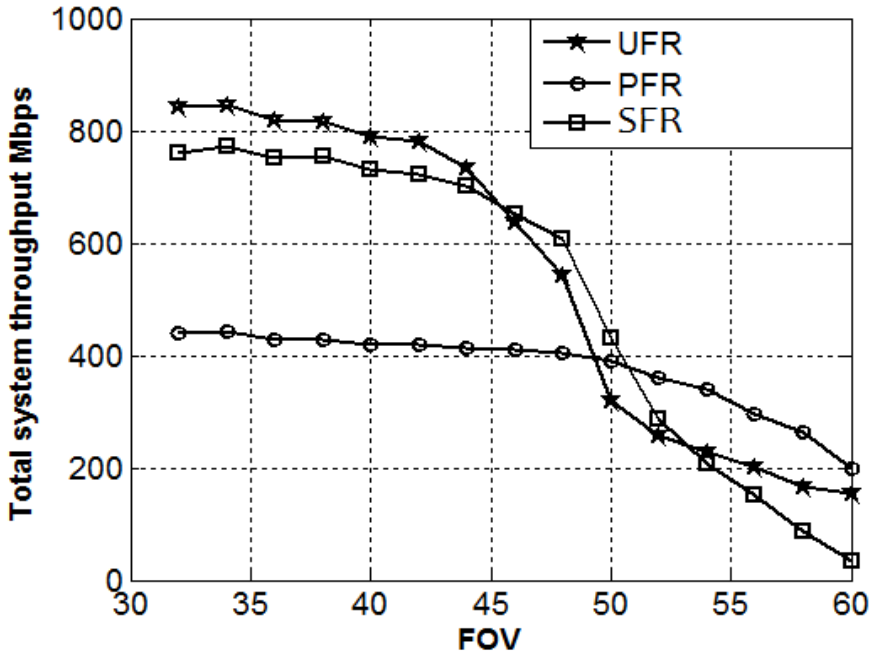

FIGURE 4-9. Total system throughput with OCO, ACO, ADO-OFDM

Fig. 4-10 shows the effect of different resource allocation algorithms by using OCO-OFDM with shared interference band, on the total system throughput. As can be seen, the overall system throughput is increased with the max-min fairness algorithm while the proposed algorithm decreases the overall system throughput due to that some users have rate constraints which cannot be satisfied, then the users will be blocked, and the capacity utilization $\boldsymbol{\rho} \neq \mathbf{1}$.

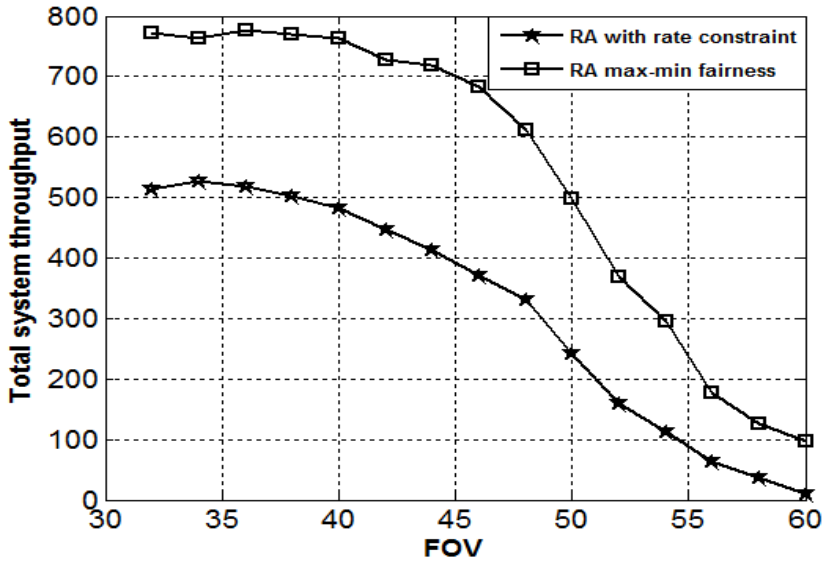

FIGURE 4-10.. Total system throughput with different resource allocation and shared band

Fig. 4-11, and Fig. 4-12 show the effect of FOV and frequency reuse techniques on the outage probability in the DCO-OFDM and the OCO-OFDM schemes, respectively. As it can be seen, the outage probability of the PFR and SFR is better than the UFR in all modulation techniques as well as, at the optimum FOV ($\mathbf{40^o}$) the PFR and SFR provide a zero-outage probability.

Finally, we can conclude that the PFR, which proposed in this paper with two different resource allocation schemes, can achieve a throughput of up to 800 Mbps with around zero outage probability at an optimum FOV.

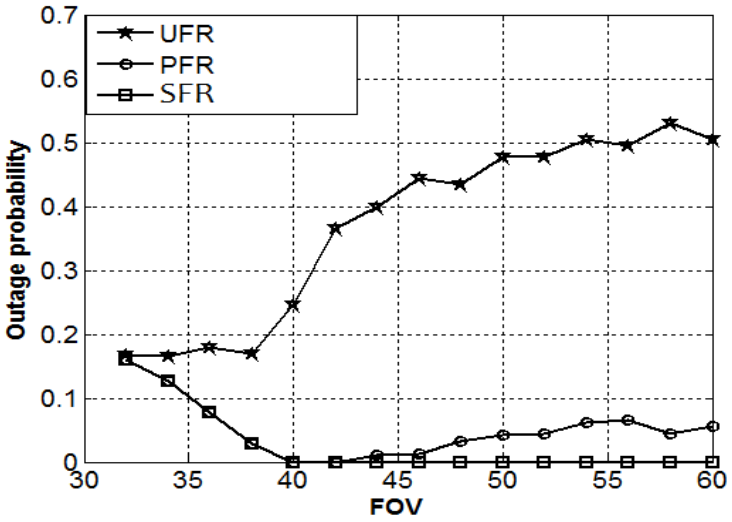

FIGURE 4-11.. Outage probability with DCO-OFDM

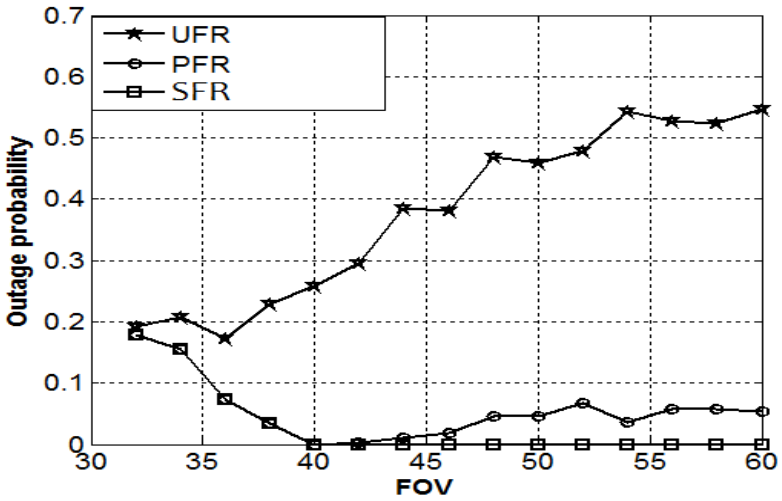

FIGURE 4-12. Outage probability with OCO, ACO, ADO-OFDM

Chapter 5 : Big Data Analytics and Clustering - Based RRH-BBU Assignment for Green Communication Network

5.1 Introduction

Network architecture is envisioned to support diverse services with low latency and high reliability. This arises the concept of the software defined network (SDN) that is based on the concept of decentralizing the data plane that allows supporting different quality of service over the common shared infrastructure [98]. Heterogeneous centralized radio access network (HCRAN) presents the fundamentals of decentralizing the data plane by providing base band unit (BBU) pool and remote radio heads (RRH), that cover different cell sizes [99]. The CRAN architecture poses different challenges as the functionality is split between the RRH and the BBU, the fronthaul network and the RRH to BBU mapping. The RRH to the BBU assignment is proposed as an optimization problem, as it significantly influence the CRAN network efficiency. Many researchers proposed ways of association based on maximizing certain objective function. In this paper we present the problem of RRH-BBU association with targeting the network power consumption minimization, as a way for green communication network in 5G architecture. Power saving constraint is reached by switching off the underutilized RRH and BBU. We introduce an RRH to BBU assignment that reduces the power and the handover rates between the BBU, the problem is formulated as NLP hard optimization problem. The proposed algorithm firstly, deployed time series-based clustering technique on the CDR data to study the network utilization over the time. Secondly, it provides second level spatial clustering that divides each temporal cluster into geographical zones to enhance the inter BBU handover rate. Finally, it computes the required number of BBUs for each temporal-spatial cluster and efficiently optimize the number of active BBUs using bin packing optimization algorithm. The proposed algorithm simplifies the problem by dividing it into clusters of joint RRH and BBU. Parallel processing, enabled by dividing the resource allocation for each cluster, divides the optimization problem into multiple simplified optimization problems. The problem is divided into two levels, in the first

level the RRH are clustered based on real collected call detailed records (CDR) of real network. In the second level, based on the clustered RRH, the BBUs are assigned to each clustered group of RRH.

5.2 Literature review and contribution

5.2.1 Related work

In this section, we propose the previous work that consider the RRH-BBU association problem. The problem is divided into two parts. First, we discuss the proposed research of the BBU RHH assignment problem, then the proposed research of clustering the BBU and RRH.

A. RRH to BBU assignment

The problem of the RRH-BBU mapping has been proposed in much research recently targeting maximizing objective function, as energy saving, and fulfil certain constraints, as quality of service (QOS). In [105] the author proposed CRAN architecture with separated computational resources from the RRH, as the RRH are deployed as small cells with only transmission functionalities. The allocation problem is described as two-level scheduling algorithm. In the first level the resources are assigned from cells to each user, while satisfying quality of service (QOS) and continuity of the service. In the second level, the problem of assigning resource from each BBU to RRH is proposed as an optimization problem, that maintains the power consumption and minimizing the computing resources. The mapping of each BBU to RRH depends on assigning physical machine (set of BBUs) to all the RRH in its coverage area. The author of [106] proposed two stage dynamic resource allocation for CRAN, that assign user equipment (UE) to each RRH with power transmission constraint jointly with RRH- BBU real time association. The problem of RRH-UE assignment is described as Mixed Integer Non-Linear Program (MINLP) with signal to interference noise ratio constraints. Based on the UE-RRH assignment, the optimal number of the BBU is computed in the second phase and the RRH-BBU association is described as Multiple Knapsack Problem (MKP) solved by linear solvers. In the work of [107] the author proposed BBU assignment that optimizes the

efficiency of the BBU pool, the problem is described as a bin packing. The assignment of RRH to BBU considers the resource requirements and the communication between the RRH by representing the network as weighted graph. The algorithm improves the power consumption up to 20% and 30% handover reduction by decreasing the communication overhead. In [113] the author proposed spatial based clustering technique by grouping neighbors RRH, the proposed model minimizes the number of active BBU and reduces the number of handovers. The problem is formulated as bin packing with Np hard optimal solution, the author proposed heuristic algorithm to drive the optimal solution in large networks. In [114] the author proposed dynamic BBU virtualization scheme that packs the dynamics of traffic load as bins with finite computing resources in the BBU. The proposed scheme targets minimizing the power consumption of the BBU. While, the author of [115] proposed joint activation and clustering scheme that maximizes the network coverage with QOS constraints.

Based on traffic analysis, in [116] the author proposed traffic aware RRH-BBU assignment algorithm, the study divided the problem into two parts. First, clustering the RHH based on spatio-temporal variation model, as the author modeled the traffic load of RRH as an exponential function with time varying rate parameter. Then, the clustered RRH association with the BBU is described as bin packing optimization problem with BBU as bin and RRH as item set. The author proposed a dynamic RRH assignment algorithm that offloads RRH from an overloaded BBU to a less loaded BBU.

B. Clustering algorithms

In this section we propose the related work of different clustering algorithms that have been recently used in literature to analyze the targeted problem, as the spatial, temporal and spatio-temporal clustering. For the perspective of clustering the RRH problem predictive data analysis, data mining and AI for decision making based CDR have been proposed in different studies recently. [108], [109], [110] propose supervised mobile traffic signature trained by prior knowledge of ground truth information for specific areas. Whereas in [111] the author proposed unsupervised cell classification based on mobile signature algorithm that classifies the mobile loads in efficient manner verified by ground-truth information, the proposed technique has been applied on

real mobile data collected from ten cities. While, in [112] the author proposed heat map drawings of the significant human activities based on mobile signature characterization without prior knowledge of the ground truth information. As geographical mobile signatures are mainly driven by the land use, this produces common pattern of user traffic in different cities and countries [109] and motivates the spatial clustering of the CDR. Accordingly, different research proposed dynamic RRH-BBU association based on longitude and latitude of the RRH using spatial clustering [117]. Residential, entertainment and work zones show different traffic load during the week. As residential zones have highest during the night hours, while the peak traffic load of work zones is during day hour and on weekends for entertainment zones.

On other side, the temporal clustering of the CDR has been proposed in literature, as the human behavior under stationary and normal circumstances is periodically repeated and this influences the aggregated network load over certain period. The real collected CDR shows similar behaviors over certain period. The CDR supported by the mobile operator describe the traffic load at specific time stamps, usually the network traffic load is captured every ten minutes. The CDR is stored as time series at specific time and date. Clustering this complex temporal data is a challenge, as the massive data points of CDR represents single object. The network load temporal clustering has been proposed recently in research considering certain events as planned [118] and unplanned events [119]. The author of [120] extended this work to include the fine-tuned clustering of snapshots of the traffic demand over multiple periods. The clustering of the times series is utilized to discover frequent and rare patterns of the time series. Time series clustering propose different tasks as recognizing dynamic changes caused by planned and unplanned events as in [118,119], predicting future patterns and discovering and classify different patterns [121]. In literature the time series clustering methods are classified into three types of the whole time series clustering and, the other two categories target clustering single long time series based on either subsequence clustering or time point clustering [122].

Different research extended the clustering to include the spatial-temporal clustering. As we described the CDR of each cell over a week as a time series, this data is described as geo-referenced time series with

spatial temporal data as it records time changing values at fixed locations. The traditional temporal and spatial clustering methods represent one way clustering methods, we focus mainly on co-clustering that clusters the data in two dimensions. The concept of data matrix clustering has been first proposed in [123], later this concept has become used in data analysis of different fields as bioinformatics data mining and weather temperature records. More researchers extended the co clustering algorithms to tri-clustering that considers all the values of the recorded data at certain time and fixed location represented by 3D data matrix. In [124] the author proposed 2D clustering algorithm (BBAC_I) that deals with an average of the data recorded over a year at fixed position in a 2D matrix. And extended the work to 3D clustering algorithm (BACT_I) that considers the recorded data at each time stamp over the total considered time interval at a fixed position represented by a 3D matrix.

5.2.2 Contribution

Our contributions are concluded as: We propose a novel RRH-BBU assignment technique, as we proved that dividing the BBU into two level clusters, based on the same clustering algorithm of RRH, reduces the system power consumption and decreases the inter BBU handover rate. To the best of our knowledge this is the first research extended the RRH clusters to be applied on the BBU in the RRH-BBU assignment phase. We propose RRH clustering based on real collected CDR. The RRH clustering algorithm is described as time series clustering algorithm that classify RRH based on its temporal activity. To the best of our knowledge this is the first research describes the CDR as time series. We propose space- time series clustering that represents two nested clustering levels based on the CDR and the latitude and longitude of each cell. We compute the optimum number of the BBU to accommodate the maximum real traffic load for each cluster. And finally we enhanced the system power consumption as we extended the sleep mode to be applied on also the BBU based on the assignment technique. As we reduce the power consumption by 28.8 %, while in literature the author of [107] proposed 20% power saving based on weighted graph that depends on user mobilities and neglects the traffic loads.

5.3 System model and problem formulation

In this section, we describe the suggested CRAN architecture for large cities and we study the effect of different clustering algorithms for the CRAN architecture on the network performance. We propose BBU to RRH mapping scheme based on different clustering algorithms and compare their influences on the power consumption and the backbone handover rate.

5.3.1 CRAN based network architecture

. Optical transport network is considered as the best candidate for the fronthaul network, as it connects the BBU and the RRH with reliable and energy efficient network that provide low latency, high capacity as it connects massive number of RRHs, and scalability [100,101]. On the other side, the functionality split highly influence the system performance and the fronthaul network capacity. As the BBU performs base band functionalities and located at a remote office while the RRH, provides the radio functionalities to the end user scheme increases the rate of the fronthaul links [102]. Whereas, in the flexible functional split scheme, which loads the RRH with more base band functionalities, enhances the capacity loaded on the fronthaul network and the power consumption [104,105]. In CRAN architecture with separated BBU pool and RRH and optical fronthaul transport network, we consider decentralization scheme of all base band operations at the BBU pool, as the RRH performs only the radio operations for the attached user equipment (UE). Based on the traffic analysis and user requests the resources of the BBU pool must be allocated to each RRH. Mainly the allocation algorithms aim to reducing the network power consumption and meeting the quality of service.

The proposed HCRAN architecture, the radio operations in the coverage area of the Femto cells are supported by the distributed RRH, while Macro base stations serve the cells with offloaded RRH during sleep modes. As turning off the underutilized units highly improves the power consumption, so Macro base stations introduced to maintain the radio operations in dead zones during low traffic loads as shown in Fig. 5-1. The proposed clustering algorithms aim to grouping some RRH based on specific feature and assign resources from the connected BBU to this cluster.

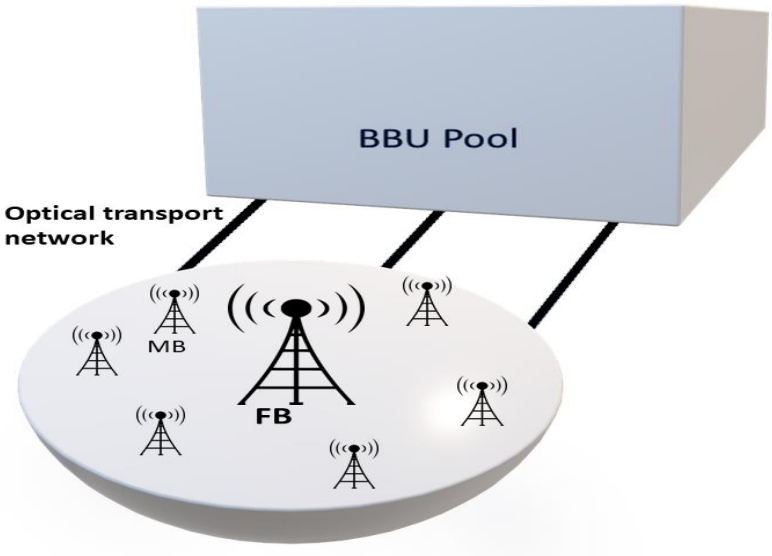

FIGURE 5-1. HCRAN (femto and micro base stations) architecture connected via optical transport network to BBU pool

5.3.2 Problem formulation

In the proposed model, we assume M BBUs in the BBU pool with equal physical resources and computing capabilities, measured by million operations per time slot (MOPTS). The assigned BBU performs all the baseband operations for the attached RRHs. The required resources for baseband operations of RRH I depends on the traffic load and noted as $R_{i.}$ Assuming each BBU have C MOPTS and up to N RRHs can be attached to each.

$$C_j \geq \sum_{i=1}^{N} \mu_{i,j} \, R_{i,j} \tag{5.1}$$

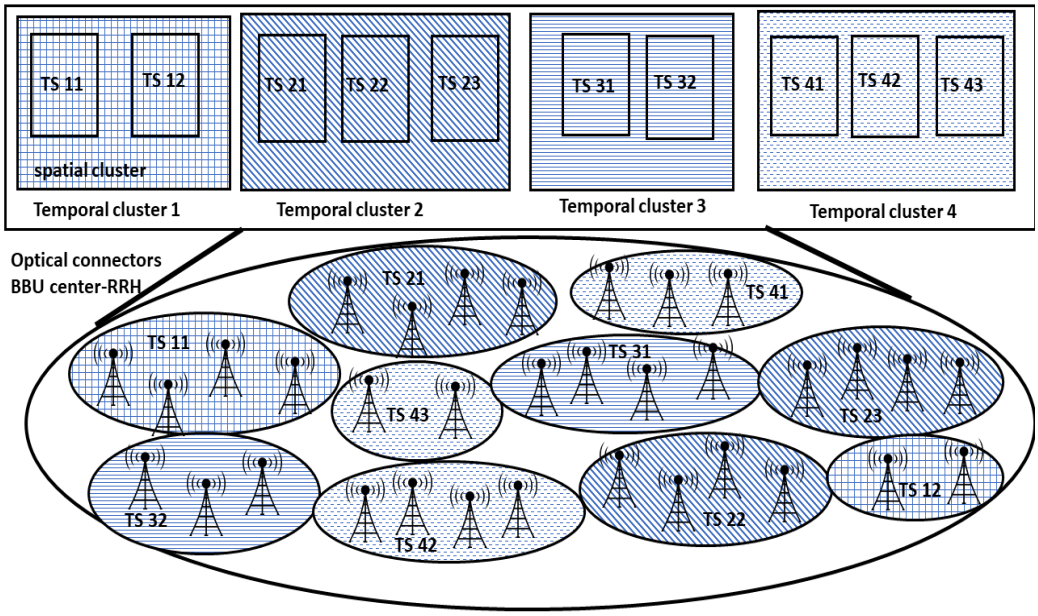

FIGURE 5-2. The proposed clustering model for temporal and spatial clusters in CRAN (TS11: spatial cluster 1 of temporal cluster 1)

Where $\mu_{i,j}$ is the assignment coefficient of RRH i to BBU j

$$\mu_{i,j} = \begin{cases} 1 & RRH\ i\ attached\ to\ BBU\ j \\ 0 & Oterwise \end{cases} \quad (5.2)$$

The power consumption of each BBU represents the base band power, $P_{Dynamic}$ represents the dynamic power incurred by the traffic load and can be expressed as a linear function of it.

$$P_{BB} = P_{Dynamic} + P_{Static} \quad (5.3)$$

$$P_{Dynamic} = P_{filter} + P_{OFDM} + P_{DPD} + P_{FEC} + P_{CPU} + P_{CRPI} \quad (5.4)$$

$$P_{Dynamic} = \beta\, R \quad (5.5)$$

β is the load–power coefficient and R is the traffic load.

Where P_{filter} , P_{OFDM} , $P_{DPD}, P_{FEC}, P_{CPU}, P_{CRPI}$ are the consumed power of the filtering, the OFDM transceivers, digital pre-distortion, CPU, encoder, serial link to backbone network, respectively.

The problem of assigning RRH to each BBU is described as a Bin Packing Problem (BPP). That can be solved using Knapsack algorithm, with the RRH as objects and BBU capacity as knapsack. Clustering the BBU pool divides this single problem into multiple joint optimization problem. The algorithm assigns one item (object) to each bin (knapsack) such that the total weights of all objects do not exceed the capacity of the knapsack and minimize the number of the used knapsacks (BBUs).

The proposed network architecture has N RRHs and M BBUs, each RRH can be only associated to a single BBU. The mathematical formulation of this problem, described by equ. (5.6),(5.9), represents an optimization problem that minimizes the number of active BBU with capacity constraint.

$$minimize \qquad \sum_{i=1}^{K} B_i \tag{5.6}$$

Subject to $\sum_{j=1}^{k} w_j \mu_{i,j} \leq C_i B_i \quad i \in \{1,..,n\}$ (5.7)

$\sum_{i=1}^{N} \mu_{i,j} = 1 \quad j \in \{1,..,k\}$ (5.8)

where $B_i = \begin{cases} 1 & if\ BBU\ i\ is\ used \\ 0 & otherwise \end{cases}$ (5.9)

$$w_j \leq C \tag{5.10}$$

Where C_i represents the resources of the BBU i and w_j represents the weight of the resources assigned from each BBU to all attached RRHs. The first constraint in ensures that the total assigned resources for all RRH attached to the BBU i are less than the total available resources at this BBU. While the second constraint verifies that each RRH must be served and attached to single BBU.

5.4 The proposed algorithm

The proposed problem described as multi objective optimization problem, that targets minimizing the network power consumption and the handover between the BBUs. The algorithm depends on first temporally clustering the BBUs and the RRHs

based on the CDR, which enables switching off the BBUs and RRHs of each cluster during the low traffic periods and minimizing the power. Secondly, spatial clustering is performed for each temporal cluster to ensure serving all nearby RRH by certain BBUs to minimize the handovers between the BBUs. Finally, the assignment process is performed for each cluster individually with reduced computational complexity as shown in the algorithm.

5.4.1 Clustering the BBU & RRH

In literature the tri-clustering algorithms have been proposed to deal with geo-referenced time series, these algorithms analyze the CDR at certain instant over the time interval at each RRH position. Although for the proposed application the RRH needs to be clustered based on its total activity. Based on this we proposed a two-level clustering algorithm that first clusters the CDR of the RRH as a temporal clustering then clusters temporal cluster based on the location of the attached RRH. We describe the CDR as multi variant time series and refer to the network temporal clustering as time series clustering. In which, the whole series clustering is considered as a single object and classified based on its similarities. These similarities are measured based on different distance measurements as discrete time Wrapping (DTW) and Euclidean distance.

Algorithm 1 Clustering algorithm

RH_i : i^{th} RRH where i ϵ {1,…,n}

BU_j : j^{th} RRH where j ϵ {1,…,k}

TC_u : u^{th} temporal clustering

SC_t : t^{th} spatial clustering

R_{iw} : The traffic load of i^{th} RRH over week w

NT : Number of temporal clusters

NSP : Number of temporal clusters

No_BBU_{ij} : Number of BBUs of temporal cluster i and spatial cluster j

BBU_RRH_{ij} : RRH to BBU assignment of temporal cluster i and spatial clusterj

Begin:

data processing R_{iw} to define:

Cell id_i

Time $interval_i$

R_{iw} =Total activity

For 3<= n_clusters <8

Apply DTW time series clustering (R_{iw}).

Compute the distortion of each cluster.

End

NSP=min (distortion)

For 1<i< NT

NSP= DBscan(cluster(i))

End

For 1<i< NT

For 1<j< NSP

No_BBU_{ij}=max (sum (R_{iw}))

BBU_RRH_{ij}=Bin_packing (R_{iw})

End

End

Agglomerative time series clustering algorithm, up-bottom approach, is proposed for clustering the CDR of RRH as a temporal clustering. Temporal clustering is applied first on the CDR of each RRH, we propose K-means discrete time wrapping (DTW) time series clustering. First the dataset is divided into K clusters and randomly select k centroids, then apply DTW to assign each time series to the nearest cluster centroid and update the centroid based on the new assigned time series. Where the DTW clustering finds all possible paths between two time series to provide a distance matrix with cumulative minimum distance of the three neighbors. Then it selects the minimum distance between two series [126]. In the proposed algorithm the number of the clusters is determined by measuring the distortion factors of each clusters number to find the optimum number of clusters.

The proposed spatial clustering algorithm divides the RRH of the CRAN architecture into clusters based on the longitude and latitude of each RRH. DBSCAN, K-means and many different clustering algorithms are defined to cluster geographical data based on the longitude and latitude. DBSCAN is a dense based clustering technique that forms a cluster based on dense connectivity analysis. BDSCAN is based on identifying a radius of connected area with minimum number of objects for each object in a cluster. There are two main parameters for the DBSCAN, as for each point of a cluster the neighborhood of a distance (R) must contain at least number of points equals (Minpts) [126].

5.4.2 RRH to BBU assignment

As mentioned, various RRH to BBU assignment techniques with different objectives have been proposed in literature. The objective of power reduction in the communication network rises as an application for the green networks with reduced power consumption. We introduce an RRH to BBU assignment with power reduction and reducing handovers between the BBUs. The problem is formulated as bin packing optimization problem that is considered as NP hard problem. The proposed algorithm simplifies the problem by dividing it into clusters of joint RRH and BBU. Parallel processing, enabled by dividing the resource allocation for each cluster, divides the optimization problem into multiple simplified problems. The best fit bin packing optimization is proposed, in which the item is packed into a bin by leaving smallest residual space.

The complexity order of the optimization problem is $O(n\ logn)$, where n is the number of the available bins (BBUs). The complexity order of the optimization

problem based on clustered model with M temporal clusters, P_j spatial clusters in temporal cluster j and n_{jk} BBU in temporal cluster j and spatial cluster k is given by (5.11).

$$O(\sum_{j=1}^{M} \sum_{k=1}^{P_j} n_{jk} \log n_{jk}) \tag{5.11}$$

5.5 Results and analysis using real traffic: Milan city

In this section we present simulation results of the proposed RRH-BBU assignment based on clustering algorithm.

5.5.1 Data

The CDR of Milan city is used as a case study area to simulate the proposed algorithm using big data analytics of collected real mobile traffic. The Italian telecom operator shared a CDR record for 10,000 cells with 235×235 m spatial resolution covers the area of Milan city [26]. The data records mobile activities sample each 10 minutes over 2 months from the first of November till the end of December 2013. The recorded activities are divided into call activities, SMS activities, and internet activities. The data has been processed and stored as data frames with multiple columns represent the square id, time interval, and the total activity (aggregated call, SMS, and internet activity). Each RRH is served with only BBU and multiple RRHs can share the same BBU based on the aggregated traffic load. Each cell is served by multiple RRHs, and the proposed CDR is considered as load of single RRH.

5.5.2 Simulation results

The procedure of the applied algorithm on the CDR is shown in Algorithm 1, the data is processed using big data analytics as Dask data frames [124]. The total activity of the cellular mobile user is studied to classify and study the nature of the geographical area. First the data is grouped by the square id and time intervals to analyze the traffic of each cell over the total period. We propose the observations of a week from Monday (4^{th} November) to Sunday (10^{th} November) as a first training set, the time samples representing this period are 1008 sample. The samples of each cell are treated as a time series producing 10,000 time series to be clustered. The values of the traffic are

normalized to ensure accurate measurements, as the cells show records with enormous variations. The time series clustering is based on K-Means algorithm that uses DTW as similarity metric between different time series. As stated in the algorithm, the number of clusters is determined in iterative manner, and the best number of clusters is chosen based on the first minimal distortion level among different number of clusters. For the proposed data the cells are clustered into 7 clusters, as at 7 clusters the distortion level begins to be constant as shown in Fig.5-3.

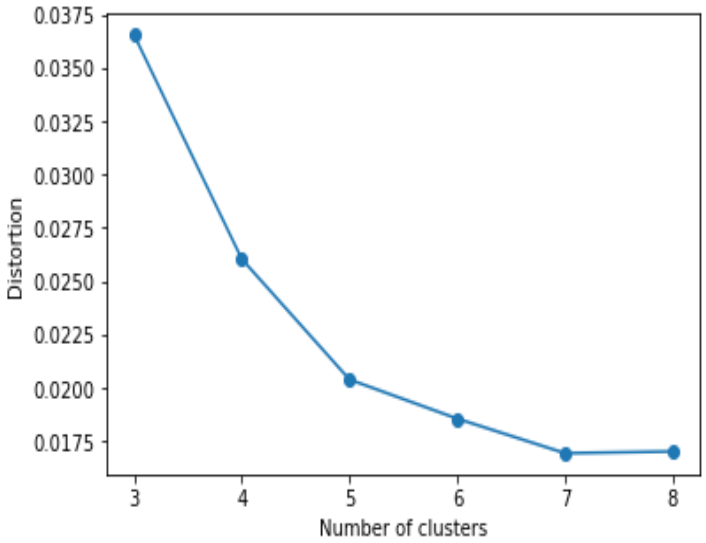

FIGURE 5-3. Distortion of different clustering number

Fig. 5-4 shows the cluster centers of the seven clusters and the activity of the cells belong to each one. Each cluster center can indicate the nature of the geographical area, as clusters 2, and 6 show pure workspace area with low traffic during the week ends and high traffic during the weekdays. Whereas cluster 3 represents residential area with high traffic load during night hours. Some clusters show different behaviors composed of the basic classifications (residential, entertainment, transportation, and work area). These different combinations produce different clusters as shown in clusters 5, and 7. As cluster 5 shows moderate activities during all the hours of day and night, that shows mixed area of workspace and entertainment area. Moreover, it is noticed that some cells show low traffic records comparing with other cells as in cluster 1, and 4. The low traffic load cells are distributed over the total area of Milan and representing areas with low population ratio and transportations.

The results of the clustering system have been verified by comparing the results of the clustering algorithm and the land use of the Milan city. Fig. 5-5.A shows the published land use map of Milan city, while Fig. 5-5.B shows the proposed simulated temporally clustered cells of Milan using the cell location given in Fig. 5-6. As shown in Fig. 5-5, the agriculture area and the green areas represented by cluster1 with low normalized traffic at the city edges. Whereas the city center has highest traffic load represented by cluster 3 as residential area and cluster 2 as workspaces. Moreover, various clusters are shown at the city center representing entertainment and other activities as clusters 4, 5, and 7.

The second phase of clustering represents a spatial clustering for each temporal cluster, this cluster phase reduces the handover between different BBUs by assigning near RRHs to the same BBU. The accurate handover rate can be computed using the mobility of each user between different RRHs, in this work, we proposed the algorithm without computing the handover rate due to lake of user mobility data. The DBSCAN proposes a spatial clustering based on connectivity with minimum distance between different objects. In Milan CDR data the square id represents the cell position as telecom Italy shared a map for the distribution of the cell over the covered area as in Fig. 5-6. DBSCAN algorithm is applied on each temporal cluster individually to produce inner spatial clusters. Changing the radius highly affects the number of the produced spatial clusters, so this radius must be carefully studied and picked according to the case.

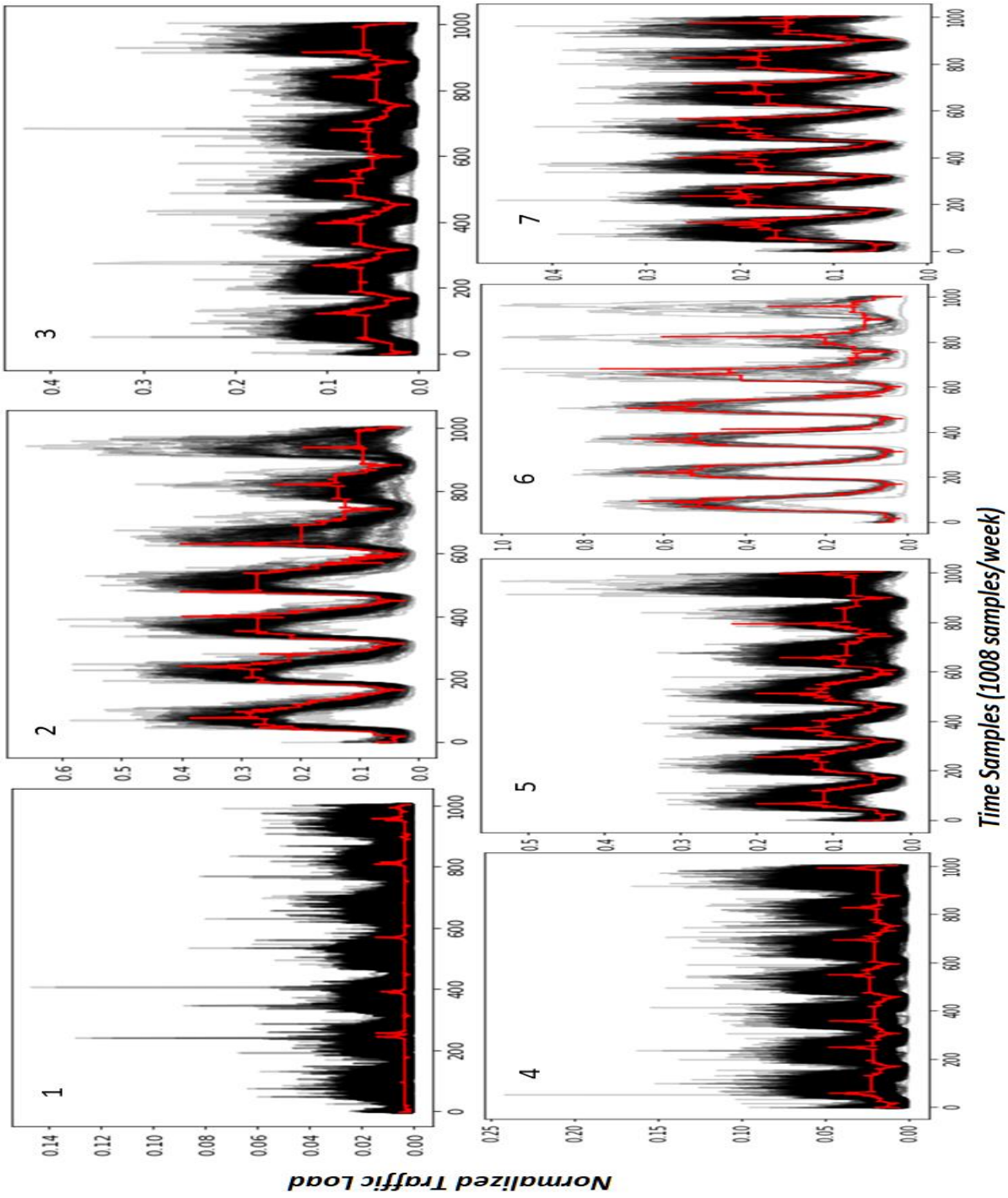

FIGURE 5-4. Normalized traffic load of different clusters and cluster centers over week (Monday - Sunday)

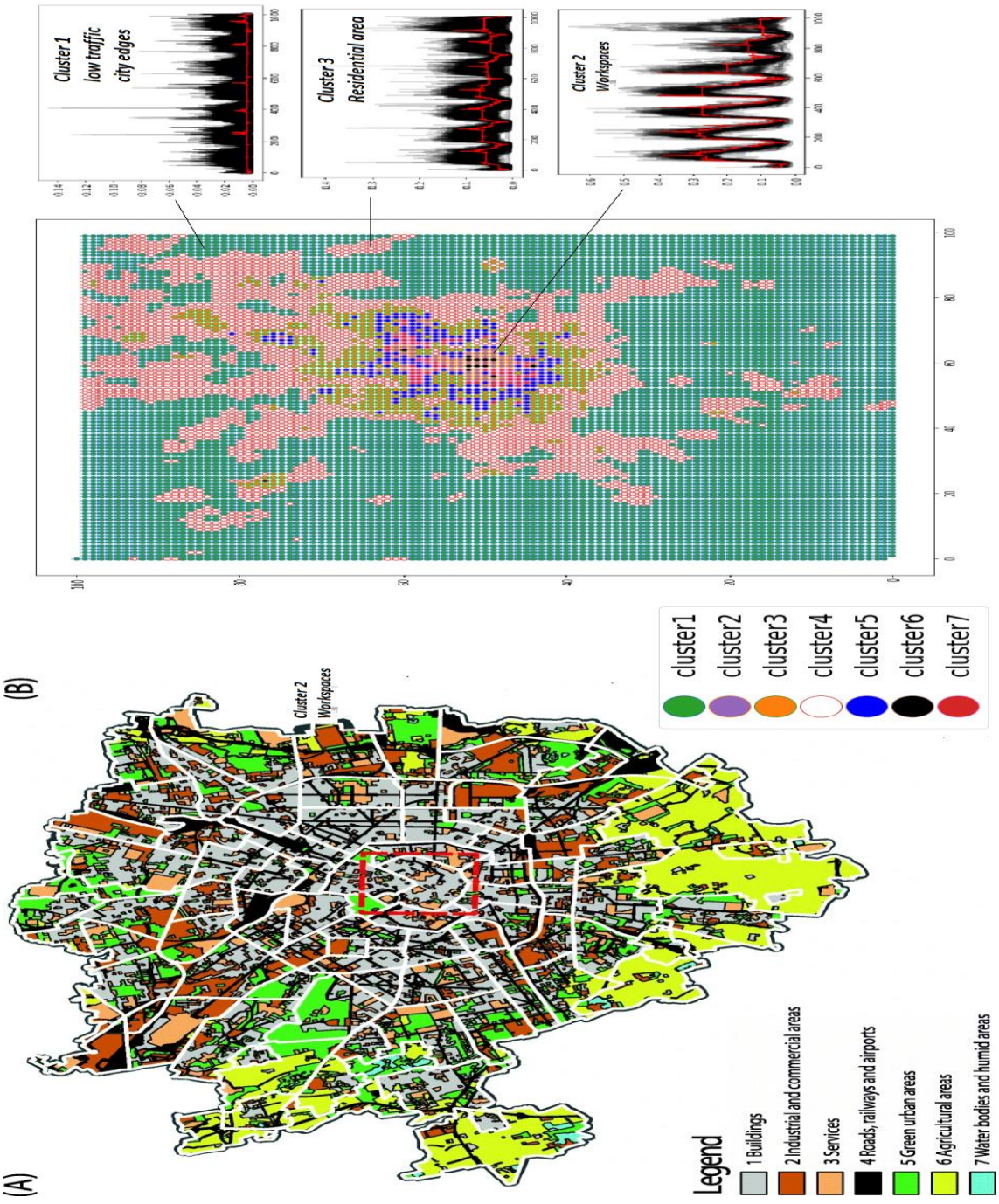

FIGURE 5-5. A. published Milan land use map / B. The land use map based on the time series clustering.

9901	9902	……	9999	10000
9801	……	……	9899	9900
……	……	……	……	……
101	102	……	……	200
1	2	3	……	100

Figure 5-6. Milan cell Grid

The cell id is translated into cartesian coordinates based on the published cell map given in Fig. 5-6, as shown the distance between two adjacent cells in the vertical axis is 100 and 1 in the horizontal axis. According to the Euclidian distance, the radius of the connected area, for the used data, adjusted to $\sqrt{2}$ after normalizing the vertical distance to 1. Minimum number of points of each cluster (Minpts) parameter of DBSCAN needs to be computed carefully, as it highly influences the number of formulated clusters and causes some random points represent the un-clustered points.

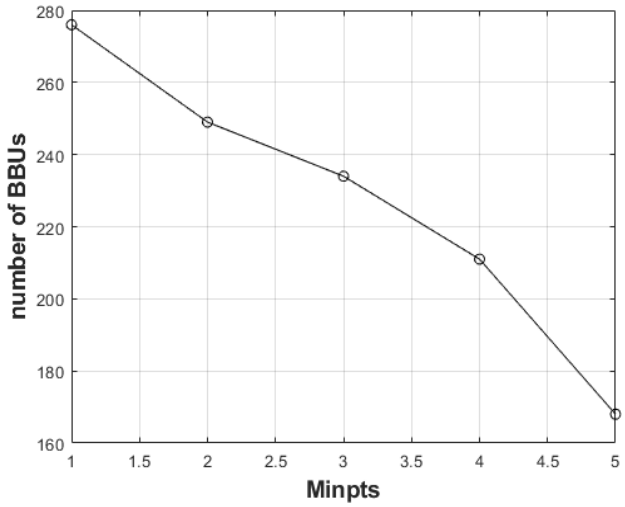

FIGURE 5-7.. The effect of the Minpts of the DBSCAN algorithm on the number of the spatial clusters.

As shown in Fig. 5-7, increasing the Minpts decreases the number of the used BBUs. As increasing the Minpts increases the random points, which will be ignored in the BBU assignment process. This tradeoff, between neglecting some points and increasing the installed BBUs, is resolved by measuring the required BBUs for the traffic of the neglected point and compare it with the corresponding number of saved BBUs from the neglection.

As shown in Fig. 5-8, for 3 Minpts the neglected random points save 42 BBUs , while it can be served by assigning 21 BBUs. The optimum point is at 3 as it verifies the tradeoff between saving the number of BBU, while serving all the cells. On the other side, at 3 Minpts the additional BBUs cannot be included in the turning off BBU algorithm, as they serve random points with different temporal behavior. Consequently, this scheme decreases the power efficiency of the network, so the performance metrics have been studied at 1 Minpts. Fig. 5-9 shows the spatial clustering for single temporal cluster (cluster 1), all the near connected cells are grouped in single spatial cluster.

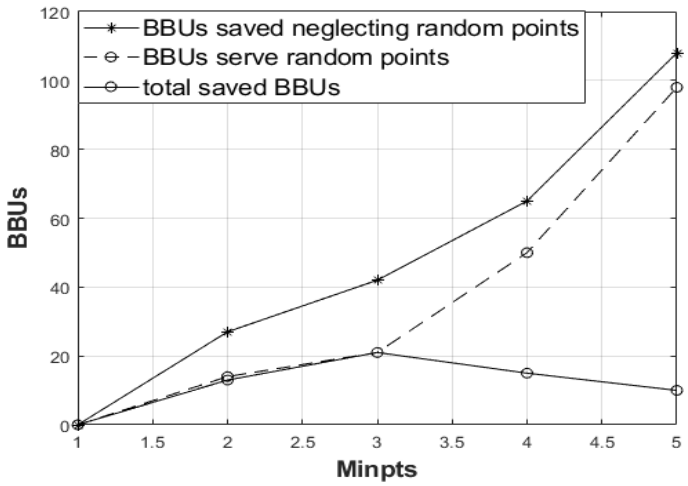

FIGURE 5-8. The effect of the Minpts of the DBSCAN algorithm on the number of the added and reduced BBUs to serve the neglected.

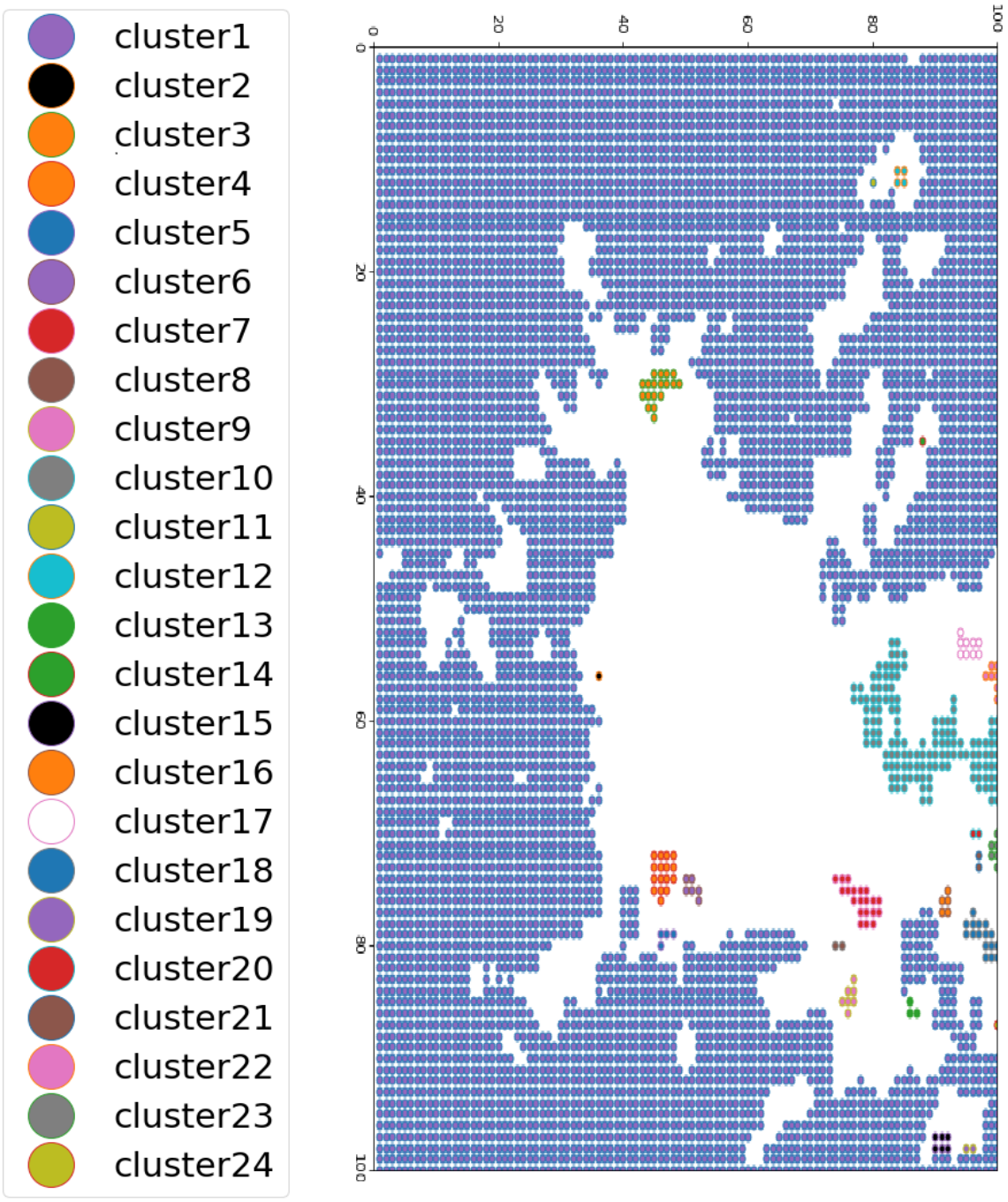

FIGURE 5-9. A. published Milan land use map / B. The land use map based on the time series clustering.

Table II shows the number of the inner spatial cluster, number of RRHs, and number of required BBUs of each temporal cluster. The number of the required BBUs is computed based on the normalized traffic required by computing and ceiling the traffic of each spatial cluster TR_k, according to (5.12).

$$BBU= £ \sum_{j=1}^{M} \left[\sum_{k=1}^{P_j} T\ R_k \right] \quad (5.12)$$

where £ is the mapping ratio between the traffic load and the number of the required BBUs.

TABLE II: Number of spatial clusters and RRHs in each temporal cluster

Temporal Clusters	No. of BBU		Spatial Cluster		No. of RRHs	
	1	**3**	**1**	**3**	**1**	**3**
Cluster 1	51	31	24	16	6657	
Cluster 2	15	9	13	5	36	
Cluster 3	56	49	66	27	613	
Cluster 4	75	71	64	32	2319	
Cluster 5	40	31	43	14	249	
Cluster 6	7	2	5	2	10	
Cluster 7	32	22	26	10	116	
Random Cells	-	21	-	-	-	168

Table III shows the total number of BBUs and the power consumption of 1, 3 Minpts clustered system and the un-clustered system. The required BBUs for un-clustered system using the traffic load of all the RRHs by adding the traffic load and ceiling it according to (5.13).

$$BBU= £ \left[\sum_{u=1}^{V} TR_u \right] \quad (5.13)$$

where V is number of the RRHs in the system. As expected, the number of the clustered system is higher than the un-clustered system due to the multiple ceiling function used in the clustered system, as the assigned number of each temporal cluster must be integer.

TABLE III. Number of BBU in each cluster

	Clustered system		UN- Clustered system
	1	3	
No. of BBU	276	255	226
Power savings	28.8%	26.89%	0%

The proposed algorithm computes the required number of BBUs for each cluster based on the maximum value of the RRHs total traffic. Then, as mentioned, the algorithm performs nested loops over the temporal and the inner spatial clusters to assign the RRHs to the proposed BBUs. For the study case of Milan, we propose the number of the active BBUs over the time. The proposed bin packing assignment is performed every one hour based on the maximum traffic load over this time interval, as the maximum traffic load is computed and the required number of BBUs to serve the required traffic load using bin packing algorithm. Fig. 5-10 shows the number of required active BBUs to serve the load demand based on DBSCAN with 1 Minpts, the required objectives are achieved on two phases. First, each spatial cluster is treated as a single entity to ensure the objective of minimizing inter BBUs handover. The accurate handover enhancement rate is computed with user movement scheme between different cells. As this data is not shared from the operator, we depend on decreasing the total handover rate with grouping all the nearby cells. Then, the algorithm is performed separately on each temporal cluster to decrease the power consumption by turning off the under-utilized BBUs over the monitoring time interval (1 week). The power saving of DBSCAN algorithm with 1 and 3 Minpts are compared using the average power saving in each scheme according to (5.14).

$$\text{Power\_saving} = \frac{BBUun - \sum_{t=1}^{time\_points(168)} BBU\_CLU_t}{BBUun} \tag{5.14}$$

Where BBU_{UN} represents the total BBUs of the un-clustered system, and BBU_CLUt represents the total active BBU of clustered system at time t. As shown in Table II, DBSCAN with 1 Minpts saves 28.8% of the total power consumption of the un-clustered system, while 3 Minpts scheme saves 26.89%. taking into consideration, the higher number of installed BBUS in the 1 Minpts scheme.

Finally, the RRH-BBU assignment as a bin packing problem assignment. The assignment problem is divided into multiple problems based on the number of temporal and spatial clusters.

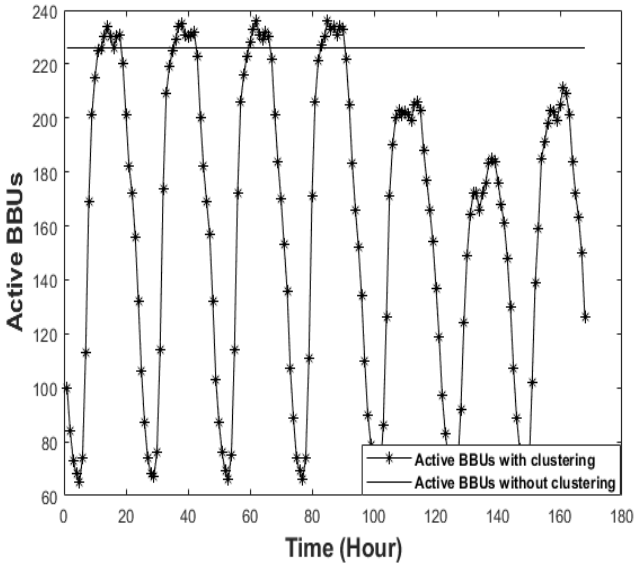

FIGURE 5-10. . The number of active BBUs over one hour using clustering and traditional schemes

Chapter 6 : Conclusion and Future Work

Throughout this thesis we addressed 5G network challenges. The non-coherent optical modulation tradeoff has been addressed, as we proposed FBMC and artificial intelligence-based schemes. The proposed schemes are proved to solve the spectral and the power efficiency trade off in non-coherent optical modulation schemes. Then we addressed the problem of interference management for indoor and outdoor networks. We evaluated the proposed scheme for VLC network and for the fronthaul optical network. The proposed schemes show significant enhancement in the network behavior regarding the power saving and network management.

6.1 Non-coherent optical modulation schemes

6.1.1 Artificial intelligent based schemes

A. Neural network

Chapter 1 presented non-coherent optical modulation transceiver based on artificial neural network. . It is shown that nonlinear regression provides the best system performance, over linear and polynomial regression, as it offers better feature extraction. Among different nonlinear regression activation function the PReLU shows the best performance as it offers linearity for positive received signal and nonlinearity for the negative parts. Evaluating the communication system parameters shows that increasing the subcarrier spacing and decreasing the modulation order highly influence the NN size and the system complexity.

B. Decision tree

In chapter 1, we presented non-coherent optical modulation transceiver based on decision regression tree, that eliminates the

clipping distortion produced by clipping the transmitted signal over optical channel. The proposed transceiver overcomes the tradeoff between the spectral and the power efficiency of the noncoherent optical modulation, by transmitting the symbols over all the subcarriers without DC component. The proposed RDT reduces the complexity of the NN architecture , moreover it shows better performance and enhanced BER for high subcarrier spacing. On the other side, reducing the subcarrier spacing highly influences the RDT scheme, as it increases the BER and the complexity of the scheme. It is shown that the AI based transceiver enhances the BER of the DCO-OFDM, as the BER reaches 10^-3 at 5 db SNR with the same spectral efficiency.

6.1.2 ACO-FBMC

While in chapter 2, the optical ACO-FBMC scheme for direct detection modulation was presented. We have shown that the proposed scheme eliminates self-frame interference and suffers from inter-frame interference. Interframe interference is eliminated using the proposed iterative receiver. Our transceiver model is based on an FFT operation and an iterative receptive method to reduce the clipping distortion. The proposed ACO-OFDM removed the guard interval, which increased spectral efficiency. Also, the ACO-FBMC enhances the BER performance of the ACO-OFDM with the perfect rectangular pulse shaping and eliminating the emission of the filter bank out of the band. Our system model has higher spectral efficiency than the classic ACO-OFDM, as FBMC shows better spectral efficiency by removing the guard interval. Moreover, it has been shown that the ACO-FBMC with 8 overlapping factors improves the BER performance of the ACO-OFDM by 4 dB due to the perfect rectangular pulse shaping and the elimination of the out-band emission of the filter bank.

6.2 Interference management schemes

6.2.1 Indoor VLC interference management

This section is proposed in chapter 4, we addressed the problem of interference management in a VLC indoor system with multi-user access. The performance of the system applying the SRF technique compared to UFR and PFR. The results showed that the proposed approach improves system performance in terms of total system throughput, outage probability, and SINR. It solved the problem of high SINR at the cell edge as experienced by UFR and improved the overall system throughput as compared with PFR. Moreover, the proposed technique combined with OCO-OFDM achieved total system throughput up to 800 Mbps with 12 users, and zero outage probability as it enhanced the SINR at the cell edge to 40 dB.

6.2.2 Interference management for green fronthaul network

In chapter 5, we proposed RRH-BBU assignment based on clustering algorithm that targets minimizing the power consumption and the inter BBU handover. The proposed algorithm computes the required number of installed BBUs to accommodate the maximum traffic load, deploys time series clustering as temporal clustering method, and applies DBSCAN algorithm to divide each temporal cluster into several spatial cluster based on the cell location. Then the problem of assigning RRH of each cluster is described as a bin packing optimization problem to find the optimum number of BBUs for each cluster. The proposed algorithm has been validated using real world CDR of Milan city and it is verified the published Milan land use map. The inter BBU handover signals have been enhanced by assigning near RRHs to the same spatial cluster and same BBU, to avoid inter BBU handover. The accurate handover rate can be computed using the user mobility between different RRHs, as stated we provide the algorithm without computing the handover rate due to lake of user mobility data. It is showed that the algorithm reduces the total power consumption of the current deployed network by 28.8 %, by assigning all the active RRHs to certain BBUs based on the traffic load and switching off the unassigned BBUs.

6.3 Future work

Throughout this work, we addressed major challenges of indoor and outdoor optical networks introduced by the 5G network architecture. Firstly, this work can be extended to propose more RRH-BBU assignment with different objectives, as we mainly focused in our proposed scheme on the power savings and the hand over rate. This has to be extended to propose different assignment schemes based on different objectives. Secondly, the optical modulation schemes need more research activities to cover coherent optical modulation and more studies must be proposed to manipulate more AI capabilities. Thirdly, the AI capabilities need to be strongly used in the 5G network to enhance the network performance and overcome major challenges, as increasing the data transfer rate, and eliminating the system noise.

Appendix A

In this Appendix, we present the interference analysis derivation of the ACO-FBMC to prove that ACO-FBMC frames have distortion at the even subcarriers components and the real part of the odd subcarriers, Whereas the imaginary part of the odd subcarriers (loaded by the data) are not affected by the clipping distortion.

The ACO-FBMC performance affected by the two sources of distortion inter frame interference and self-frame interference. Hard clipping of transmitted signal causes distortion on specific sub-carriers. The clipping distortion interfere with the data carried by the same frame and the data carried by the adjacent frames. In this section the clipping distortion and its effect on the data carried by the same frame is proposed. The FBMC-OQAM transmitted signal is introduced in (1) and $\theta_{l,k}$is the phase to shift the interference to the imaginary domain and given by

$$\theta_{l,k} = \frac{\pi}{2} * (k + l) \tag{A.1}$$

For simplicity the clipping distortion is studied at k=0 for the odd ACO-FBMC frame

$$x_0(t) = p(t) * \sum_{l=0}^{L-1} e^{j2\pi lFt} * e^{j\frac{\pi}{2}*(l)} X_l \tag{A.2}$$

For discrete time signal x(n) = x(nT)

Reference to the Bussgang's theorem, the non linear effect of the clipping negative parts on the transmitted signal is represented as an additional distortion to the original signal [14]. So that, the received signal can be expressed as

$$X(l) = X_{clipped}(l) + D(l) \tag{A.3}$$

$$X_{clipped}(l) = \sum_{n=0x(n)>0}^{N-1} x(n)\, e^{-\frac{j2\pi nl}{N}} e^{-\theta_{l,0}} \tag{A.4}$$

where D(l) is the clipping distortion and N is the total number of the subcarriers

Appendix A

$$D(l) = \sum_{n=0x(n)<0}^{N-1} x(n)\, e^{-\frac{j2\pi nl}{N}} e^{-\theta_{l,0}} \tag{A.5}$$

$$= \sum_{n=0x(n)<0}^{N/2-1} x(n)\, e^{-\frac{j2\pi nl}{N}} e^{-j\theta_{l,0}} + \sum_{n=N/2x(n)<0}^{N-1} x(n)\, e^{-\frac{j2\pi nl}{N}} e^{-j\theta_{l,0}}$$

First, by using the odd ACO-OFDM property x(n + N2) = x(N2 − n) and changing the variables. It can be shown that

$$D(l) = \sum_{n=0x(n)<0}^{N/2-1} x(n)\, e^{-\frac{j2\pi nl}{N}} e^{-j\theta_{l,0}e^{-j\pi l}} + \sum_{l=N/2x(n)<0}^{N-1} x(n)\, e^{-\frac{j2\pi nl}{N}} e^{-j\theta_{l,0}e^{j\pi l}} \tag{A.6}$$

Where

$$\theta_{l,0} = \frac{\pi}{2} * l \tag{A.7}$$

TABLE IV Even and Odd subcarriers

	Even subcarriers	Odd subcarriers
$\cos(\frac{3\pi l}{2})$	$(-1)^{\frac{l}{2}}$	0
$\cos(\frac{\pi l}{2})$	$(-1)^{\frac{l}{2}}$	0
$\sin(\frac{3\pi l}{2})$	0	$-(-1)^{\frac{l-1}{2}}$
$\sin(\frac{\pi l}{2})$	0	$(-1)^{\frac{l-1}{2}}$

Appendix A

$$D(l) = \sum_{n=0(x(n)>0}^{N/2-1} x(n)\left(\cos(\frac{2\pi nl}{N}) - j*\sin(\frac{2\pi nl}{N})\right)\times\left(\cos(\frac{3\pi l}{2}) - j*\sin(\frac{3\pi l}{2})\right) \quad (A.8)$$
$$+ \sum_{l=N/2x(n)>0}^{N-1} x(n)\left(\cos(\frac{2\pi nl}{N}) - j*\sin(\frac{2\pi nl}{N})\right)\times\left(\cos(\frac{\pi l}{2}) + j*\sin(\frac{\pi l}{2})\right)$$

So real part of the distortion equals

$$Re(D(l)) = \sum_{n=0(x(n)>0}^{N/2-1} x(n)\left(\cos(\frac{3\pi l}{2})\times\cos(\frac{2\pi nl}{N}) - \sin(\frac{2\pi nl}{N})\times\sin(\frac{3\pi l}{2})\right) \quad (A.9)$$
$$+ \sum_{l=N/2x(n)>0}^{N-1} x(n)\left(\cos(\frac{\pi l}{2}\times\cos(\frac{2\pi nl}{N}) + \sin(\frac{2\pi nl}{N}))\times\sin(\frac{\pi l}{2})\right)$$

Substituting using values in table 1 for even subcarriers l

$$Re(D(l)) = \left(\sum_{n=0(x(n)>0}^{N/2-1} x(n)\cos(\frac{2\pi nl}{N})\right. \quad (A.10)$$
$$\left. + \sum_{l=N/2x(n)>0}^{N-1} x(n)\ \cos(\frac{2\pi nl}{N}))\right)\times(-1)^{\frac{l}{2}}$$

similarly for odd subcarriers l

$$Re(D(l)) = \left(\sum_{n=0(x(n)>0}^{N/2-1} x(n)\sin(\frac{2\pi nl}{N})\right. \quad (A.11)$$
$$\left. + \sum_{l=N/2x(n)>0}^{N-1} x(n)\ \sin(\frac{2\pi nl}{N}))\right)\times(-1)^{\frac{l-1}{2}}$$

and imaginary part of the distortion equals

Appendix A

$$Im(D(l)) = \sum_{n=0(x(n)>0)}^{N/2-1} x(n)\left(-\sin(\frac{3\pi l}{2}) * \cos(\frac{2\pi nl}{N}) - \cos(\frac{3\pi l}{2}) * \sin(\frac{2\pi nl}{N})\right) + \sum_{l=N/2(x(n)>0)}^{N-1} x(n)\left(\sin(\frac{\pi l}{2}) * \cos(\frac{2\pi nl}{N}) - \cos(\frac{\pi l}{2}) * \sin(\frac{2\pi nl}{N})\right) \quad (A.12)$$

Substituting using values in table 1 for even subcarriers l

$$Im(D(l)) = \left(-\sum_{n=0(x(n)>0}^{N/2-1} x(n)\sin(\frac{2\pi nl}{N}) - \sum_{l=N/2x(n)>0}^{N-1} x(n)\ \sin(\frac{2\pi nl}{N}))\right) \times (-1)^{\frac{l}{2}} \quad (A.13)$$

similarly for odd subcarriers l

$$Im(D(l)) = \left(\sum_{n=0(x(n)>0}^{N/2-1} x(n)\cos(\frac{2\pi nl}{N}) + \sum_{l=N/2x(n)>0}^{N-1} x(n)\ \cos(\frac{2\pi nl}{N}))\right) \times (-1)^{\frac{l-1}{2}} \quad (A.14)$$

where

$$X(l) = -D(l) + X_{clipped}(l) \quad (A.15)$$

for even subcarriers X(l)=0

$$X_{clipped}(l) = -D(l) \quad (A.16)$$

for odd subcarriers Re(X(l))=0

$$Re(X_{clipped}(l)) = -Re(D(l)) \quad (A.17)$$

And

$$Im(X(l)) = Im(X_{clipped}(l)) + Im(D(l)) \quad (A.18)$$

substituting in equ.10

Appendix A

$$Im(X_{clipped}) = \sum_{n=0(x(n)>0}^{N-1} x(n)\cos(\frac{2\pi nl}{N}) \tag{A.19}$$

From equ. 16 and equ.20

$$\begin{aligned} Im(D(l)) &= (-1)^{\frac{l-1}{2}} * Im(X_{clipped}) \\ &= Im(X_{clipped}) \end{aligned} \tag{A.20}$$

as $(-1)^{\frac{l-1}{2}} = -1$ for odd l

$$Im(X(l)) = \frac{Im(X_{clipped}(l))}{2} \tag{A.21}$$

As proved odd ACO-FBMC frames have distortion at the even subcarriers components and the real part of the odd subcarriers, Whereas the imaginary part of the odd subcarriers (loaded by the data) are not affected by the clipping distortion. So the clipping distortion causes only inter-frame interference as it has distortion on the imaginary component of the even subcarriers of the even adjacent ACO-FBMC. Similarly, it can be proved that for even ACO- FBMC frames, the clipping causes inter-frame interference on the imaginary component of the odd subcarriers of the odd adjacent ACO-FBMC.

Bibliography

[1] X. Ge, H. Cheng, M. Guizani, T. Han, "5G wireless backhaul networks: Challenges and research advances," IEEE Netw., vol. 28, no. 6, pp. 6-11, Nov. 2014.

[2] X. Foukas, G. Patounas, A. Elmokash_, and M. K. Marina, "Network slicing in 5G: Survey and challenges," IEEE Commun. Mag., vol. 55, no. 5, pp. 94{100, May 2017.

[3] I. Afolabi, T. Taleb, K. Samdanis, A. Ksentini, and H. Flinck, "Network slicing and soft- warization: A survey on principles, enabling technologies and solutions," IEEE Commun. Surveys Tuts., DOI:10.1109/COMST.2018.2815638.

[4] J. Ordonez-Lucena, P. Ameigeiras, D. Lopez, J. J. Ramos-Munoz, J. Lorca, and J. Folgueira,"Network slicing for 5G with SDN/NFV: Concepts, architectures, and challenges," IEEE Commun. Mag., vol. 55, no. 5, pp. 80-87, May 2017.

[5] C. Liang and F. R. Yu, "Wireless network virtualization: a survey, some research issues and challenges,"IEEE Commun. Surveys Tuts., August 2014.

[6] M. Agiwal, A. Roy, and N. Saxena, "Next generation 5G wireless networks: A comprehensive survey," IEEE Commun. Surveys Tuts., vol. 18, no. 3, pp. 1617-1655, 3rd Quart., 2016.

[7] Z. Gao, L. Dai, D. Mi, Z. Wang, M. A. Imran, and M. Z. Shakir, "mm-Wave massive- MIMO-based wireless backhaul for the 5G ultradense network," IEEE Wireless Commun., vol. 22, no. 5, pp. 13{21, Oct. 2015.

[8] Q. Zhao and J. Li,"Rain attenuation in millimeter wave ranges," Proc. IEEE Int. Symp. Antennas, Propag. EM Theory, Oct. 2006.

[9] T. E. Bogale and L. B. Le, "Massive MIMO and millimeter wave for 5G wireless HetNet: Potentials and challenges,"Oct. 2015) [Online].

[10] ETSI GS 002 V1.1.1 "Network Virtualisation(NFV) architectural framework," Oct. 2013.

[11] "5G white paper,by NGMN Alliance," Feb 2015, available from https://www.ngmn.org/uploads/media/NGMN 5G White Paper V1 0.pdf.

[12] Y. Niu, Y. Li, D. Jin, L. Su, and A. Vasilakos, "Survey of millimeter wave communications (mm-Wave) for 5G: Opportunities and challenges," Wireless Networks, pp. 1{20, Apr. 2015.

[13] K. Zheng, L. Zhao, J. Mei, M. Dohler, W. Xiang, and Y. Peng, "10 Gb/s HetSNets with millimeter-wave communications: Access and networking { challenges and protocols," IEEE Commun. Mag., vol. 53, no. 1, pp. 222{231, Jan. 2015.

[14] C. Ranaweera, E. Wong, A. Nirmalathas, C. Jayasundara and C. Lim, "5G C-RAN With Optical Fronthaul: An Analysis From a Deployment Perspective," in Journal of Lightwave Technology, vol. 36, no. 11, pp. 2059-2068, 1 June, 2018.

[15] D. Camps-Mur et al., "5G-XHaul: A Novel Wireless-Optical SDN Transport Network to Support Joint 5G Backhaul and Fronthaul Services," in IEEE Communications Magazine, vol. 57, no. 7, pp. 99-105, July 2019.

[16] "Exploring 5G Fronthaul Network Architecture Intelligence Splits and Connectivity," Intel white paper, 26, March, 2019.

[17] M. Mossaad , “Theoretical Analysis and Simulation of IM/DD Optical OFDM Systems,” Diss. PhD. Thesis, McMaster University, 2011.

[18] C. Jiang, H. Zhang, Y. Ren, Z. Han, Kw. Chen, and L. Hanzo, “Machine learning paradigms for next generation wireless networks,” IEEE Wireless Communications, vol. 24, no. 2, pp. 98–105, 2017.

[19] D. Mulvey, C. H. Foh, M. A. Imran and R. Tafazolli, “Cell fault management using machine learning techniques,” IEEE Access, vol. 7, pp. 124 514-124 539, 2019.

[20] A. Islam, M. T. Hossan, and Y. M. Jang, “Convolutional neural network scheme–based optical camera communication system for intelligent internet of vehicles,” International Journal of Distributed Sensor Networks, vol. 14, no. 4, p. 1550147718770153, 2018.

[21] M. Jarajreh et al., “Artificial neural network nonlinear equalizer for coherent optical OFDM,” IEEE Photonics Technology Lett., vol. 27, no. 4, pp. 387-390, Feb. 2014.

[22] B. Karanov et al., "End-to-End Deep Learning of Optical Fiber Communications," in Journal of Lightwave Technology, vol. 36, no. 20, pp. 4843-4855, 15 Oct.15, 2018.

[23] M. Mossaad , “Theoretical Analysis and Simulation of IM/DD Optical OFDM Systems,” Diss. PhD. Thesis, McMaster University, 2011

[24] S. D. Dissanayake and J. Armstrong, “Comparison of ACO-OFDM, DCO-OFDM and ADO-OFDM in IM/DD systems,” IEEE J. Lightwave Technol., vol. 31, no. 7, pp.1063-1072,2013.

[25] A. Ibrahim, T. Ismail, and K. Elsayed, M. Saeed “Odd Clipping Optical Orthogonal Frequency Division Multiplexing for VLC System,” International Journal of Communication Systems, 2019.

Bibliography

[26] I. Cano, X. Escayola, V. Polo, M. Santos, and J. Prat, "Sign Labeled OFDM with Intensity-Modulation Direct Detection for PONs," in European Conference and Exhibition on Optical Communication, OSA Technical Digest (online), Optical Society of America, 2012.

[27] I. N. Cano et al., "Experimental demonstration of a statistical OFDM-PON with multiband ONUs and elastic bandwidth allocation," in IEEE/OSA Journal of Optical Communications and Networking, vol. 7, no. 1, pp. A73-A79, Jan. 2015.

[28] J.M. Hamamreh, and M. Abewa, "Non-coherent OFDM-subcarrier power modulation for low complexity and high throughput IoT applications," RS Open J. Innov. Commun. Technol, vol. 4, pp.1-13, 2020.

[29] A. Ibrahim, J. Prat & T. Ismail "Asymmetrical clipping optical filter bank multi-carrier modulation scheme," Optical Quantum Electronics journal, vol. 53, pp. 230, 2021.

[30] C. Jiang, H. Zhang, Y. Ren, Z. Han, Kw. Chen, and L. Hanzo, "Machine learning paradigms for next generation wireless networks," IEEE Wireless Communications, vol. 24, no. 2, pp. 98–105, 2017.

[31] N. Baldo, L. Giupponi, and J. Mangues-Bafalluy, "Big Data Empowered Self Organized Networks," In 20th European Wireless Conference; Proceedings of European Wireless- 2014, pp. 1-8, 2014.

[32] S. Srinivasa and V. Bhatnagar, "Big Data Analytics," vol. 7678. Berlin, Heidelberg: Springer Berlin Heidelberg, 2012

[33] M. Jarajreh et al., "Artificial neural network nonlinear equalizer for coherent optical OFDM," IEEE Photonics Technology Lett., vol. 27, no. 4, pp. 387-390, Feb. 2014.

[34] A. Ibrahim, A. Elsheikh, A. Abdelsalam, J. Prat, "Neural Network based Transceiver for Non-Coherent OFDM Optical Modulation ", 25th International Conference on Advanced Communication TGechnology Tranactions (ICACT-TACT), March, 2023.

[35] M. Segal, "Machine learning benchmarks and random forest regression," Center Bio-inform. Mol. Bio-stat., 2004.

[36] B. Yildiz, J. I. Bilbao, and A. B. Sproul, "A review and analysis of regression and machine learning models on commercial building electricity load forecasting," Renew. Sustain. Energy Rev., vol. 73, pp. 1104–1122, Jun. 2017.

[37] M. Segal, "Machine learning benchmarks and random forest regression," Center Bio-inform. Mol. Bio-stat., 2004.

[38] J. Tsai, J. Chou, and T. Liu, "Tuning the structure and parameters of a neural network by using hybrid Taguchi-genetic algorithm," IEEE Trans. Neural Networks, vol. 17, no. 1, pp. 69–80, Jan. 2006.

[39] A. Ibrahim, A. Elsheikh, A. Abdelsalam, J. Prat, "Neural Network based Transceiver for Non-Coherent OFDM Optical Modulation ", 25th International Conference on Advanced Communication TGechnology Tranactions (ICACT-TACT), March, 2023

[40] J. Wu, et al., "Hyperparameter optimization for machine learning models based on Bayesian optimization," Journal of Electronic Science and Technology, vol.17, no. 1, pp. 26-40, 2019.

[41] J. Luketina, "Hyperparameter Optimization for Machine Learning," Master's thesis, School of Science, Aalto University, 2016. [Online]. Available: http://urn.fi/URN:NBN:fi:aalto-201606292835.

[42] J. Tsai, J. Chou, and T. Liu, "Tuning the structure and parameters of a neural network by using hybrid Taguchi-genetic algorithm," IEEE Trans. Neural Networks, vol. 17, no. 1, pp. 69–80, Jan. 2006.

[43] M. Stefano, C. Papa, and C. Sansone, "Effects of hidden layer sizing on CNN fine-tuning," Future Generation Computer Systems 118, pp. 48-55, 2021.

[44] E. Paluzo-Hidalgo, R. Gonzalez-Diaz, and M. A. Gutiérrez-Naranjo, "Two-hidden-layer feed-forward networks are universal approximators: A constructive approach," Neural Networks, pp. 29-36, 2020

[45] K. Hornik, M. Stinchcombe, and H. White, "Multilayer feedforward networks are universal approximators," Neural networks, vol. 2, no. 5, pp. 359–366, 1989.

[46] S. Ellen Haupt, A. Pasini, and C. Marzban, "Artificial intelligence methods in the environmental sciences," Springer Science & Business Media, 2008.

[47] S. Sharma and A. Athaiya, "Activation functions in neural networks," International Journal of Engineering Applied Sciences and Technology, Vol. 4, Issue 12, pp. 310-316, 2020.

[48] A. L. Maas, A. Y. Hannun, and A. Y. Ng, "Rectifier nonlinearities improve neural network acoustic models," in Proc. ICML, pp. 1–6, 2013.

[49] Martín Abadi et al., 'TensorFlow: Large-Scale Machine Learning on Heterogeneous Systems'. 2015. https://www.tensorflow.org/learn

[50] F. Chollet and Others, 'Keras', 2015. [Online]. Available: https://github.com/fchollet/keras.

[51] W. McKinney and Others, 'Data structures for statistical computing in python', in Proceedings of the 9th Python in Science Conference, vol. 445, pp. 51–56, 2010. https://pandas.pydata.org/

[52] F. Pedregosa et al., 'Scikit-learn: Machine Learning in Python', Journal of Machine Learning Research, vol. 12, pp. 2825–2830, 2011. https://pypi.org/project/scikit-commpy/

Bibliography

[53] M. Barbareschi, S. Del Mario Prete, F. Gargiulo, A. Mazzeo and C. Sansone, "Decision tree-based multiple classifier systems: An FPGA perspective", Proc. 12th Int. Workshop Multiple Classifier Syst. (MCS), pp. 194-205, 2015.

[54] R. Narayanan, D. Honbo, G. Memik, A. Choudhary and J. Zambreno, "An FPGA Implementation of Decision Tree Classification," 2007 Design, Automation & Test in Europe Conference & Exhibition, 2007, pp. 1-6, doi: 10.1109/DATE.2007.364589.

[55] A.M. Abdelsalam, A. Elsheikh, S. Chidambaram, et al. , " POLYBiNN: Binary Inference Engine for Neural Networks using Decision Trees," Journal of Signal Processing Systems, vol. 92, PP. 95–107, 2020. https://doi.org/10.1007/s11265-019-01453-w

[56] C. Ranaweera, E. Wong, A. Nirmalathas, C. Jayasundara and C. Lim, "5G C-RAN With Optical Fronthaul: An Analysis From a Deployment Perspective," in Journal of Lightwave Technology, vol. 36, no. 11, pp. 2059-2068, 1 June, 2018.

[57] P. Iovanna, F. Cavaliere, F. Testa et al., "Future proof optical network infrastructure for 5G transport," Journal of Optical Communications and Networking, vol. 8, no. 12, p. B80, 2016.

[58] A. Sahin, I. Guvenc, and H. Arslan, "A survey on multicarrier communications: Prototype filters, lattice structures, and implementation aspects," IEEE Communication Surveys and Tutorials, Dec. 2013.

[59] P. Siohan, C. Sicletand, and N. Lacaille, "Analysis and design of OFDM/OQAM systems based on filter bank theory," IEEE Transaction of Signal Processing, vol. 50, pp. 1170-1183, May 2002.

[60] R. Chen, K.-H. Park, C. Shen, T. K. Ng, B. S. Ooi, and M.-S. Alouini, "Visible light communication using DC-biased optical filter bank multicarrier modulation," in Proc. Global LIFI Congress (GLC), Paris, France, Feb. 2018.

[61] R. Nissel, S. Schwarz, and M. Rupp, "Filter bank multicarrier modulation schemes for future mobile communications," IEEE J. Sel. Areas Commun., vol. 35, no. 8, pp. 1768–1782, Aug. 2017.

[62] H. Lin and P. Siohan, "OFDM/OQAM with hermitian symmetry: Design and performance for baseband communication," in IEEE International Conference on Communications, (ICC '08), pp. 652–656, Beijing 2008.

[63] A. Ibrahim, T. Ismail, K. Elsayed and M. Saeed, "Odd Clipping Optical Orthogonal Frequency Division Multiplexing for VLC System," International Journal of Communication Systems, Wiley, e3942, vol. 32, no. 16, Sep. 2019.

[64] H. Elgala, R. Mesleh, and H. Haas, "Indoor broadcasting via white LEDs and OFDM," in IEEE Transaction Consumer Electronics, vol. 55, no. 3, pp. 1127-1134, 2009.

[65] S. Dissanayake and J. Armstrong, "Comparison of ACO-OFDM, DCOOFDM and ADO-OFDM in IM/DD systems," in Journal of Light Wave Technology, vol. 31, no. 7, pp. 1063-1072, 2013.

[66] S. Sarmiento, J. A. Altabas, S. Spadaro, and J. A. Lazaro, "From 4.2Gbps Asymmetrical Clipping (ACO)-OFDM to 8.7Gbps Layered- ACO-FBMC with Intensity-Modulation Direct-Detection for PONs," in 2019 Conference on Lasers and Electro Optics Europe and European Quantum Electronics Conference, OSA Technical Digest (Optical Society of America, 2019).

[67] R. Haas and J.-C. Belfiore, "A time-frequency well-localized pulse for multiple carrier transmission," Wireless Personal Communications, vol. 5, no. 1, pp. 1–18, 1997.

[68] M. Bellanger, D. Le Ruyet, D. Roviras, M. Terre, J. Nossek, L. Baltar, Q. Bai, D. Waldhauser, M. Renfors, T. Ihalainen et al., "FBMC physical layer: a primer," PHYDYAS, January, 2010.

[69] H.A. Ali, R.M. Zaki, M.M. Tantawy, "Overlapping factor effect on the prototype filter response proposed for FBMC trans multiplexer system," ICENCO 2018 - 14th International Computer Engineering Conference, 2019.

[70] A. Jovicic, J. Li, and T. Richardson, "Visible light communication: opportunities, challenges and the path to market," in IEEE Communications Magazine, vol. 51, no. 12, pp. 26-32, 2013.

[71] N. Komuro and H. Habuchi, "Intensity Modulation Direct Detection Optical Wireless Communication with Nonorthogonal Code Shift Keying," 2019 IEEE 8th Global Conference on Consumer Electronics (GCCE), Osaka, Japan, 2019.

[72] M.Y. Liu, T.L. Wang and S.M. Tseng, "Throughput Performance Analysis of Asynchronous Optical CDMA Networks with Channel Load Sensing Protocol," IEEE Photonics Journal, vol.9, no. 3, 2017.

[73] S.H. Chen and C.W. Chow, "Color-shift Keying Code-division Multiple access Transmission for RGB-LED Visible Light Communications using Mobile Phone Camera," IEEE Photonics Journal, vol.7, no.6., Dec. 2014.

[74] H. Elgala, R. Mesleh, and H. Haas, "Indoor broadcasting via white LEDs and OFDM," in IEEE Transaction Consumer Electronics, vol. 55, no. 3, pp. 1127-1134, 2009.

[75] M. Aminikashani, W. Gu, and M. Kavehrad, "Indoor positioning in high speed OFDM visible light communications," in 13th IEEE Annual Consumer Communications and Networking Conference (CCNC), 2016.

[76] S. Dissanayake and J. Armstrong, "Comparison of ACO-OFDM, DCOOFDM and ADO-OFDM in IM/DD systems," in Journal of Light Wave Technology, vol. 31, no. 7, pp. 1063-1072, 2013.

[77] A. Ibrahim, T. Ismail, K. Elsayed and M. Saeed, "Odd Clipping Optical Orthogonal Frequency Division Multiplexing for VLC System," International Journal of Communication Systems, Wiley, e3942, vol. 32, no. 16, Sep. 2019.

Bibliography

[78] C. Chen, W. D. Zhong, and D. Wu, "Non-Hermitian symmetry orthogonal frequency division multiplexing for multiple-input multiple-output visible light communications," in IEEE/OSA Journal of Optical Communication and Networks, vol. 9, no. 1, pp. 36–44, 2017.

[79] Basnayaka, A. Dushyantha, and H. Haas, "Hybrid RF and VLC systems: Improving user data rate performance of VLC systems," in 81st Vehicular Technology Conference (VTC Spring), UK, 2015.

[80] G. W. Marsh and J. M. Kahn, "Channel reuse strategies for indoor infrared wireless communications," in IEEE Transactions on Communications, vol. 45, no. 10, pp. 1280-1290, 1997.

[81] R. Mondal, M. Chowdhury, N. Saha, and Y. M. Jang, "Interference aware optical resource allocation in visible light communication," in International Conference on ICT Convergence, pp. 155-158, 2012.

[82] C. Chen, N. Serafimovski, and H. Haas, "Fractional frequency reuse in optical wireless cellular networks," in the 24th Annual International Symposium on Personal, -- Indoor, and Mobile Radio Communications (PIMRC), UK, 2013.

[83] S. Ali and V. C. M. Leung, "Dynamic frequency allocation in fractional frequency reused OFDMA networks," in IEEE Transactions on Wireless Communications, vol. 8, pp. 4286–4295, Aug. 2009.

[84] A. A. Gebremariam, T. Bao, D. Siracusa, T. Rasheed, F. Granelli, and L. Goratti, "Dynamic strict fractional frequency reuse for software-defined 5g networks," in IEEE International Conference on Communications (ICC), May 2016.

[85] H. Liu, P. Xia, Y. Chen, L. Wu, "Interference graph-based dynamic frequency reuse in optical attocell networks," Optical Communication, vol. 402, pp. 527–534, Nov. 2017.

[86] Y. Chen, S. Li, H. Liu, "Dynamic frequency reuse based on improved tabu search in multi-user visible light communication networks," IEEE Access, vol. 7, pp. 35173–35183, Feb. 2019.

[87] K. X. Zhou, C. Gong, and Z. Y. Xu, ''Color planning and intercell interference coordination for multicolor visible light communication networks,'' in Journal of Light Wave Technology, vol. 35, no. 22, pp. 4980–4993, Nov. 2017.

[88] Y. Fan, J. Liu, Q. Li, and X. Zhang, ''Downlink channel allocation of visible light communication network based on graph coloring and traffic fairness,'' in Proceeding of Computer Science, pp. 667–673, Jan. 2017.

[89] A. Ibrahim, T. Ismail and K. Elsayed, "Optimized radio resource allocation scheme for indoor optical wireless communication," in International Conference on Transparent Optical Networks, Gerona, Spain, July 2017.

[90] W. Rhee and J. M. Cioffi, "Increase in capacity of multiuser OFDM system using dynamic sub channel allocation," 51st Vehicular Technology Conference (VTC), Tokyo, Japan, May 2000.

[91] S. Dimitrov, S. Sinanovic, and H. Haas, "Clipping noise in OFDM-based optical wireless communication systems," IEEE Trans. Commun., vol. 60, no. 4, pp. 1072–1081, Apr. 2012.

[92] J. Armstrong and B. J. C. Schmidt, "Comparison of asymmetrically clipped optical OFDM and DC-biased optical OFDM in AWGN," IEEE Commun. Lett., vol. 12, no. 5, pp. 343–345, May 2008.

[93] M. Vadivel and H. Ranganathan, "Optimization of Dynamic Resource Allocation and Rate Adaptation in OFDMA Systems," in International Journal of Computer Applications, vol. 47, no. 25, p.p. 15-19, June 2012.

[94] T. Mehrdad and L. Farshad, "Discrete Rate Interfering Cognitive Link Adaptation Design with Primary Link Spectral Efficiency Provisioning," IEEE Transactions on Wireless Communications, vol. 10, no. 9, pp. 2929-2939, July 2011.

[95] S. Sadr, A. Alagan, and R. Kaamran, "Suboptimal Rate Adaptive Resource Allocation for Downlink OFDMA Systems," in International Journal of Vehicular Technology, vol. 10, 2009.

[96] A. Noliya and S. Kumar, "Performance Analysis of Resource Scheduling Techniques in Homogeneous and Heterogeneous Small Cell LTE-A Networks," Wireless Personal Communications vol. 112, p.p. 2393–2422, Jan. 2020.

[97] B. Ghimire and H. Haas, "Resource allocation in optical wireless networks," in the 22nd Annual IEEE International Symposium on Personal, Indoor and Mobile Radio Communications, Canada, pp. 11-14, 2011.

[98] J. Ordonez-Lucena, P. Ameigeiras, D. Lopez, J. J. Ramos-Munoz, J. Lorca, and J. Folgueira, "Network slicing for 5G with SDN/NFV: Concepts, architectures, and challenges," IEEE Commun. Mag., vol. 55, no. 5, pp. 80-87, May 2017.

[99] China Mobile Research Institute, Beijing, China, "C-RAN: The road towards green RAN," White Paper, 2013. [Online]. Available: http://labs. chinamobile.com/cran/

[100] C. Ranaweera, E. Wong, A. Nirmalathas, C. Jayasundara and C. Lim, "5G C-RAN with Optical Fronthaul: An Analysis from a Deployment Perspective," in Journal of Lightwave Technology, vol. 36, no. 11, pp. 2059-2068, 2018.

[101] D. Camps-Mur et al., "5G-XHaul: A Novel Wireless-Optical SDN Transport Network to Support Joint 5G Backhaul and Fronthaul Services," in IEEE Communications Magazine, vol. 57, no. 7, pp. 99-105, July 2019.

[102] C.-Y. Chang et al., "Impact of packetization and functional split on C-RAN fronthaul performance," in Proc. IEEE ICC, 2016.

[103] Chia-Yu Chang, et al, "FlexCRAN: A flexible functional split framework over ethernet fronthaul in Cloud-RAN," 2017 IEEE International Conference on Communications (ICC). IEEE, 2017.

Bibliography

[104] Y. Zhou, et al. "Flexible functional split design for downlink C-RAN with capacity-constrained fronthaul." IEEE Transactions on Vehicular Technology, vol. 68, no.6, pp. 6050-6063 ,2019.

[105] E. Aqeeli, A. Moubayed, and A. Shami, "Power-aware optimized RRH to BBU allocation in C-RAN," IEEE Transactions on Wireless Communications, vol.17, no.2, pp. 1311-1322, 2017.

[106] M. Y. Lyazidi, N. Aitsaadi, and R. Langar, "Dynamic resource allocation for Cloud-RAN in LTE with real-time BBU/RRH assignment," 2016 IEEE international conference on communications (ICC). IEEE, 2016.

[107] Sahu, Bharat JR, et al. "Energy-efficient bbu allocation for green c-ran." IEEE Communications Letters, vol. 21, no. 7, pp. 1637-1640, 2017.

[108] F. Girardin, J. Blat, F. Calabrese, F. Dal Fiore, C. Ratti, "Digital Foot printing: Uncovering Tourists with User-Generated Content," IEEE Pervasive Computing, vol. 7, no. 4, pp. 36–43, 2008.

[109] R.A. Becker, R. Caeres, K. Hanson, J.M. Loh, S. Urbanek, A. ´ Varshavsky, C. Volinsky, "A Tale of One City: Using Cellular Network Data for Urban Planning," IEEE Pervasive Computing, vol. 10, no. 4, pp. 18–26, 2011.

[110] J.L. Toole, M. Ulm, M.C. Gonzalez, D. Bauer, "Inferring land use ´ from mobile phone activity," ACM SIGKDD UrbComp, Beijing, PRC, Aug. 2012.

[111] E. Aqeeli, A. Moubayed, and A. Shami, "Power-aware optimized RRH to BBU allocation in C-RAN," IEEE Transactions on Wireless Communications, vol.17, no.2, pp. 1311-1322, 2017.

[112] P. Secchi, S. Vantini, V. Vitelli, "Analysis of Spatio-Temporal Mobile Phone Data: A Case Study in the Metropolitan Area of Milan," Statistical Methods & Applications, vol. 24, no. 2, pp. 279–300, 2015.

[113] K. Boulos, M. E. Helou, and S. Lahoud, "RRH clustering in cloud radio access networks," in Proc. Int. Conf. Appl. Res. Comput. Sci. Eng.(ICAR), Beirut, Lebanon, Oct. 2015, pp. 1–6.

[114] M. Qian, W. Hardjawana, J. Shi, and B. Vucetic, "Baseband processing units virtualization for cloud radio access networks," IEEE Wireless Commun. Lett., vol. 4, no. 2, pp. 189–192, Apr. 2015.

[115] H. M. Soliman and A. Leon-Garcia, "QoS-aware joint RRH activation and clustering in cloud-RANs," in Proc. IEEE Wireless Commun. Netw. Conf., Doha, Qatar, Apr. 2016, pp. 1–6.

[116] D. Mishra, et al. "Load-aware dynamic RRH assignment in cloud radio access networks." IEEE Wireless Communications and Networking Conference. IEEE, 2016.

[117] Z. H. Fakhri, M. Khan, F. Sabir, and H. S. Al-Raweshidy, "A resource allocation mechanism for cloud radio access network based on cell differentiation and integration concept," IEEE Trans. Netw. Sci. Eng., Oct. 2017

[118] F. Calabrese, F.C. Pereira, G. Di Lorenzo, L. Liu, C. Ratti, "The Geography of Taste: Analyzing Cell-Phone Mobility and Social Events," Pervasive Computing, 2010.

[119] J.P. Bagrow, D. Wang, A.-L. Barabasi, "Collective Response of Human Populations to Large-Scale Emergencies," PLoS ONE, 6(3), 2011.

[120] D. Naboulsi, R. Stanica, M. Fiore, "Classifying Call Profiles in Large-scale Mobile Traffic Datasets," IEEE INFOCOM, 2014.

[121] S. Aghabozorgi, A. Shirkhorshidi, and T.Wah. , "Time-series clustering–a decade review," Information Systems, vol. 53, pp. 16-38, 2015.

[122] E. Keogh, J., Lin, "Clustering of time-series subsequences is meaningless: implications for previous and future research," Knowledge and information systems, vol. 8, no. 2, pp. 154–177, 2005.

[123] Telecom Italia, "Telecommunications - SMS, Call, Internet – MI," Harvard

[124] Dataverse,2015. https://doi.org/10.7910/DVN/EGZHFV .

[125] Barlacchi, G. et al., "A multi-source dataset of urban life in the city of Milan and the Province of Trentino," . Sci. Data 2:150055 doi: 10.1038/sdata.2015.55 , 2015.

[126] K. Khan, et al. , "DBSCAN: Past, present and future," The fifth international conference on the applications of digital information and web technologies (ICADIWT 2014). IEEE, 2014.

[127] L. Buitinck et al., 'API design for machine learning software: experiences from the scikit-learn project', in ECML PKDD Workshop: Languages for Data Mining and Machine Learning, pp. 108–122, 2013.